UNIVERSITY OF TECHNOLOGY OF COMPIEGNE

PHD Thesis

to obtain the title of

PHD of the University of Technology of Compiegne
Discipline: Information and Systems Technologies

by

Nadia Ben Abdallah

Modelling sea-level rise uncertainties for coastal defence adaptation using belief functions

prepared at UTC, Decision & Image (DI) Team

defended on 12th March, 2014

Jury:

Walter Schon	-	Professor at UTC
Didier Dubois	-	CNRS Research Advisor
Minh Ha-Duong	-	CNRS Research Advisor
Scott Ferson	-	Senior Scientist at Applied Biomathematics
Thierry Denoeux	-	Professor at UTC
Nassima Mouhous-Voyneau	-	Associate professor at UTC

To my grandfather

Acknowledgments

Foremost, I would like to express my thanks and gratitude to my supervisor, Thierry Denoeux, for his support, guidance, and precious advice during these three years. I have been really pleased to conduct this thesis under his supervision, and benefited a lot from his extended knowledge and mastery. I hope I will have the opportunity to further exchange and work with him. My thanks go also to Nassima Voyneau, my co-supervisor, for the inner interest she demonstrated in my work. Her confidence, encouragements, and kindness helped me overcome some tough moments only PHD students experience.

I would express my sincere thanks to Didier Dubois, Minh-Ha Duong, Walter Schon, and Scott Ferson for kindly agreeing to be members of the committee, and for the time they devoted to read and review the manuscript. I was really honored to have them in the jury. I thank them for their suggestions and the various discussions we had. Particular thanks go to Didier Dubois and Scott Ferson for their insightful comments on the manuscript, their benevolence, and encouragements.

I express my deepest gratitude to my professor, mentor, and master thesis supervisor: Alain Chateauneuf. I owe him my interest in research and the willingness to pursue a PHD. He is a source of inspiration and admiration, both on human and scientific sides.

It was not easy to cope with me lately. I thank my friends and colleagues who have been understanding, patient, and caring. Siwar, Haythem, Nabil: you're gold friends. I thank Aya, JiaMin, Chakib, Ameni, Imene, Aurélie, Sawsan, Nicole, Jérémy, Marion, Katherine, and Fernanda for their support, from near and far.

My last and not least thanks go to my parents, sisters, and brothers for their love, support and encouragement throughout my entire life. I owe you all, and my accomplishments are yours. Anis, you deserve an entire PHD chapter of acknowledgments. I thank you for your unconditional love, patience, and strength of will to be part of my (messy) life.

Contents

Introduction 3

I Belief functions theory: a framework for probabilistic and statistical reasoning 7

1 Reasoning under uncertainty 9
1.1 Introduction . . . 9
1.2 Taxonomies of uncertainty . . . 9
1.3 Probabilistic modelling of uncertainty and its issues . . . 11

2 Belief functions theory 13
2.1 Mathematical fundamentals of evidence theory: finite domain . . . 14
2.2 Belief functions in infinite spaces: random intervals . . . 17
2.3 Connection with alternative uncertainty frameworks . . . 18
2.4 Combining evidence from different sources . . . 20
2.4.1 Dempster's rule of combination . . . 21
2.4.2 Discounting rule . . . 22
2.4.3 Averaging rule . . . 24
2.5 Propagation of belief functions . . . 26
2.5.1 The extension principle . . . 26
2.5.2 Monte Carlo approximation . . . 28

3 Statistical inference 29
3.1 Background . . . 29
3.2 Dempster's approach . . . 30
3.3 Likelihood-based inference extended to DST . . . 32
3.3.1 Formal description . . . 32
3.3.2 Addressing the incompatibility with Dempster's rule . . . 34
3.3.3 Discussion . . . 35

4 Conclusion 36

II Global warming and sea-level rise 39

1 Introduction 41

2 A review of uncertainties in future global warming projections 41
2.1 Greenhouse gas emissions . . . 41
2.2 Future global warming . . . 44

3 Sea-level rise **46**
3.1 Controlling processes . . . 47
3.1.1 Thermal expansion of oceans . . . 47
3.1.2 Melting of mountain ice and glaciers . . . 47
3.1.3 Ice sheet dynamics . . . 47
3.2 Future projections . . . 49
3.2.1 Process-based projections . . . 49
3.2.2 Past observations to predict the future: the semi-empirical approach . . . 50
3.2.3 Climate expert elicitation . . . 52

4 Conclusion **54**

III Quantifying uncertainty in future sea-level projections **57**

1 Process-based projections **59**

2 Projections derived from statistical fit to historical data **63**
2.1 Analysis method . . . 64
2.2 Quantifying uncertainty of the model statistical fit . . . 69
2.3 Representing evidence on future temperature projections . . . 70
2.4 Propagation results: SLR projections . . . 72

3 Projections derived from climate expert judgments **74**
3.1 Representing expert judgments with belief functions . . . 75
3.2 Pooling expert judgments . . . 77
3.3 Propagation results: combined ice sheets contribution and global sea-level rise projections . . . 83

4 Comparative analysis and conclusion **85**

IV Coastal design and adaptation to climate change **89**

1 Coastal defence structures and hydrographic loading **91**
1.1 Defence structures . . . 91
1.2 Hydrographic loads . . . 92
1.2.1 Still water level . . . 92
1.2.2 Waves . . . 93
1.3 Functional failure mechanisms . . . 94
1.3.1 Overflowing . . . 94
1.3.2 Wave overtopping . . . 94

2 Coastal design **96**
2.1 Univariate design variable: the level of overflowing 96
2.2 Multiple design variables: the level of overtopping 98
2.2.1 Copulas: a multivariate model 99
2.3 Impact of climate change 100
2.3.1 Impact of climate change on sea conditions 100
2.3.2 Adapting to climate change: an analytical approach 101
2.3.3 Uncertainty in coastal adaptation 101

3 Conclusion **103**

V Adapting under uncertainty: a methodologically-oriented case study **105**

1 Description of the study site **107**

2 Extreme sea-level analysis **108**
2.1 Models and assumptions 108
2.1.1 Extreme value statistics for present-day conditions from statistical evidence 108
2.1.2 Impact of climate change on extreme sea levels 110
2.2 Application to the Havre data 111
2.2.1 Extreme sea-level statistics under present-day conditions . . . 111
2.2.2 The impact of climate change 112
2.2.2.1 Sensitivity analysis 113
2.2.2.2 Uncertainty analysis 113

3 Overtopping hazard analysis **116**
3.1 Models and assumptions 116
3.2 Application to the Havre site 118
3.2.1 Multivariate analysis of storm waves and surges 118
3.2.1.1 Data preparation 118
3.2.1.2 Modelling dependence with copulas 119
3.2.2 Joint design conjunction 122
3.2.3 Centennial overtopping 124
3.2.4 Adapting to uncertain climate change 125

4 Conclusion **127**

Conclusion **131**

VI Appendices **135**

1 Statistical inference **137**
1.1 Frequentist perspective: an exemple to illustrate inconsistency 137
1.2 Formal description of Bayesian perspective of inference 137
1.3 Axiomatic justification of the likelihood principle 138

2 Correlation analysis in time series **140**

3 Multivariate analysis through copulas **141**
3.1 Archimedean copulas family 141
3.2 Genest and Rivest goodness-of-fit test 141

4 Expert Elicitation: intermediate results **143**

Bibliography **145**

List of Figures

1.1 Uncertainty classification for structural enginnering 10
1.2 Uncertainty classification for policy and risk analyses 10
1.3 Random code setup. 15
1.4 Random closed interval induced by a possibility distribution 19
1.5 Random closed interval induced by a p-box 20
2.1 Uncertainty sources in the integrated climate change impact assessment 42
2.2 Projections of anthropogenic GHG emissions in the next century . . 43
2.3 IPCC projections of future global warming in the coming century . . 45
2.4 Earth's ice sheets: Antarctica and Greenland 48
2.5 IPCC projections of global sea-level rise by 2100 50
2.6 Observed vs reconstructed rate of sea-level rise 51
2.7 Projection of sea-level rise from 1990 to 2100 52
2.8 Range plots of individual responses by experts 53
2.9 Distribution of sea-level rise from ice sheets contribution 54
3.1 Contour functions and cdfs of random sets on SLR by 2100 62
3.2 Contour plot of belief functions 62
3.3 contour plot of plausibilities 63
3.4 Annual temperature anomaly relative to the 1950-1980 average . . . 65
3.5 GISS annual temperature anomaly and smoothed data 65
3.6 Church and White annual sea-level and sea-level rate 66
3.7 Residuals plot. 67
3.8 Correlation and partial autocorrelation functions 67
3.9 Observation-based rate of sea-level vs predictions 68
3.10 Observations-based sea-level compared with that predicted by RV09 69
3.11 Joint and marginal contour plausibilities on RV09 parameters 70
3.12 Contour plausibility of the random set on the a (a) and T_0 (b) parameters. 71
3.13 IPCC temperature anomaly projections 71
3.14 Contour functions and ω-level cuts 72
3.15 Consecutive ω-cuts of the random intervals on T 73
3.16 Contour plausibility and cumulative plausibility and belief on SLR . 74
3.17 Expert's assessments of the contribution of ice sheets to SLR 76
3.18 Cumulative belief and plausibility on θ 77
3.19 Contour plausibility of the WAIS contribution 79
3.20 Effect of discounting 80
3.21 Contour plausibility of the WAIS contribution 82
3.22 WAIS, EAIS, and GrIS combined assessments 82
3.23 Ice sheets contribution to SLR 83
3.24 PDF for the rate of SLR due to ice sheets contribution 84
3.25 The contribution of ice sheets to SLR 84
3.26 Cumulative belief and plausibility on SLR projections from expert's judgments 85
3.27 Upper and lower CDFs on SLR from three predictive methods 86

4.1 A generic dike and the main hydrographic loads . . . 92
4.2 The components of still sea-level . . . 92
4.3 Overflowing process on a dike . . . 94
4.4 Wave overtopping process on a dike . . . 95
5.1 The Havre location . . . 108
5.2 Empirical CDF of sea level annual maxima . . . 112
5.3 Contour and marginal contour plausibility plots . . . 112
5.4 Contour plausibility of Z_T . . . 113
5.5 Return period curves for current and future climate conditions . . . 114
5.6 Contour plausibility on SLR for different ϕ functions . . . 115
5.7 Contour plausibility on Z'_{100} . . . 116
5.8 CDFs induced by the random interval on Z'_{100} . . . 117
5.9 Offshore Wave-surge conjunctions (gray dots) and storm events (blue stars). 119
5.10 QQ plot for storm waves (a) and surges (b) variables. . . . 119
5.11 GOF graphical plots . . . 121
5.12 Random sample (U, V) from Gumbel copula with parameter $\lambda = 3$ (a) and $\lambda = 1.26$ (b). . . . 122
5.13 Contour plausibility induced by the random interval on θ . . . 123
5.14 return period is-lines . . . 123
5.15 CDFs induced by the random interval on the joint return period . . . 124
5.16 Kernel density of High tides. . . . 125
5.17 Contour plausibility induced by the belief function on the centennial overtopping (under current climate conditions). . . . 126
5.18 Crest elevation: contour plausibility . . . 127

Modelling sea-level rise uncertainties for coastal defence adaptation using belief functions

Abstract

Coastal adaptation is an imperative to deal with the elevation of the global sea level caused by the ongoing global warming. However, when defining adaptation actions, coastal engineers encounter substantial uncertainties in the assessment of future hazards and risks. These uncertainties may stem from a limited knowledge (e.g., about the magnitude of the future sea-level rise) or from the natural variability of some quantities (e.g., extreme sea conditions). A proper consideration of these uncertainties is of principal concern for efficient design and adaptation.

The objective of this work is to propose a methodology for uncertainty analysis based on the theory of belief functions – an uncertainty formalism that offers greater features to handle both aleatory and epistemic uncertainties than probabilities. In particular, it allows to represent more faithfully experts' incomplete knowledge (quantiles, intervals, etc.) and to combine multi-sources evidence taking into account their dependences and reliabilities. Statistical evidence can be modeled by likelihood-based belief functions, which are simply the translation of some inference principles in evidential terms. By exploiting the mathematical equivalence between belief functions and random intervals, uncertainty can be propagated through models by Monte Carlo simulations. We use this method to quantify uncertainty in future projections of the elevation of the global sea level by 2100 and evaluate its impact on some coastal risk indicators used in coastal design. Sea-level rise projections are derived from physical modelling, expert elicitation, and historical sea-level measurements. Then, within a methodologically-oriented case study, we assess the impact of climate change on extreme sea conditions and evaluate the reinforcement of a typical coastal defence asset so that its functional performance is maintained.

Keywords: Belief functions, random intervals, expert opinions, likelihood-based inference, Monte Carlo, copulas, extreme value theory, climate change, uncertainty analysis, coastal design.

Utilisation des fonctions de croyance pour la modélisation des incertitudes dans les projections de l'élévation du niveau marin pour l'adaptation côtière

Résumé

L'adaptation côtière est un impératif pour faire face à l'élévation du niveau marin, conséquence directe du réchauffement climatique. Cependant, la mise en place d'actions et de stratégies est souvent entravée par la présence de diverses et importantes incertitudes lors de l'estimation des aléas et risques futurs. Ces incertitudes peuvent être dues à une connaissance limitée (de l'élévation du niveau marin futur par exemple) ou à la variabilité naturelle de certaines variables (les conditions de mer extrêmes). La prise en compte des incertitudes dans la chaîne d'évaluation des risques est essentielle pour une adaptation efficace.

L'objectif de ce travail est de proposer une méthodologie pour la quantification des incertitudes basée sur les fonctions de croyance – un formalisme de l'incertain plus flexible que les probabilités. Les fonctions de croyance nous permettent de décrire plus fidèlement l'information incomplète fournie par des experts (quantiles, intervalles, etc.), et de combiner différentes sources d'information. L'information statistique peut quand à elle être décrite par de fonctions des croyance définies à partir de la fonction de vraisemblance. Pour la propagation d'incertitudes, nous exploitons l'équivalence mathématique entre fonctions de croyance et intervalles aléatoires, et procédons par échantillonnage Monte Carlo. La méthodologie est appliquée dans l'estimation des projections de la remontée du niveau marin global à la fin du siècle issues de la modélisation physique, d'élicitation d'avis d'experts, et de modèle semi-empirique. Ensuite, dans une étude de cas, nous évaluons l'impact du changement climatique sur les conditions de mers extrêmes et évaluons le renforcement nécessaire d'une structure afin de maintenir son niveau de performance fonctionnelle.

Mots-clés: Fonctions de croyance, intervalles aléatoires, avis d'experts, inférence statistique basée sur la vraisemblance, Monte Carlo, copules, théorie des valeurs extrêmes, changement climatique, analyse d'incertitude, dimensionnement côtier.

Abbreviations

ACF	auto-correlation function
AIC	Akaike's information criterion
AIS	Antarctica ice sheets
BVN	bivariate normal
ANEMOC	atlas numérique des états de Mer céaniques et côtiers
AOGCMs	atmosphere-ocean global circulation models
AR4	fourth assessment report
CANDHIS	Centre d'Archivage National de Données de Houle in Situ
AR1	first order autoregressive process
CLASH	Crest Level Assessment of coastal Structures by full scale monitoring, neural network prediction and Hazard analysis on permissible wave overtopping
ARMA	autoregressive moving average
CDF	cumulative distribution function
CETMEF	Centre d'Etudes Techniques Maritimes et Fluviales
CGCM	climate global circulation models
CMH	Cote Marine du Havre
CP	conditionality principle
DS	Dempster–Shafer
DST	Dempster–Shafer theory
EAIS	East Antarctica ice sheet
EML	exact maximum likelihood
EE	expert elicitation
EU	Europe
EVT	extreme value theory
GEV	generalized extreme value

GHG greenhouse gases

GICC Gestion et Impacts du Changement Climatique

GISS Goddard Institute for Space Studies

GOF goodness-of-fit

GPD generalised Pareto distribution

GrIS Greenland ice sheet

Gt gigaton

IFM inference functions for margins

IPCC Intergovernmental Panel on Climate Change

IS ice sheet

MC Monte Carlo

MLE maximum likelihood estimate

NASA National Aeronautics and Space Administration

PACF partial auto-correlation function

p-box probability box

PDF probability distribution function

POT peak over threshold

PSMSL permanent service for mean sea level

RONIN Réseau d'Observation du Niveau de la Mer

SAO POLO Strategies d'Adaptation des Ouvrages de Protection marine ou des modes d'Occupation du Littoral

SHOM Service Hydrographique et Océanographique de la Marine

SLR sea-level rise

SP sufficiency principle

SRES special report on emission scenarios

SSA singular spectrum analysis

SWL sea-water level

UN	United Nations
WAIS	West Antarctica ice sheet

Introduction

Context & Motivation

Since the late nineteenth century, the Earth climate has been showing noticeable changes in extreme events frequency, temperature ranges, seasonal patterns, etc. The scientific community is unequivocal about the causes of these changes: the increasing concentrations of greenhouse gases (GHG) produced by human activities. Just one month ago, the Intergovernmental Panel on Climate Change (IPCC), a scientific international body dedicated to climate issues, said in its latest report that it is "'95% confident that humans are behind the climate change". Global warming, referring to the rise of the average temperature of Earth's atmosphere and oceans due to the greenhouse gas emissions, is recognized by the scientific community as an underway process that poses significant risks to ecological and human systems.

To deal with global warming, two complementary policy responses exist: mitigation and adaptation. The objective of mitigation is to reduce anthropogenic (i.e., induced by humans) GHG emissions via international and local policies, such as the Kyoto Protocol. Mitigation strategies raise some issues as they are difficult to implement and require long time before they can meet their expectations. The second policy to deal with climate change is adaptation, and consists in making adjustments of natural and human systems to prevent, or at least to minimise, the climate-related risks and hazards. Adaptation is increasingly recognised as an unavoidable strategy at the local and international levels. In its very recent report issued in October 2013, the IPCC devoted an entire chapter to adaptation practices and options. At the European level, the European Commission adopted an EU adaptation strategy in April 2013. Since the beginning of this century, various countries have been developing their national adaptation strategies and frameworks.

The increase of sea levels is amongst the most hazardous impacts of global warming. The rising sea levels increase the vulnerability of low-lying areas to natural hazards (inundations, shoreline erosion, etc). They also threaten the safety of coastal and offshore transportation and energy infrastructures, such as ports, nuclear installations, or power platforms. Worldwide, 200 million people are concerned with the elevation of the sea levels. Given the great human and economic issues, anticipatory coastal adaptation is urgently needed for coping with the increasing sea levels in the very coming decades. Coastal adaptation strategies involve the construction of new structures, or the reinforcement of the existing ones. The methodological scheme that an effective coastal adaptation strategy should follow is the following:

(A) Collect the most reliable and up-to-date scientific evidence on the climate change impacts.

(B) Estimate the potential risks on the defence structure related to the climate change.

(C) Assess the vulnerability of the infrastructures to the climate-related risks.

(D) Calculate the costs of the required adaptation.

In the latest decade, states with coastal areas have been developing their national coastal planning strategies. At the national level, the Gestion et Impacts du Changement Climatique (GICC) organism has launched in 2007 a project, named Strategies d'Adaptation des Ouvrages de Protection marine ou des modes d'Occupation du Littoral (SAO POLO), to assess the impact of the sea-level rise on certain French coasts and evaluate the costs of local adaptation strategies.

Efficient coastal design and adaptation require the estimates of the hydraulic risks, the vulnerability and the costs determined in each of the three tasks (B), (C) and (D) to be as accurate as possible. However, coastal engineers are often confronted when undertaking these tasks to different uncertainties. Some of these uncertainties are not very challenging as they can be reduced. This is the case of the uncertainties stemming from the inaccuracy of the models used to assess the hazard and the vulnerability and the imprecision of the measurements. They can be narrowed, respectively, by the development of site-specific numerical models and the investment in precise measurement devices. A more challenging uncertainty – probably the most challenging in coastal adaptation – is the magnitude of climate change impacts, and particularly the magnitude of future sea-level rise that is assessed in task (A). Indeed, projections of future sea-level rise provided by the climate community are substantially uncertain with estimates for the end of the century ranging between 0.3 to 5 meters.

The large uncertainty in future sea-level projections is due to the limited understanding of many loops in the sea-level rise processes, such as the ice sheets dynamics, and the inability to model them with an acceptable level of confidence. Extensive research on sea-level rise is ongoing since the nineties to better understand and quantify the future sea level tendency based on different sources of evidence (expert opinions, collection of data, scientific research, etc). The objective is to improve the projections by narrowing them as much as possible and facilitate the anticipatory adaptation.

Despite a significant improvement in the scientific understanding of the mechanisms controlling sea-level elevation, the use of the projections for adaptation purposes remain quite challenging for at least two reasons. The first reason is related to the lack of agreement in the climate community on a "best" method and model for assessing sea-level increase. Different models and methods are used in the climate literature and they lead to a very large interval on climate impacts projections. The second reason is that, even if a method was agreed on, there is generally no likelihood attached to its associated projections. Because of these two factors, integrating sea-level projections in risk analyses is challenging for coastal engineers. To-date methods are based on conducting risk (then vulnerability) analyses considering particular sea-level rise scenarios, such as the higher estimate in the literature. This deterministic approach has been used within the SAO POLO project. Such an approach masks the uncertainty and gives policy makers an unjustified security in their policy. The quantification of the uncertainties in the most reliable sea level projections in the literature is critical for a faithful description of the effective scientific state of knowledge on the climate change and for an "intelligent" adaptation.

Since the last decade of the previous century, there has been a growing scientific interest in quantifying uncertainty in future climate change. Different uncertainty formalisms have been used for estimating future temperatures, whereas only few works addressed the uncertainty in the future sea-level rise. These works used, exclusively, the probabilistic framework to quantify future sea-level projections. However, this formalism proved its inadequacy to handle certain aspects of uncertainty in climate-related assessments.

Objective

The objective of this work is to propose an alternative methodology to the existing ones for the quantification and propagation of uncertainty in climate change impacts (the sea-level rise in particular) and related risks analyses. In particular, we intend to demonstrate the applicability of a particular uncertainty framework, the Dempster–Shafer theory, in handling different dimensions of uncertainty and illustrate its potential in climate and engineering applications.

The proposed methodology was applied in two analyses. The first application concerns task (A). We propose to conduct an assessment of the sea-level rise induced by the global warming in the the coming century. The second application is the hydraulic risk assessment (task (B)) for a typical defence structure in a context of changing climate.

Outline of the Dissertation

The dissertation is structured around three main parts. In chapter 1, we introduce the uncertainty formalism we intend to use in this work, namely, the belief functions framework. First, we introduce the concept of uncertainty and describe the different definitions that can be associated to it. Then, we describe the traditional framework for modelling uncertainty, i.e., the probability theory and discuss its adequacy for addressing certain aspects of uncertainty. In particular, we show that this formalism can not handle severe uncertainty that is often encountered in climate-related analyses, and that more general theories are required. In the third and last part, we introduce the belief functions theory – an alternative framework for reasoning under uncertainty. We describe its mathematical foundations and its features for probabilistic and statistical reasoning.

Chapter 2 and 3 are dedicated to the sea-level rise assessment. In chapter 2, we describe the physical processes controlling the elevation of the sea level, namely, the expansion of oceans and the melting of glaciers and the two main ice sheets. We describe in detail the origins of uncertainty in the future global warming and sea-level rise assessment and review the recent state of the art of the formalisms used to quantify the main uncertainties. We finally describe the most reliable and up-to-date sources of evidence on future sea-level rise and report their projections. Chapter 3 presents the belief functions-based methods used to provide qualitative

assessments of the sea-level projections at the end of the century and presents the results for the three most reliable sources of evidence.

Chapter 4 and 5 are dedicated to the coastal risks assessment in a context of changing climate. In chapter 4, we describe some indicators of coastal risk used in design and adaptation. Then, we present a hypothetical case-study on coastal hazards and risks under climate change uncertainty. This application illustrates the Dempster–Shafer based approach in representing uncertainty in two entities involved in the estimation of the risk indicators.

Part I

Belief functions theory: a framework for probabilistic and statistical reasoning

1 Reasoning under uncertainty

1.1 Introduction

Uncertainty, referring to the lack of certainty and sureness, is encountered everywhere. In our everyday life, we are rarely completely sure and often doubtful: about the outcomes of our actions and decisions, about what tomorrow will be made of, etc. In the scientific field, uncertainty is pervading and is inherent to every system and analysis in whatever area (economics, engineering, medicine, etc.). When the state of knowledge is limited, we still need to reason to derive conclusions and take decisions. In the last century, reasoning under uncertainty gained a lot of attention, with intensive research on the quantification of uncertainty and the psychology behind decision making under uncertainty [Kahneman 1982]. Uncertainty analyses, consisting of identifying uncertainties, quantifying, and integrating them in the decision process, are becoming the rule rather than the exception in many scientific fields.

In this work, we are concerned with the credal level of uncertainty, i.e., the identification and representation aspects, in opposition to the decision level. The objective is to provide some background on the uncertainty concept and describe some models to make probabilistic reasoning and statistical inference in the presence of uncertainty. In the first chapter, we give a brief survey of uncertainty meanings and classifications based on their sources and introduce the particular epistemic/aleatory dual classification. Then we discuss some uncertainty models. We begin with a discussion of probability – the classical model for addressing uncertainty. We briefly recall the different views used to interpret probabilities (frequentist and subjectivist) and emphasise the limitations of this model in handling in a natural way the epistemic uncertainty. The inappropriateness of this formalism for addressing all types of uncertainty has motivated the development of alternative frameworks, e.g., possibility, fuzzy sets, or belief functions theories. In the third part of this chapter, we focus on the last theory. We describe its mathematical foundations, note connections to alternative uncertainty frameworks and highlight its theoretical and practical advantages for (1) probabilistic reasoning (representing ambiguous information, combining evidence from different sources) and (2) statistical inference.

1.2 Taxonomies of uncertainty

Uncertainty is a multi-meanings term that encompasses a variety of concepts such as variability (randomness), ignorance, imprecision, conflict (disagreement between several sources), or ambiguity (inability to propose a definite interpretation). Uncertainty arises from different sources: it might originate from linguistic imprecision (what conclusion to draw from the judgment that an event is likely to occur), measurements inaccuracies (experimental error), insufficient information. Uncertainty might also arise from disagreement between sources of information (experts, for

instance) or from approximations in models (structural uncertainty), or natural variability, among other causes [Morgan 1990].

As the variety of meanings and sources of uncertainty might be confusing, it motivated the definition of some classification schemes. There are different criteria on which classification can be based, and accordingly, different typologies can be defined. These typologies are often defined specifically to scientific fields. Indeed, the classifications and associated definitions adopted in social sciences differ from those in systems engineering or those in physical sciences. A comprehensive survey of classifications and definitions from various fields can be found in works concerned with uncertainty [Morgan 1990, Krupnick 2006]. Examples of classification schemes in structural engineering and policy and risk analyses as reported in [Thunnissen 2003] are shown in Figures 1.1 and 1.2.

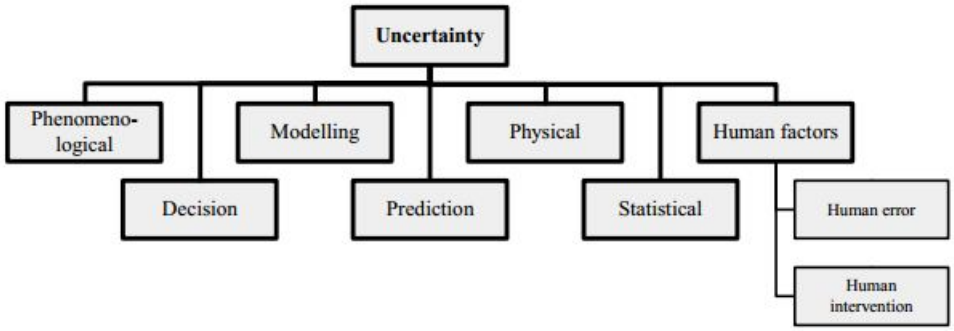

Figure 1.1: Uncertainty classification for structural engineering.

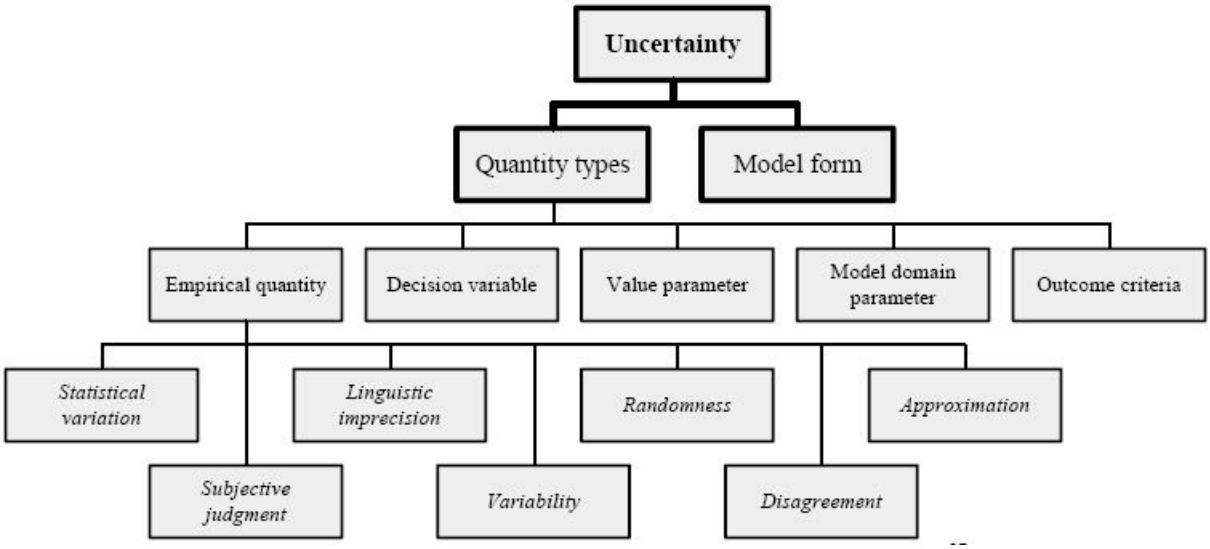

Figure 1.2: Uncertainty classification for policy and risk analyses.

One general method of categorisation that applies to all fields distinguishes un-

certainty due to randomness and natural variability of observations from uncertainty due to lack of information. In formal terms, the dual nature of uncertainty is described using the aleatory/epistemic terminology:

- Aleatory uncertainty: This type stems from the inherent variability of the system under consideration. It is also referred to as variability, stochastic uncertainty, or type A uncertainty. It is an inherent attribute of the system of interest and can not be reduced via increased knowledge.
- Epistemic uncertainty: This type reflects a state of limited knowledge of the system. Contrary to the aleatory uncertainty, epistemic uncertainty can be reduced as additional data or information are collected. An example of epistemic uncertainty is the rise in global temperature by 2100.

Once the uncertainties have been identified and categorized, the next step of an uncertainty analysis consists in their quantification. The common approach is based on the use of probabilities. However, this formalism has some weaknesses in handling certain dimensions of uncertainty, particularly the epistemic one. The probabilistic formalism, as well as the issues it may raise, are discussed in the following section.

1.3 Probabilistic modelling of uncertainty and its issues

Probability is the most common formalism for representing uncertainty. Conventionally, all uncertainties, regardless their source and type, are described using probabilities. If the tool is the same for both types (aleatory and epistemic), its interpretation differs.

There are two distinct views of probability: the classical frequentist view and the Bayesian view (also known as subjectivist or evidential). Within the classical view, probability is an objective state of the world defined as "*the value to which the long-run frequency converges as the number of trials increases*" [Morgan 1990]. By the way it is defined, frequentist probability is meaningful only in situations where the repetition of the process or experiment is possible (e.g., reliability analyses, etc.). In applications that involve non-repeatable processes, the frequentist interpretation does not apply and some uncertainty measures, such as the confidence interval (interval that includes, in the long run with data from many samples, the true value with a given high frequency), lose their relevance.

Bayesians [Laplace 1814, Savage 1954, de Finetti 1974] propose a different interpretation of probability. In the Bayesian perspective, probability quantifies personal belief defined based on one's state of knowledge. Bayesian probability can thus be defined in situations where no random process is involved. Contrary to the frequentist interpretation, evidential probability in not an objective state of the world, but a subjective entity that depends on individuals and on the context.

Frequentist probability can naturally describe aleatory uncertainty, but it fails in capturing epistemic one, particularly when the available evidence for the quantity of interest is poor. Consider the case where all we know about a certain variable

θ is that it lies between $\underline{\theta}$ and $\overline{\theta}$. Describing this state of knowledge using a probabilistic model requires assigning an exact degree of belief to every possible value within the possible interval (Bayesian dogma of precision). Eliciting such an accurate probability distribution solely from the evidence at hand involves inevitable arbitrariness. When the available evidence is too poor to justify a precise probability model, for instance in situations of complete ignorance, Bayesians resort to some selection principles such as Laplace's principle of insufficient reason [Savage 1954]. This principle, also known as indifference principle, suggests to describe the state of ignorance (when no information is available) by a precise model that assigns the same probability to all possible realizations of an uncertain variable. We illustrate this principle with a simple example. Two experts are asked to forecast the winner of a cycling race among three favorites (C_1, C_2, C_3). The first expert, who is quite familiar and experienced with this kind of races, claims, based on the observation of previous races, that the three of them seem to have the same performance. This implies that the favorites have the same probability of winning (the probability is $\frac{1}{3}$ for each). The second expert, who is rather specialized in (let's say) Formula1 races, claims having no idea about the outcome of this race. A Bayesian translates both opinions by a probabilistic model that assigns a probability (of winning) of $\frac{1}{3}$ for each of the favorites. Clearly, both experts do not provide the same information: the information provided by the first is much more precise than the second's, however, they are modeled alike.

The indifference principle is used when making Bayesian inference in situations where no prior evidence is available on the quantity of interest. Uniform priors, supposed to be uninformative, fail in capturing ignorance as they reveal additional precise information. They have been intensively discarded and several objections to their use have been reported in the literature, for instance in [Walley 1991].

The use of subjective probabilities in situations that involve deep epistemic uncertainty is constantly challenged. In a recent study, Millner et al. [Millner 2012] conducted an empirical experiment to attempt to answer the question *'Do probabilistic expert elicitations capture scientists' uncertainty about climate change?"*. In particular, the authors were interested in assessing whether the experts' knowledge of climate sensitivity – a key climate metric that characterises the equilibrium temperature change in response to a doubling of the radiative forcing – can be captured by subjective probabilities elicited from the experts' beliefs. By comparing the elicited subjective probabilities with choices over bets with uncertain outcomes, they detected ambiguity in the experts' beliefs. Due to this ambiguity, experts violate (probability) axioms that must be satisfied for subjective probabilities to adequately describe their knowledge. The empirical analysis leads to the conclusion that "by automatically presupposing the existence of subjective probabilities, the existing elicitation studies might qualitatively understate the extent of the experts' uncertainty relative to climate change". The authors recommended the use of alternative frameworks when eliciting climate expert beliefs about poorly known and unobservable climate variables.

Different formal mathematical theories have been proposed since the fifties to

cope with situations involving epistemic uncertainty. They include the interval analysis [Moore 1966], the fuzzy sets theory [Zadeh 1965], the possibility theory [Zadeh 1978, Dubois 1988], the imprecise probabilities [Walley 1991], the belief functions theory [Dempster 1967, Shafer 1976], etc. In the interval approach, uncertainty is described by an upper and lower bound, and no assumption is made on the likelihood of the elements within this interval (unknown probability). Zadeh [Zadeh 1965] extended the interval approach by quantifying the degree of belonging to a set through the concept of gradual membership of elements to sets. Dempster [Dempster 1967] and Shafer [Shafer 1976] proposed a model that assigns degrees of beliefs to sets and not to singletons, as is the case with probabilities.

The uncertainty framework proposed by Dempster and Shafer, referred to as Dempster–Shafer theory (DST) or the theory of belief functions is a promising alternative to the classical probabilistic theory. Indeed, belief functions have a great expressive power that makes them an adequate tool to handle very general forms of information. In addition to the credal level, they can be used to make decision based on limited information. Since the nineties, the theory has been applied in a variety of fields involving different dimensions of uncertainty, such as risk and reliability [Kay 2007, Inagaki 1991], classification [Bloch 1996, Denoeux 2001], expert systems [Shenoy 1992] and signal processing [Boston 2000], among others.

The remaining of this chapter is concerned with the description of the fundamental concepts of the belief functions theory. First, we describe the mathematical foundation and introduce the main definitions of the uncertainty measures. A second section provides a review of the information fusion techniques within DST, and several combination rules and their properties are presented. In the third section, we address the question of uncertainty propagation. The last part is concerned with the statistical inference problem with the description of two inference methods using belief functions. The chapter does not pretend to cover in a very comprehensive way all the aspects of the the belief functions theory. In particular, it does not address the decision level. It is rather expected to explain how the DS framework can (better) handle epistemic uncertainty (than probabilities), and provide a sufficiently detailed description of the main tools we will be using in the application part (chapters III and V).

2 Belief functions theory

In the middle of the 1960s, Arthur P. Dempster developed a theory based on upper and lower probabilities [Dempster 1966, Dempster 1967]. Dempster's theory was originally proposed as a tool to make statistical inference (this point will be discussed in detail in Section 3). One decade later, Shafer developed Dempster's theory and extended its scope to become a well-established theory of evidential reasoning in his reference book "*A Mathematical Theory of Evidence*" [Shafer 1976].

In the first section, we recall the mathematical fundamentals of evidence theory. We discuss the position of belief functions with respect to the classical theory of

uncertainty (the probability theory) and alternative uncertainty frameworks. An important aspect of this theory is the combination of evidence obtained from multiple sources and the modelling of conflict among them. In the second section, we describe the main aggregation modes as well as the requirements for their use. The third section of the chapter is concerned with the propagation of belief functions throughout a model. Finally, we address statistical inference and describe two approaches based on belief functions to make statistical inference. The content of this chapter is based on a recent paper by myself, T. Denoeux and N. Voyneau [Ben-Abdallah 2013].

2.1 Mathematical fundamentals of evidence theory: finite domain

Belief functions theory relaxes the assumptions of probability theory in situations in which the available information is too poor (ambiguous, conflicting, incomplete, etc.) to allow a precise assessment of an exact probability distribution (without making some arbitrary choices). In a finite and discrete space, belief functions can be viewed as a generalisation of classical probability theory. In this formalism, degrees of belief are assigned to sets (and not to exclusive singletons) by means of the *mass function*.

Mass function: Let θ be a variable that takes values in a finite domain Θ known as the *frame of discernment*. Uncertain evidence for θ may be represented by a *mass function* m defined as a mapping from the power-set of the discernment space into the unit interval $[0, 1]$:

$$m : 2^{\Theta} \rightarrow [0, 1]. \tag{1.1}$$

Function m, also known as the basic probability assignment (BPA), assigns an evidential weight to every subset $A \subseteq \Theta$ from the available evidence. The quantity $m(A)$ is interpreted as a measure of the *degree of belief* attached to the exact proposition $\theta \in A$ and to *no more specific propositions*, based on some evidence. Every set $A \subseteq \Theta$ such that $m(A) > 0$, i.e., there exists some evidence that supports the statement "$\theta \in A$", is referred to as a *focal element*. The pair $(\mathcal{F}, m)$, where $\mathcal{F}$ is the core and denotes the set of all focal elements of m, is referred to as a *body of evidence*. The function m fulfills $m(\emptyset) = 0$ and

$$\sum_{A \subseteq \Theta} m(A) = 1, \tag{1.2}$$

which describes a normalisation requirement.

A clear distinction must be made between a probability mass function and a mass function. The former is defined on Θ, whereas the latter is defined on the power set 2^{Θ}. In other words, a probability assigns a weight of evidence to every possible hypothesis (singleton), whereas the mass function allows a more coarse distribution of the total belief. In addition, m does not satisfy probability axioms such as

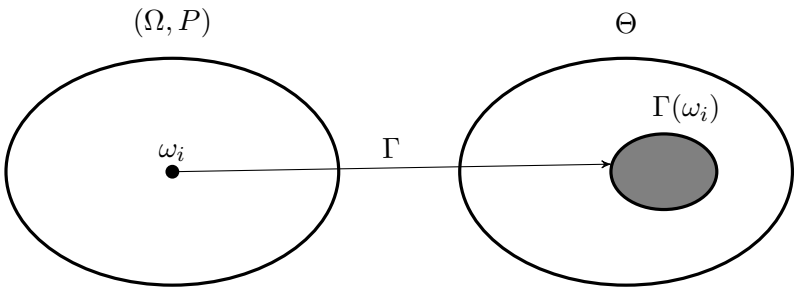

Figure 1.3: Random code setup.

monotonicity (i.e., $m(A) \leq m(B)$ if $A \subseteq B$) or additivity (i.e., $m(A) + m(A^c) = 1$, where A^c refers to the complement of A). However, if all of the focal elements are singletons, then the mass function is equivalent to a probability distribution and is referred to as a *Bayesian mass function*. Another special case is the *vacuous mass function* that assigns the unit degree of belief to the entire space of possibilities, i.e., $m(\Theta) = 1$. A mass function is said to be *consonant* if the focal elements A_i $(i = 1, ..., n)$ are nested (i.e., $A_1 \subseteq A_2 \subseteq ... \subseteq A_n$).

As argued by Shafer [Shafer 1976], the meaning of the degree of belief can be better understood by assuming that we have compared our evidence to a canonical chance set-up. The set-up proposed by Shafer consists of an encoded message and a set of codes $\Omega = \{\omega_1, \omega_2, ..., \omega_n\}$, exactly one of which is selected at random. We know the list of codes as well as the chance p_i of each code ω_i being selected. Decoding the encoded message using code ω_i produces a message of the form " $\theta \in A_i$" for some $A_i \subseteq \Theta$, as illustrated in Figure 1.3. Therefore

$$m(A) = \sum_{\{1 \leq i \leq n : A_i = A\}} p_i \tag{1.3}$$

is the chance that the original message was "$\theta \in A$". Stated differently, it is the probability of knowing that $\theta \in A$ and nothing more. In particular, in this setting, $m(\Theta)$ is the probability that the original message was vacuous, i.e., the probability of knowing nothing.

The above setting thus consists of a set Ω, a probability P on Ω and a multi-valued mapping $\Gamma : \Omega \to 2^\Theta \setminus \emptyset$ such that $A_i = \Gamma(\omega_i)$ for each $\omega_i \in \Omega$. This is the framework initially considered by Dempster in [Dempster 1966]. The triple (Ω, P, Γ) is known as a *source* and formally defines a finite *random set* [Nguyen 2006]: mass functions are thus exactly equivalent to random sets from a mathematical point of view. However, the meaning of mass functions differs from the usual interpretation of a random set as the chance of a random experiment. Hence, $m(A)$ is not the chance that A was selected, but it can be viewed as the chance of the evidence that θ is in A [Shafer 1981]. As discussed later, the concept of a random interval is more general than that of a belief function. Indeed, a source can be used in the infinite case to generate belief functions even if a mass function does not exist.

Belief and plausibility DST defines two measures of uncertainty: belief and plausibility. Given the frame of discernment Θ and a body of empirical evidence $(A_i, m(A_i))$ $(i = 1, ..., n)$, we can quantify the uncertainty of the proposition $A \subseteq \Theta$ using upper and lower probabilities, defined, respectively, by:

$$Bel(A) = P(\{\omega \in \Omega | \Gamma(\omega) \subseteq A\}) = \sum_{B \subseteq A} m(B), \tag{1.4}$$

and

$$Pl(A) = P(\{\omega \in \Omega | \Gamma(\omega) \cap A \neq \emptyset\}) = \sum_{B \cap A \neq \emptyset} m(B). \tag{1.5}$$

The belief quantity $Bel(A)$ is interpreted as the degree to which the evidence supports the claim "$\theta \in A$", whereas $Pl(A)$ can be interpreted as the maximum amount of specific support that could be given to the same claim, or in other words, the degree to which the evidence does not contradict that claim.

Functions m and Bel are equivalent representations of a body of evidence and can be recovered from each other by the so-called *Mobius transformation* [Shafer 1976]:

$$m(A) = \sum_{B \subseteq A} (-1)^{|A-B|} Bel(B). \tag{1.6}$$

Bel and Pl are mutually dual in the sense that one of them can be uniquely determined from the other using the relation $Pl(A) = 1 - Bel(A^c)$ for all $A \subseteq \theta$. The function pl defined on the space of discernment Θ to the unit interval $[0, 1]$ by:

$$pl(\theta) = Pl(\{\theta\}). \tag{1.7}$$

is called the *contour plausibility function* associated to m.

The following inequality always hold: $Bel(A) \leq Pl(A)$, for all $A \subseteq \Theta$. Belief functions are sub-additive probabilities that satisfy the following conditions [Shafer 1976]:

- Boundary conditions: $Bel(\emptyset) = 0$ and $Bel(\Theta) = 1$.
- Monotonicity: For every A, $B \subseteq \Theta$, if $A \subseteq B$, then $Bel(A) \leq Bel(B)$.
- Infinite order (complete) monotonicity: for any $k \geq 2$ and any sequence $A_1, ..., A_k$ of subsets of Θ

$$Bel\left(\bigcup_{i=1}^{k} A_i\right) \geq \sum_{\emptyset \neq I \subseteq \{1,...,k\}} (-1)^{|I|+1} Bel\left(\bigcap_{i \in I} A_i\right), \tag{1.8}$$

where $|I|$ denotes the cardinality of the set I. Using the dual identity between belief and plausibility (i.e., $Pl(A) = 1 - Bel(A^c)$, for any $A \subseteq \Theta$), it can be shown that the plausibility function satisfies the following property:

$$Pl\left(\bigcap_{i=1}^{k} A_i\right) \leq \sum_{\emptyset \neq I \subseteq \{1,...,k\}} (-1)^{|I|+1} Pl\left(\bigcup_{i \in I} A_i\right). \tag{1.9}$$

If the mass is Bayesian, then the Bel and Pl functions are equal and are a probability measure, i.e.,

$$Bel(A) = Pl(A) = P(A) \tag{1.10}$$

for any $A \subseteq \Theta$. In this case, the contour plausibility pl corresponds to the probability mass function. If the mass function is consonant, the plausibility function is a possibility measure [Zadeh 1978, Dubois 1988] (section 2.2 provides a brief description of the possibility theory) with possibility distribution $pl = \pi$, i.e., the plausibility function can be recovered from the contour function as follows:

$$Pl(A) = \sup_{\theta \in A} \pi(\theta). \tag{1.11}$$

As it allows degrees of belief to be assigned to sets rather than to singletons, DST allows to cope naturally with partial information. In particular, it captures extreme scenarios of partial knowledge that correspond to perfect knowledge and total ignorance. Total ignorance is described by a vacuous mass function, whereas perfect knowledge is described by a Bayesian mass.

Returning to the example proposed in the introduction, belief functions allow to distinguish between both expert's assessments as they can be modeled using different belief functions: the first expert's evidence is modeled with a Bayesian belief function $(\mathcal{F}_1, m_1) = \{(\{C_1\}, \frac{1}{3}); (\{C_2\}, \frac{1}{3}); (\{C_3\}, \frac{1}{3})\}$, whereas the second's is faithfully described by a vacuous mass function that naturally reflects ignorance: $(\mathcal{F}_2, m_2) = \{(\{(C_1, C_2, C_3)\}, 1)\}$.

2.2 Belief functions in infinite spaces: random intervals

The definition of belief functions and random sets in infinite spaces implies greater mathematical sophistication than it does in finite spaces [Shafer 1979, Nguyen 2006]. In this work, we restrict our discussion to random closed intervals on the real line (see e.g., [Dempster 1968b, Smets 2005, Denoeux 2009]), which constitutes a simple yet sufficiently general framework for expressing beliefs on a real variable.

Let $(\Omega, \mathcal{A}, P)$ be a probability space and $(U, V) : \Omega \to \mathbb{R}^2$ a two-dimensional real random vector such that $P(\omega \in \Omega | U(\omega) \leq V(\omega)) = 1$. Let Γ be a mapping that maps each $\omega \in \Omega$ to the closed interval $[U(\omega), V(\omega)]$. This setting defines a random interval, as well as the belief and plausibility functions on $\mathbb{R}$, respectively, by

$$Bel(A) = P(\{\omega \in \Omega | [U(\omega), V(\omega)] \subseteq A\}) \tag{1.12}$$

and

$$Pl(A) = P(\{\omega \in \Omega | [U(\omega), V(\omega)] \cap A \neq \emptyset\}), \tag{1.13}$$

for all elements A of the Borel sigma-algebra $\mathcal{B}(\mathbb{R})$ on the real line [Dempster 1968b]. The intervals $[U(\omega), V(\omega)]$ are referred to as the focal elements of $[U, V]$. We note that if U and V are continuous, the notion of the mass function should be replaced

by that of a mass density function defined by $m([u,v]) = p(u,v)$ where $p(u,v)$ denotes the joint probability density function (*pdf*) of (U,V).

Plausibility and belief yield upper and lower cumulative distribution functions, respectively, by:

$$\overline{F}(x) = Pl((-\infty, x]) \tag{1.14}$$

and

$$\underline{F}(x) = Bel((-\infty, x]), \tag{1.15}$$

for all $x \in \mathbb{R}$.

2.3 Connection with alternative uncertainty frameworks

- **Connection with possibility theory**

An alternative framework for uncertainty quantification is *possibility theory* [Zadeh 1978, Dubois 1988]. This theory represents the state of knowledge using a *possibility distribution* π (an upper semi-continuous mapping from the parameter space Θ to the unit interval) that measures the degree of possibility that the true value is θ. If $\pi(\theta) = 0$ for a given $\theta \in \Theta$, the state θ is considered impossible, whereas modal values (i.e., values such that $\pi(\theta) = 1$) are completely possible. Perfect knowledge is captured by a possibility function that satisfies: $\pi(\theta_0) = 1$ for some θ_0 and $\pi(\theta) = 0$ for all the other states. Complete ignorance is captured by a vacuous possibility function that assigns a level of possibility 1 to all values in Θ (i.e., $\pi(\theta) = 1$ for all θ in Θ) [Dubois 1988].

Possibility theory provides two evaluations of the likelihood of an event: the possibility (denoted Π) and the necessity (denoted N). They are defined as follows:

$$\Pi(A) = \sup_{x \in A} \pi(x) \tag{1.16}$$

and

$$N(A) = 1 - \Pi(A^c). \tag{1.17}$$

The possibility measure satisfies the *maxitivity* axiom:

$$\Pi(A \cup B) = \max(\Pi(A), \Pi(B)) \quad \forall A, B \subseteq \Theta. \tag{1.18}$$

Possibility distributions can be interpreted as particular random sets that correspond to random sets whose focal elements are nested. In particular, a continuous and unimodal possibility distribution on the real line ($\Theta = \mathbb{R}$) can be defined by the Lebesgue probability measure P on the unit interval ($\Omega = [0,1]$) and a multi-valued mapping Γ from the unit interval to $\mathbb{R}$, defining a family of nested intervals [Dubois 1987]. The multi-valued mapping assigns to each $\omega \in [0,1]$ the set defined by:

$$\Gamma(\omega) = \{x \in \mathbb{R} | \pi(x) \geq \omega\}. \tag{1.19}$$

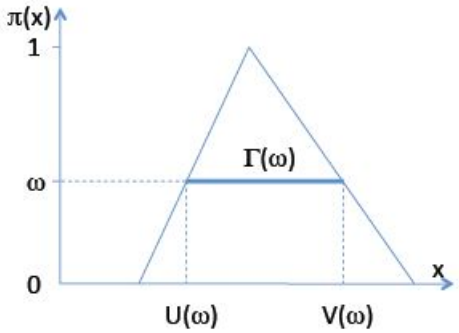

Figure 1.4: Random closed interval induced by a possibility distribution.

The quantity $\Gamma(\omega)$ is a closed interval $[U(\omega), V(\omega)]$ known as the ω-level cut of π (see Figure 1.4). Given P, the Lebesgue measure on Ω, $[U, V]$ is a random closed interval, and π is the contour function, i.e., $pl(x) = \pi(x)$ for all $x \in \mathbb{R}$. Such a random interval is consonant because its focal intervals $\Gamma(\omega)$ are nested. Indeed, if $\omega_1 > \omega_2$, then $\Gamma(\omega_1) \subseteq \Gamma(\omega_2)$. The intervals $\Gamma(1)$ and $\{x \in \mathbb{R} | \pi(x) > 0\}$ are referred to, respectively as, the core and the support of π.

- **Connection with p-boxes**

Let P be a probability measure on the real line $\mathbb{R}$. Its cumulative distribution F is a nondecreasing mapping from $\mathbb{R}$ to $[0, 1]$ such that for any $x \in \mathbb{R}$, $F(x) = P(]-\infty, x])$. A p-box [Ferson 2003, Destercke 2008b] is defined as a pair of cumulative distributions $[\underline{F}, \overline{F}]$ such that:

1. $\underline{F}$ is non-decreasing and right-continuous;
2. $\overline{F}$ is non-decreasing and left-continuous;
3. $\underline{F} \leq \overline{F}$.

Consider the p-box $[\underline{F}, \overline{F}]$ and the pseudo-inverses of $\underline{F}$ and $\overline{F}$ defined, respectively, as:

$$\underline{F}^{-1}(\omega) = \inf \{x \in \mathbb{R} | \underline{F}(x) \geq \omega\},$$
$$\overline{F}^{-1}(\omega) = \inf \left\{x \in \mathbb{R} | \overline{F}(x) \geq \omega\right\}$$

for each $\omega \in \Omega = [0, 1]$. The mapping Γ from $[0, 1]$ to the set of real intervals such that:

$$\begin{aligned}\Gamma(\omega) &= [\overline{F}^{-1}(\omega), \underline{F}^{-1}(\omega)] \\ &= [U(\omega), V(\omega)]\end{aligned}$$

is a closed interval (see Figure 1.5).

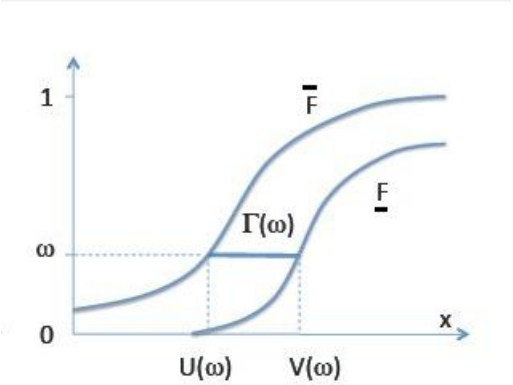

Figure 1.5: Random closed interval induced by a p-box.

2.4 Combining evidence from different sources

Often, evidence is provided by different sources. For instance, expert elicitation involves more than one expert. Once the assessment step has been performed, the evidence issued from various knowledge sources (e.g., expert judgments) need be combined to yield an overall assessment that reflects the global opinion.

The combination of evidence from different sources has been intensively addressed in the probabilistic framework [**?**]. The linear opinion pool, which weights the individual probabilistic assessments and combines them linearly, is the most used combination method .

An important feature of the belief functions framework is that it provides a wide variety of combination rules (compared to probabilities) that allow to address specific fusion problems by taking into account the reliability of the sources, their dependences, the conflict among them, etc. In particular, the *conjunctive* mode, based on the transfer of beliefs to the intersections of focal elements of individual masses, is used in situations where all sources of evidence are reliable.The most used conjunctive rule in DST is the Dempster's rule. In situations where there is at least one reliable source (with no information on which one it is). The *disjunctive*, based on the transfer of beliefs to the unions of the focal elements of elemental masses, is more appropriate. This combination mode is often very conservative and does not lead to informative results. The most commonly used disjunctive rule is a disjunctive version of Dempster's rule proposed by Dubois and Prade [Dubois 1986, Dubois 1992].

In situations where none of these extreme scenarios on the reliability of the sources holds, alternative pooling modes need to be used. A large body of literature on evidence combination in DST has been developed since the seventies by authors such as [Smets 1993, Murphy 2000, Zhang 1994, Yager 1978, Denoeux 2008]. A comprehensive survey of the existing aggregation techniques can be found in [Sentz 2002]. In the following, we describe three pooling modes: the fundamental *Dempster's* rule, the weighted-average combination and the discount and combine

rule.

2.4.1 Dempster's rule of combination

Dempster's rule of combination plays a central role in DST and is the basic mechanism for combining evidence and updating probabilities. According to Shafer [Shafer 1981] "Dempster's rule of combination is the most important single tool of the theory". Dempster's rule can be naturally derived using the random code metaphor described previously as follows. Let m_1 and m_2 be two mass functions induced by triples $(\Omega_1, P_1, \Gamma_1)$ and $(\Omega_2, P_2, \Gamma_2)$ interpreted under the random code framework as before. Let us further assume that the codes are selected independently. For any two codes $\omega_1 \in \Omega_1$ and $\omega_2 \in \Omega_2$, the probability that they both are selected is $P_1(\{\omega_1\})P_2(\{\omega_2\})$, in which case we can conclude that $\theta \in \Gamma_1(\omega_1) \cap \Gamma_2(\omega_2)$. If $\Gamma_1(\omega_1) \cap \Gamma_2(\omega_2) = \emptyset$, we know that the pair of codes (ω_1, ω_2) could not have been selected: consequently, the joint probability distribution on $\Omega_1 \times \Omega_2$ must be conditioned, eliminating such pairs [Shafer 1981]. This line of reasoning yields the following combination rule, which is referred to as Dempster's rule [Shafer 1976] and denoted $\oplus$:

$$m_1 \oplus m_2(C) = \begin{cases} \sum\limits_{A \cap B = C} \frac{m_1(A)m_2(B)}{1-K} & \text{if } C \neq \emptyset \\ 0 & \text{if } C = \emptyset, \end{cases} \tag{1.20}$$

where:

$$K = \sum_{A \cap B = \emptyset} m_1(A)m_2(B). \tag{1.21}$$

The number K is a measure of the inconsistency between the two sources and is known as the *degree of conflict*. If $K = 1$, a logical contradiction exists between the two pieces of evidence and they can not be combined. The commutativity and associativity of the rule allow the modeler to combine the evidence from different sources. The vacuous mass function is a neutral element for $\oplus$.

Note that Bayes theorem can be shown to be a particular case of Dempster's rule of combination. Indeed, when a Bayesian prior is available and is combined with the belief function encoding the evidence, the result coincides with the Bayesian posterior calculated with Bayes' rule (the rule is recalled in the Appendices, Section 1.2).

Dempster's rule emphasises the agreement between the different sources of evidence by transferring evidence to the intersection of focal elements. It ignores the conflicting evidence as it normalises the mass of resultant focal elements by the factor $(1 - K)$ to ensure that we remain in the closed world (i.e., $m(\emptyset) = 0$). For the rule to be used, the sources of evidence need to be (1) independent and (2) reliable (i.e., that their estimates overlap). When these two preconditions are not met, Dempster's rule generates inconsistent results. Counter-intuitive examples were reported mainly by Zadeh [Zadeh 1979, Zadeh 1986]. Zadeh's main example is

a story of doctors and diagnosis: *"A patient consults two doctors $D1$ and $D2$ about a disease. They give him the following diagnosis: $D1$ believes the patient has either a meningitis, with a probability of* 0.99*, or concussion, with a probability of only* 0.01*. $D2$ believes the patient has a brain tumor, with a probability of* 0.99*, or concussion, with a probability of* 0.01*."* Encoding these statements and applying Dempster's rule leads to $m(concussion) = 1$. Dempster's rule of combination yields an unexpected result because it implies a total support for the diagnosis considered as unlikely by both doctors.

To overcome the counter-intuitive results that Dempster's rule can lead to, many authors proposed modified versions of this rule [Yager 1978, Zhang 1994]. In Smets's terms [Smets 2007], there is currently a " jungle" of combination rules developed to deal with conflicting evidence. Each of these versions proposes a different way to define and distribute the conflict in the combination [Sentz 2002, Smets 2007].

Using Dempster's rule to aggregate evidence requires all sources to be equally reliable. However, in many applications, all of the sources may not have the same reliability or importance. Alternative combination modes based on *discounting* make it possible to cope with different reliabilities and ensure a rational combination result.

2.4.2 Discounting rule

It is important to account for the reliability of the different sources of evidence in the aggregation process. If a source of evidence is unreliable, its contribution in the resultant mass should be penalised because it is of limited relevance. Within the belief functions theory, discounting [Shafer 1976] allows to weaken the information of an unreliable source and to reduce its impact in the combined assessment. Discounting consists in weakening a mass function by multiplying it by a discounting factor $\alpha \in [0, 1]$ and transferring the lost mass to the universe Θ as follows:

$$m^{\alpha}(A) = \begin{cases} (1-\alpha)m(A) & \text{if } A \subset \Theta, \\ \\ (1-\alpha)m(\Theta) + \alpha & \text{if } A = \Theta. \end{cases} \tag{1.22}$$

In equation (1.22), α is the discount rate and $1-\alpha$ is the coefficient of reliability. If the source is entirely reliable, $\alpha = 0$, whereas if the source is unreliable, $\alpha = 1$. Discounting can alternatively be applied to the plausibility function [Zeng 2007]. In that case, the plausibility is discounted with a power rather than with a coefficient as in the original discounting.

The estimation of the reliability of a source (and thus its discounting rate) in the aggregation process is a major step. It may happen to the modeller to have an à priori knowledge of the reliability of the source (collected from expert assessment, literature, etc.). In such situations, he can directly use this information in the discounting process. If there is no meta-knowledge of the reliability, the modeler can make some learning through different techniques, exclusively developed in multi-sensor data fusion applications. These techniques include (1) contextual

discounting [Mercier 2005, Mercier 2008] (the method considers that the reliability of a source depends on the context and quantifies the reliability conditionally on hypotheses on the values of the parameter of interest), (2) optimisation-based discounting [Elouedi 2004] (Elouedi defines the discounting factor as the value that minimises the discrepancy between observations –the pignistic probability– and sensor outputs), and (3) (dis)agreement-based discounting [Martin 2008, Ramon 1991], etc.

The disagreement-based discount relies on the principle of majority [Yang 2013]. According to this principle, an intuitive measure of reliability on a given set of sources can be the dissimilarity among them. In other words, if a body of evidence is supported by the others, it should be considered as reliable. In contrast, if a body of evidence highly disagrees with the others, it can be treated as an "outlier" and should have smaller weight in the overall combination result. The distance between two bodies of evidence is an intuitive measure used to determine the degree of dissimilarity. Different distances have been proposed in the literature in many applications, e.g., the Euclidean, betting commitment, plausibility-based and *Jousselme*'s [Jousselme 2001] distances. A comprehensive survey of the existing research related to distances in evidence theory was reported by Jousselme [Jousselme 2012].

Jousselme's distance is the first based on a geometric interpretation of the evidence and contains convenient distance properties. It is among the most commonly used distances [Denoeux 2008, Martin 2008]. It is defined, in the finite case, for two bodies of evidence $(\mathcal{F}_1, m_1) \times (\mathcal{F}_2, m_2)$ by:

$$d_J(m_1, m_2) = \sqrt{(\boldsymbol{m_1} - \boldsymbol{m_2})^t D(\boldsymbol{m_1} - \boldsymbol{m_2})}, \tag{1.23}$$

where $\boldsymbol{m_1}$ and $\boldsymbol{m_2}$ are $2^{|\Theta|}$-dimensional vectors of the basic belief masses corresponding to m_1 and m_2. D is a square matrix of size $2^{|\Theta|}$ known as the *Jaccard's matrix*, and its elements represent the similarity between focal elements (A, B) in $\mathcal{F}_1 \times \mathcal{F}_2$:

$$D(A,B) = \begin{cases} 1 \text{ if } A = B = \emptyset \\ \\ \frac{|A \cap B|}{|A \cup B|} \text{ otherwise.} \end{cases} \tag{1.24}$$

According to this distance, the farther m_1 and m_2 are from each other, the more disagreement exists between the two bodies of evidence. It should be noted at this point that disagreement is a notion different from conflict; the latter refers exclusively to the mass of the empty set as defined in *Dempster's* rule. Different methods exist for assigning a global weight of dissimilarity to a given expert i in a set of experts $E = \{1, 2..., n\}$. For instance:

$$Diss(m_i) = \frac{1}{n-1} \sum_{\substack{j=1...n \\ j \neq i}} d_J(m_i, m_j), \tag{1.25}$$

or

$$Diss(m_i) = d_J(m_i, m_{n-i}), \tag{1.26}$$

where m_{n-i} is the resultant mass from the combination (in term of average or DS rule) of all masses in E except for i. Yang [Yang 2013] proposed the difference between the scatter of the set of all original bodies of evidence (i.e., the average distance between any body of evidence in the ensemble and the center of the ensemble) and the scatter of the bodies of evidence after the expert i is removed from the original ensemble as a distance-based degree of disagreement (or dissimilarity). If expert i shows a high (low) dissimilarity from the average, s/he is considered as unreliable (reliable). Any decreasing function of the dissimilarity into $[0, 1]$ could thus provide an indicator of the relative reliability $(1 - \alpha_i)$. For instance, Martin [Martin 2008] proposed:

$$1 - \alpha_i = 1 - Diss(m_i). \tag{1.27}$$

Alternative approaches to discounting pieces of evidence based on new approaches of conflict management have been proposed in recent literature. Klein [Klein 2010] and Shubert [Schubert 2011] investigated sequential discounting, which is performed in a sequence of incremental steps with the conflict (or falsity by Shubert [Shubert 1996]) or the dissimilarity (by Klein [Klein 2010]) updated at each step until a predefined acceptable level is reached.

2.4.3 Averaging rule

The averaging mode is an extension of the probabilistic linear opinion pool. It's a two stage process that assigns first a degree of importance c_i $(i = 1...n)$ to each of the n estimates supplied by n experts, then averages the weighted masses $m_{1,...,}m_n$:

$$m(A) = \sum_{i=1}^{n} \frac{c_i}{\sum\limits_{k=1...n} c_k} m_i(A) \tag{1.28}$$

for all $A \subseteq \Theta$.

The major difficulty of this method is related to the way weights are defined and calculated. When the modeller has no information on the weight of the different experts, the common approach is to use some default weighting scheme that assigns equal weights to all of them (averaging method proposed by Murphy [Murphy 2000]). Alternatively, weights can be derived from expert credentials (literature, etc.). In this case, the averaging rule is known as Trade-off rule [Sandri 1995]. An alternative method to weighting experts is empirically using performance assessment in a manner similar to that described by Cooke in the theory of weights [Cooke 1988]. In the following, we briefly recall some key elements of the original theory of weights developed by Cooke and describe how this paradigm can be extended to the belief functions theory.

In Cooke's model, experts are first solicited to give their estimates of the values of a range of quantiles for a set of calibration (seed) variables. A calibration set is a collection of judgments of uncertainty on some (seed) variables (drawn from the context of the elicitation) the actual values of which are already known to the analyst. From the answers, the performance of every expert can be quantified with

a quality score. Cooke developed a definition of the performance of an expert which is related to his accuracy and informativeness. An expert is accurate if his probabilistic assessment is close to the real distribution of the (seed) variable. Accuracy is measured statistically by a calibration index (CI) that corresponds to the "probability that the deviation between the expert's proposed probability and the empirical probability derived from observations of seed variables might have arisen by chance" [Aspinall 2008]. Informativeness, the second scoring criterion, measures the degree to which the expert's uncertainty distribution is concentrated relative to a completely uninformed distribution (commonly the uniform measure is used). Cooke defines the performance of an expert as the product of both calibration and information scores. The weight assigned to the expert in the pooling step is proportional to his/her performance score.

Analogous scoring indexes can be estimated if expert's assessment is described in alternative uncertainty schemes, such as the possibility theory or DST [Sandri 1995, Destercke 2008a].

Let x be a seed variable whose true value x^* is known. An expert e is asked to supply his/her knowledge of x on the support $[\underline{x}, \overline{x}]$. The analyst represents this information with a body of evidence $(\mathcal{F}, m)$. The accuracy of the expert e on the variable x, denoted $CI(e, x)$, can be assessed by:

$$CI(x, e) = pl(x^*). \tag{1.29}$$

The greater the plausibility of the true value assigned by the expert, the more accurate s/he is. Indeed, if $pl(x^*) = 1$, i.e., there is a total confidence that x^* is the right value, the expert can be considered as totally accurate with respect to x. However, if $pl(x^*) = 0$, the expert totally misses x^* and s/he is completely inaccurate in that sense. The second aspect experts are rated on is the precision. In DST, an intuitive measure of the imprecision is based on the aggregation of the widths of all focal elements in $\mathcal{F}$:

$$PI(x, e) = \sum_{A \in \mathcal{F}} m(A)|A|, \tag{1.30}$$

where the width of an interval $A = [a, b]$ is $|b - a|$. The specificity can be derived by:

$$Sp(x, e) = 1 - \frac{PI(x, e)}{\sup(PI(x, e))}. \tag{1.31}$$

The background measure used to calculate $\sup(PI(x, e))$ is the vacuous mass function associated with the support, i.e., $m([\underline{x}, \overline{x}]) = 1$. For an expert to have good performance, s/he must fulfill both accuracy and precision criteria. His/her score is therefore:

$$Q(x, e) = Sp(x, e) \times CI(x, e). \tag{1.32}$$

To derive a global performance score of a source e, the evaluation requires a high number of seed variables x_j $(j = 1...J)$. The global score is therefore:

$$Q(e) = \frac{1}{J} \sum_{j} Q(x_j, e), \tag{1.33}$$

and is used to weight the expert e in formula (1.28).

The discounting approach can be combined with the averaging mode and the reliability factor assessed by different discounting methods can also be used as the weight of the expert in the averaging formula (1.28).

2.5 Propagation of belief functions

2.5.1 The extension principle

Together with the quantification and combination aspects, propagation of uncertainties throughout a model is a major step within a comprehensive uncertainty analysis.

Let f be a function from the Cartesian product $\times_{i=1}^{n} X^i$ of inputs spaces X^i to the output space Y. We are interested in propagating the uncertainty bearing on the inputs $X_i (i = 1, ..., n)$ and calculating the system response Y. Suppose that the n parameters are independent. In the probability theory, the joint probability distribution of n random variables $(X_1, ..., X_n)$ is calculated, under the independence assumption, as the product of the marginal distributions:

$$P(x_1, x_2, ...x_n) = P_1(x_1)...P_n(x_n). \tag{1.34}$$

where P_i is the marginal probability distribution of variable X_i. Suppose now that each parameter is described by a body of evidence $(\mathcal{F}^i, m^i)$ on the space X^i $(i = 1, ...n)$, with $\mathcal{F}^i = (A_1^i, ..., A_{L_i}^i)$ (i.e., variable X_i has L_i focal elements). We denote the joint random set of the inputs $(\mathcal{F}, m)$. $\mathcal{F}$ is the Cartesian product of $\mathcal{F}^i$ $(i = 1, ..., n)$, i.e., $\mathcal{F} = \mathcal{F}^1 \times ... \times \mathcal{F}^n$, or more explicitly

$$\mathcal{F} = \left\{ A = A_s^1 \times A_u^i ... \times A_v^n \right\} \tag{1.35}$$

for all combinations of $s, u, ..., v$ in $[1, L_1] \times [1, L_2] \times ... \times [1, L_n]$. The joint basic probability assignment is defined for every element $A = A_s^1 \times A_u^i ... \times A_v^n \in \mathcal{F}$ as:

$$m(A) = m^1(A_s^1) \times m^2(A_u^2) \times ...m^n(A_v^n). \tag{1.36}$$

The resulting joint random set $(\mathcal{F}, m)$ is referred to as a *stochastically decomposable random Cartesian product* [Dubois 1991].

The extension principle [Yager 1986] is used to propagate the joint random set $(\mathcal{F}, m)$ through f. The principle yields a random set $(\mathcal{F}', M)$ that constrains Y, defined as follows:

$$\mathcal{F}' = \{B = f(A); A \in \mathcal{F}\} \tag{1.37}$$

and

$$M(B) = \sum_{A \in \mathcal{F} | f(A) = B} m(A). \tag{1.38}$$

The construction of $\mathcal{F}'$ consists of mapping every joint focal element $A \in \mathcal{F}$ into $f(A)$. If sets A are Cartesian products of closed intervals defined on the real line,

computing $f(A)$ requires the resolution of two optimisation problems:

$$f(A) = [l, u], \tag{1.39}$$

where

$$l = \min_{x \in A} f(x) \tag{1.40}$$

and

$$u = \max_{x \in A} f(x). \tag{1.41}$$

Different optimisation algorithms can be used to resolve the system of equations. These algorithms may involve more or less complex calculations, depending on the properties of f (monotonicity, dimension, continuity, etc.). When function f is monotonous, the resolution can be performed easily using the vertex method [Dong 1987]. This method calculates the interval response simply by identifying the minimum and maximum values among all the vertices (i.e., the upper and lower bounds) of the joint focal elements A.

Here is an example that illustrates the use of the extension principle. Suppose that two uncertain numbers X and Y are described, respectively, by the DS structures $(\mathcal{F}^X, m^X) = \{([1,2], 0.3), ([2,4], 0.7)\}$ and $(\mathcal{F}^Y, m^Y) = \{([0,1], 0.2), ([0,4], 0.3), ([1,2], 0.5)\}$. Suppose that X and Y are independent and we are interested in estimating the DS structure of the sum of the variables $Z = f(X,Y) = X + Y$. Results are reported in the following table where the focal elements of X, respectively of Y, and their associated masses (in bold) are arrayed in the leftmost column, respectively in the top row.

X \ Y	$[0,1]$ **0.2**	$[0,4]$ **0.3**	$[1,2]$ **0.5**
$[1,2]$ **0.3**	$[1,3]$ **0.06**	$[1,6]$ **0.09**	$[2,4]$ **0.15**
$[2,4]$ **0.7**	$[2,5]$ **0.14**	$[2,8]$ **0.21**	$[3,6]$ **0.35**

Table 1.1: Cartesian product of X and Y.

Variables X and Y have, respectively, 2 and 3 focal elements. The output Z has $2 \times 3 = 6$ focal elements obtained by summing all the combinations of the marginal focal elements. Since the addition operator is strictly increasing, the focal elements on Z can be calculated using the vertex method. For instance, the image of the joint focal element $A = A_1^X \times A_1^Y = [1,2] \times [0,1]$ is simply:

$$f(A) = [f(\min(A_1^X), \min(A_1^Y)), f(\max(A_1^X), \max(A_1^Y))] = [1+0, 2+1] = [1,3]. \tag{1.42}$$

The mass of the focal element A is:

$$m(A) = m^X(A_1^X) \times m^Y(A_1^X) = 0.3 \times 0.2 = 0.06. \tag{1.43}$$

2.5.2 Monte Carlo approximation

Monte Carlo simulation is a method used to estimate the statistical properties of a random variable that is related via a model to a number of random variables. The method is useful when direct calculations of probability functions of the model input are impossible to derive from the available data. The values of the random input parameters are first generated according to their probability distribution and the sampled values are propagated through the model. This operation is repeated until sufficient realisations of the output are generated to derive its pdf.

Monte Carlo approximation can be extended to the case in which the variables are constrained by random sets and not by probability densities. For situations in which the exact expression of the DS structure is difficult to derive or the computational cost required by the the extension principle is too high (e.g., in infinite domains, complex functions, etc.), the MC method turns out to be an interesting alternative as it is computationally more tractable. When the variables are defined on the real line, the MC procedure consists in:

1. Sampling an interval $[U(\omega), V(\omega)]$ (called an ω-cut, with $\omega \in [0, 1]$) in every random interval on each of the input variables.

2. Applying interval arithmetic and optimisation methods on the random intervals sampled in step 1 to estimate the model output.

Operations (1) and (2) are repeated N times. The DS measures on the model output can be approximated via equations:

$$Bel(A) = P(\{\omega \in \Omega | [U(\omega), V(\omega)] \subseteq A\}) \tag{1.44}$$

and

$$Pl(A) = P(\{\omega \in \Omega | [U(\omega), V(\omega)] \cap A \neq \emptyset\}). \tag{1.45}$$

The Cartesian product, as well as the MC approximation require independence among the input variables. When the independence does not hold, i.e., when there is partial or unknown dependence among the inputs, calculating the resultant focal elements raises further difficulties. Different methods have been proposed in the literature for reliable propagation of uncertainty through calculations involving arithmetic operations including the Distribution Envelope Determination (DEnv) [Berleant 1998], the dependency bounds convolution [Williamson 1990] and interval probabilities [Walley 1991]. Regan [Regan 2004] showed that although each of the cited methods were constructed from different types of applications and purposes, they converge to equivalent methods for positive real valued variables and are equivalent to Yager's method if the independence assumption is satisfied. A comprehensive survey of the techniques used in accounting for dependence in DST can be found in Ferson's report [Ferson 2004] dedicated to the issue of dependence in the different evidence frameworks. The report provides simple and methodological examples on the use of the different methods.

Throughout this chapter, we noted out the great potential of belief functions for probabilistic reasoning, but the question remains as to their application in statistical inference.

3 Statistical inference

3.1 Background

Statistical inference denotes the process of drawing conclusions about a population based on an observed sample data. In the statistical mainstream, Bayesian and frequentist perspectives are the most common. Both paradigms encounter, however, fundamental objections. Frequentist perspective is criticised because it violates the prominent conditionality principle (see Appendices, section 1.3). The hypothetical repeated sampling principle on which the inference relies leads to counter intuitive results in situations in which the experiment does not lend itself to repetition (an example that illustrates such inconsistency was given by Pratt [Pratt 1965] and is reported in the Appendices, Section 1.1). A more complete discussion on the limitations of the frequentist perspective can be found in [Wagenmakers , Chapter 9].

Bayesian inference (Section 1.2 in the Appendices) addresses some weaknesses of the frequentist approach, in particular, it does condition on data at hand. However it encounters a fundamental objection that concerns the arbitrariness in the specification of the prior [Gelman 2008, Efron 1986].

The controversies raised by both frequentist and Bayesian procedures motivated the development of alternative inferential methods exclusively pioneered by Fisher. Fisher proposed two different approaches. The first is the fiducial theory [Fisher 1933, Fisher 1935]. The fiducial inference is a generalisation of the Bayesian process as it relies also on the idea of inversion. The difference with the Bayesian inference is that it does not involve a a prior distribution. Savage described it as "*an attempt to make the Bayesian omelet without breaking the Bayesian eggs* " [Savage 1963] . Fiducial inference raised a lot of controversy and was not accepted in the statistical community as it was considered quite ambiguous [Gelman 2008]. A detailed account of the development and criticisms of Fisher's fiducial theory can be found in [Zabell 1992, Efron 1986, Efron 1998].

Fisher [Fisher 1973] proposed an alternative conceptual approach for inference referred to as the likelihood approach. It is based on the Fisherian likelihood concept, and more formally on the likelihood principle stating that all inference conclusions should solely be drawn from the likelihood function (the formal statement of this principal and the basics of its justification are reported in the Appendices, Section 1.3). A detailed proof of the theorem in the discrete case can be found in [Robert 2001, pages 18-19] and in [Berger 1984] for the continuous case.

The use of Fisherian inference in practical applications remained quite limited, though its underlying reasoning has inspired many statisticians dealing with the inference issue. For instance, Dempster was inspired by the fiducial argument. His

work was originally dedicated to the extension of the fiducial statistical inference, which justifies the initial designation of his theory: *Dempster's theory of inference*. When extending the original theory to a well-establishing theory of evidential reasoning, Shafer, who was a proponent of the likelihood approach, proposed an alternative inference method based on the Fisherian likelihood principle.

It seemed essential to dedicate a section of this thesis to the statistical inference topic because it was a key point in the development of the DS uncertainty theory. The original approach by Dempster [Dempster 1966] is briefly described in the following subsection. Shafer's approach is then recalled and discussed in Subsection 3.3.1.

3.2 Dempster's approach

In the 1960s, Dempster developed a model to draw inferences of unknown parameters without calling on a prior distribution. He proposed an inference theory based on the concept of the multinomial DS model – a general tool based on a pivotal quantity that induces a set-valued mapping from a probability space to the parameter space once the observations have been collected [Dempster 1966, Dempster 1968a, Dempster 1968b]. In the following, we describe the general concepts underlying this inference method based on recent papers by Martin and Denoeux [Martin 2010, Denoeux 2013a].

Let $X \in \mathbb{X}$ denote the observable data described probabilistically by a parametric model $f(x, \theta)$, where $\theta \in \Theta$. The objective is to make probabilistic statements about θ. The key idea underlying Dempster's inferential method is to consider the observed variable as a function of the parameter of interest (θ) and an auxiliary unobservable variable $U \in \mathbb{U}$, referred to as a pivotal quantity, with a known probability distribution p defined on measurable subsets of $\mathbb{U}$ and independent of θ:

$$X = a(\theta, U). \tag{1.46}$$

Equation (1.46) is known as the *auxiliary-equation*. This representation is familiar in the context of data generation [Fraser 1968, Martin 2010]. For instance, a random variable X with a cumulative distribution function F_θ can be generated by setting $X = F_\theta^{-1}(U)$ with $U \sim Unif(0, 1)$.

Dempster exploited the Fisherian fiducial idea of exchanging the roles of X and θ when making inference. Before the observation, X is random and has a sampling distribution that depends on a deterministic quantity θ, but after the observation, its variability is transferred to θ. By assuming that each of X, θ and U is bijectively determined by the auxiliary equation given the other two, a posterior probability distribution is constructed on Θ.

Dempster's method combines this switching principle with the representation in expression (1.46) to construct a (fiducial) posterior distribution on θ. Dempster's adaptation of fiducial inference relaxes the uniqueness hypothesis mentioned above

as he does not require the sets

$$\Theta_{X,U} = \{\theta \in \Theta | X = a(\theta, U)\}$$

and

$$\mathbb{U}_{X,\theta} = \{U \in \mathbb{U} | X = a(\theta, U)\}$$

to be singletons. A posterior distribution on subsets of the parameter space Θ can thus be constructed. We briefly describe the general procedure by Dempster.

The auxiliary equation (1.46) defines a set-valued mapping Γ (known as the state space model (SSM)) from the probability space $\mathbb{U}$ into the product space of the parameter space and observation space $\mathbb{X} \times \Theta$ (frame of discernment)

$$\Gamma : U \to \Gamma(U) = \{(X, \theta) \in \mathbb{X} \times \Theta | X = a(\theta, U)\}. \tag{1.47}$$

Dempster referred to the set $\Gamma(U)$ as a focal set. The mapping Γ, together with the probability model p of the pivotal quantity on $\mathbb{U}$, specifies a DS model – a belief function (equivalently, a random set) on $\mathbb{X} \times \Theta$ defined by:

$$Bel(A) = p(U | \Gamma(U) \subseteq \lambda) \quad , \quad \forall A \subseteq \mathbb{X} \times \Theta. \tag{1.48}$$

Taking into account the evidence from an observation $X = x$, the set-valued mapping based on this information becomes

$$\Gamma_0 : U \to \Gamma_0(U) = \{x\} \times \Theta. \tag{1.49}$$

When conditioning on X (the conditioning is performed by combining (1.49) with (1.47) in the sense of Dempster), a new focal random set is produced:

$$\Gamma_X(U) = \{\theta \in \Theta | x = a(\theta, U)\}. \tag{1.50}$$

The mapping Γ_X and the pivotal measure p induce a posterior DSM on Θ, with the belief function for every $A \subseteq \Theta$ defined by

$$Bel_X(A) = \frac{\mu(U | \Gamma_X(U) \subseteq A)}{\mu(U | \Gamma_X(U) \neq \emptyset)}. \tag{1.51}$$

Dempster's method of inference raises two major criticisms. The first is related to the lack of specification when constructing the pivotal quantity and the model in (1.46), and the second is related to its costly implementation [Denoeux 2006]. Recently, some authors revisited Dempster's method [Martin 2010, Leaf 2012]. Lately, Dempster worked again on the inference topic [Dempster 2008].

In extending the original theory of Dempster, Shafer proposed an alternative approach for inference based on another Fisherian concept: the likelihood. This approach is recalled in Subsection 3.3.1. Arguments for and against this solution are discussed in Subsection 3.3.3.

3.3 Likelihood-based inference extended to DST

3.3.1 Formal description

The likelihood approach is an alternative to classical inference paradigms. It is based on viewing the likelihood as the unique basis for statistical inference, and more formally, on the likelihood principle. The principle states that [Berger 1984]:

Likelihood Principle (LP) *In making inferences or decisions about θ after x is observed, all relevant experimental information is contained in the likelihood function for the observed x. Furthermore, two likelihood functions contain the same information about θ if they are proportional to each other.*

The axiomatic justification of this principle was given by Birnbaum [Birnbaum 1962] (Appendices, Section 1.3). Convincing arguments in favour of the likelihood principle can be found in [Ghosh 1988].

Fisher [Fisher 1922, Fisher 1925] suggested to use the ratio of the likelihood function as a measure of the relative merit of two hypotheses given some observation. Shafer translated this idea in evidential terms and expressed the ratio of the likelihood function in the belief functions framework as follows:

$$\frac{L(\theta_1;x)}{L(\theta_2;x)} = \frac{pl(\theta_1;x)}{pl(\theta_2;x)} \tag{1.52}$$

for all $(\theta_1,\theta_2) \in \Theta^2$, or equivalently,

$$pl(\theta;x) = cL(\theta;x) \tag{1.53}$$

for all $\theta \in \Theta$ and some positive constant c. These definitions make inferential sense for parametric inference. The higher is the plausibility of θ, the more probable it is to observe x given this value. For instance, if $pl(\theta_1;x) = 0.01$, then we are 100 times more likely to observe x with the MLE (if it exists) than with $\theta = \theta_1$.

The least commitment principle (LCP) (stating that when the available evidence suggests several belief functions, the least informative one should be selected) then leads to giving the highest possible value to constant c, i.e., defining pl as the relative likelihood:

$$pl(\theta;x) = \frac{L(\theta;x)}{\sup_{\theta'\in\Theta} L(\theta';x)}. \tag{1.54}$$

This definition requires the denominator to be finite so that pl is not identically null. Statistical evidence about θ can equivalently be represented by the least committed plausibility function induced by pl, i.e.,

$$Pl(A;x) = \sup_{\theta\in A} pl(\theta;x) = \frac{\sup_{\theta\in A} L(\theta;x)}{\sup_{\theta'\in\Theta} L(\theta';x)}, \tag{1.55}$$

The corresponding belief function is:

$$Bel(A;x) = 1 - \sup_{\theta\notin A} pl(\theta;x) = 1 - \frac{\sup_{\theta\notin A} L(\theta;x)}{\sup_{\theta'\in\Theta} L(\theta';x)}, \tag{1.56}$$

for all $A \in \Theta$. The belief function is usually referred to as the likelihood-based belief function.

Equation (1.54) was first proposed by Shafer in [Shafer 1982] who, however, did not justify it by the LCP, but by the more questionable requirement that the belief function on Θ be consonant. In the special case where $\Theta = \{\theta_1, \theta_2\}$, Wasserman [Wasserman 1990] showed that the plausibility function (1.54) corresponds to the unique belief function $Bel(.; x)$ satisfying the following requirements:

- If $L(\theta_1; x) = L(\theta_2; x)$ then $Bel(.; x)$ should be vacuous;
- $Bel(\{\theta\}; x)$ should be nondecreasing in $L(\theta; x)$;
- If $Bel = Bel \oplus P_0$ where P_0 is a probability measure, then Bel should be equal to the Bayesian posterior.

This argument can be extended to the general case where Θ is a complete, separable metric space [Wasserman 1988b, Wasserman 1988a]. The first condition requires that a flat likelihood, as it does not carry any information about the relative plausibility of the parameter of interest, should lead to a non-informative belief function, i.e., in DST terms, to a vacuous belief function. The second condition reformulates the likelihood principle in evidential terms: it states that the higher is the likelihood of a given value, the higher should be the belief assigned to it. The last condition requires the compatibility between Bayesian and belief-function inference when a Bayesian prior is available. More precisely, let $\pi(\theta)$ be a Bayesian prior probability mass of density function on Θ. Combining it with the $Bel(.; x)$ via Dempster's rule yields a Bayesian (posterior) belief function with probability mass or density function:

$$p(\theta; x) \propto pl(\theta; x)\pi(\theta). \tag{1.57}$$

Since the posterior probability function on θ satisfies

$$p(\theta; x) \propto f(x; \theta)\pi(\theta), \tag{1.58}$$

then compatibility with Baye's rule leads to

$$pl(\theta; x) = cf(x; \theta) = cL(\theta; x). \tag{1.59}$$

for c a positive constant depending only on the likelihood function. A belief function satisfying the three conditions cited above has its focal elements defined as follows:

$$\Gamma_x(u) = \{\theta \in \Theta | pl(\theta; x) \geq u)\}, \tag{1.60}$$

for $u \in [0, 1]$.

In a recent paper, Denoeux [Denoeux 2013a], provided new arguments in favour of the evidential likelihood-based method, by showing that it can be derived from three principles: the likelihood principle, compatibility with Bayesian inference and the least-commitment principle.

3.3.2 Addressing the incompatibility with Dempster's rule

One of the main criticisms against the use of the likelihood-based plausibility function (1.54) for representing statistical evidence is its incompatibility with Dempster's rule in the case of independent observations [Shafer 1982]. More precisely, assume that X is an independent sample $(X_1, ..., X_n)$ and each observation X_i has a marginal pdf $p(x_i; \theta)$ depending on θ. We could combine the n observations at the "aleatory level" by computing $Pl(.; x)$ using (1.54) and (1.55), or we could combine them at the "epistemic level" by first computing the consonant plausibility functions $Pl(.; x_i)$ induced by each of the independent observation and applying Dempster's rule to combine them. Obviously, these two procedures yield different results in general, as consonance is not preserved by Dempster's rule [Denoeux 2013a].

In [Shafer 1982], Shafer regards the inconsistency due to the non-commutativity as strong enough to reject (1.54) as a reasonable method to statistical inference. However, Aickin [Aickin 2000] proposed to keep (1.54) but questioned Dempster's rule as a mechanism for combining statistical evidence, based on the notion of *commitment to the model*. He suggested an alternative combination rule to Dempster's which seems to be the additional piece that ensures a coherent parametric inference within the pure view of DS theory.

Let (Ω, P, Γ) be a random set corresponding to Pl. As stated above, each $\omega \in \Omega$ can be regarded as an interpretation of a given piece of evidence. These interpretations are consistent, or "committed to the model" if

$$\bigcap_{\omega \in \Omega} \Gamma(\omega) \neq \emptyset$$

which is equivalent to the condition that $pl(\theta_0) = 1$ for some $\theta_0 \in \Theta$. Aickin [Aickin 2000] argued that, in the context of statistical inference, one should be fully committed to the idea that the model actually generated the observations, which entails the plausibility functions used to represent statistical evidence should be generated by a random set that is committed to the model.

Aickin went on by defining the notion of commitment to a submodel as follows. Let $A \subset \Theta$ be a "submodel". A random set (Ω, P, Γ) is committed to A if all those $\Gamma(\omega)$ that intersect A have a non-void intersection. This property means that, after combining the random set with information stating that $\theta \in A$ for sure using Dempster's rule, our random set should be committed to the new model $A \subset \Omega$ now considered as certain.

Let Pl be an arbitrary plausibility function on Θ, pl the corresponding contour function, $c = \sup pl$, and Pl^* the consonant plausibility function defined by $Pl^*(A) = c^{-1} \sup_{\theta \in A} pl(\theta)$. Aickin [Aickin 2000, Proposition 1] showed that, if Pl is committed to A, then $Pl(A)/c = Pl^*(A)$, and the converse is true if A is compact and Pl is upper semicontinuous. A consequence of this result is that, assuming commitment to the model, i.e., $c = 1$, the two plausibility functions Pl and Pl^* coincide on all "interesting" sub-models A, and nothing is lost by replacing the former by the latter.

Let us now assume that $Pl(.;x_1)$ and $Pl(.;x_2)$ are plausibility functions on Θ induced by two independent observations x_1 and x_2. After combination by Dempster's rule, the resulting plausibility function $Pl(.;x_1) \oplus Pl(.;x_2)$ need not to be committed to the model even though $Pl(.;x_1)$ and $Pl(.;x_2)$ are, which can be considered as an argument against the use of Dempster's combination of evidence from independent observations in the context of parametric statistical model. However, commitment to the model may be restored by considering the contour function $pl(.;x_1;x_2) = pl(.;x_1) \oplus pl(.;x_2)$ corresponding to $Pl(.;x_1) \oplus Pl(.;x_2)$, recalling it so that its supremum equals 1, and computing the consonant plausibility function. We thus get

$$pl(\theta;x_1,x_2) = \frac{pl(\theta;x_1)pl(\theta;x_2)}{\sup_{\theta\in\Theta} pl(\theta;x_1)pl(\theta;x_2)} = \frac{L(\theta;x_1,x_2)}{\sup_{\theta'\in\Theta} L(\theta';x_1,x_2)} \tag{1.61}$$

for all $\theta \in \Theta$ and

$$Pl(A;x_1,x_2) = \sup_{\theta\in A} pl(\theta;x_1,x_2) = \frac{\sup_{\theta\in A} L(\theta;x_1,x_2)}{\sup_{\theta'\in\Theta} L(\theta';x_1,x_2)} \tag{1.62}$$

for all $A \subseteq \Theta$. This way of combining independent statistical evidence, which Aickin called the DS^* rule, restores the equivalence between combination at the aleatory and epistemic levels and reconciles likelihood inference with DS theory. Further arguments against the use of Dempster's rule for combining statistical evidence from statistically independent observations can be found in [Walley 1987]. In particular, Walley showed that Dempster's rule leads to the violation of the sufficiency principle (the statement of this principle can be found on the appendices, Section 1.3) when it's used to combine evidence from independent observations.

3.3.3 Discussion

The solution proposed by Shafer is considerably simpler and easier to implement than Dempster's initial proposal [Dempster 1968a] and other methods discussed in [Shafer 1982], while being more widely applicable than Smet's Generalized Bayesian theorem [Dubois 2010, Smets 1993]. The method has been successfully applied to relatively complex models such as Gaussian mixture models [Denoeux 2013b] or hidden Markov models [Ramasso 2013]. Recently, Denoeux [Denoeux 2013a] demonstrated the potential of this approach in handling low-quality data acquired through an imperfect observation process or being only partially relevant to the population of interest. Further arguments in favor of this solution are summarized in the following:

1. Combining $Pl(.;x)$ given by (1.54) with a Bayesian prior P_0 on Θ using Dempster's rule yields a Bayesian plausibility function $Pl(.;x) \oplus P_0$ which is identical to the posterior probability obtained using Baye's rule: consequently, the proposed method of inference boils down to Bayesian inference when a Bayesian prior is available.

2. Consistency with statistical practice: viewing the relative likelihood function as the contour of a consonant belief function, or, equivalently, as a possibility distribution [Zadeh 1978, Dubois 1988] is, to a large extent, consistent with statistical practice. For instance, likelihood intervals are focal elements of the relative likelihood viewed as a possibility distribution. In the case where $\Theta = (\theta_1, \theta_2) \in \Theta_1 \times \Theta_2$ and θ_2 is considered as a nuisance parameter, the relative profile likelihood function can be written

$$pl(\theta_1; x) = \sup_{\theta_2 \in \Theta_2} pl(\theta_1, \theta_2; x), \tag{1.63}$$

which is the marginal possibility distribution on Θ_1. Eventually, the usual likelihood ratio statistics $\mathbf{\Lambda}(x)$ for a composite hypothesis $H_0 \subset \Theta$ can be seen as the plausibility of H_0, as

$$\mathbf{\Lambda}(x) = \frac{\sup_{\theta \in H_0} L(\theta; x)}{\sup_{\theta \in \Theta} L(\theta; x)} = \sup_{\theta \in H_0} pl(\theta; x) = Pl(H_0; x). \tag{1.64}$$

3. The method can handle partial prior information about the parameter of interest (i.e., situations where the prior is neither vacuous nor Bayesian). In addition, the combination of the partial information with the statistical evidence does not require heavy calculations. Indeed, if Bel_p is a belief function representing prior information about θ with source $(\Theta, \mathcal{B}(\Theta), P, \Lambda)$ and consonant Bel_x, the statistical belief function generated from the observations, then, the posterior belief function $Bel = Bel_x \oplus Bel_p$ takes a special form:

$$Pl(A) = \frac{P(\overline{L}_A)}{P(\overline{L})} \quad \forall A \subseteq \Theta \tag{1.65}$$

where $L_A(\theta) = L(\theta) I_A(\theta)$, I_A is the indicator function for A, and for any bounded measurable function f on Θ, $\overline{f}$ is defined by: $\overline{f} = \sup_{\theta \in \Lambda(x)} f(\theta)$.

4 Conclusion

Epistemic uncertainty, which characterises lack of knowledge, is often prevalent in engineering applications, but it is often treated (incorrectly) as aleatory information. Among the great number of models developed to better account for epistemic uncertainty, we focused on the theory of belief functions.This chapter is concerned with the description of the mathematical foundation of the belief functions theory. Considering first the finite case, we highlighted the differences between this particular imprecise probabilities model and the probabilistic model, and illustrated its added values through some examples of situations involving poor information that does not lend itself to a precise probabilistic description. The second part was concerned with the infinite case on the real line (a particular yet sufficiently general framework) where belief functions are equivalent from a mathematical point of view to random sets (closed intervals). In this framework, connection with other

imprecise probabilities models, such as the possibility model or Ferson's p-boxes, was highlighted: both turn out to be particular belief functions (or equivalently random closed intervals). Then we addressed the fusion of multi-sources evidence, and some of the main combination modes (Dempster's, disjunctive, averaging and discounting rules) that cover different scenarios on the dependence and reliability of the sources were described. We were finally concerned with the extension of belief functions through a model. The extension principle in the finite case, and the Monte Carlo approximation in the infinite case were described and illustrated with some simple examples. The last part of this chapter was concerned with another aspect: the statistical reasoning. We briefly recalled the classical frequentist and Bayesian inference approaches, and described their limitations, basically the inability to condition on data at hand (for frequentists) and the justification of the use of uninformative priors (Bayesians). These limitations motivated the development of alternative inference methods based on more general principles and arguments (likelihood principle, fiducial inference). Dempster's first inference solution based on fiducial arguments was described. It was interesting to report this solution (even if it is of little practical use because it implies cumbersome calculations) as it shows how upper and lower probabilities (plausibility and belief) have been initially introduced and defined by Dempster. We finally described a different inference method based on the likelihood principle which axiomatic justifications was provided. This method provides a simple way to draw inference conclusions as it leads to consonant belief functions that have simple analytical expression and can be easily recovered from the evidence at hand. Additional arguments in favor of this solution were reported. Finally, we discussed some of the criticisms raised by this method, basically its inconsistency with Dempster's rule of combination in the case of independent observations. This inconsistency is not attributable to the inference model but to the rule, and it can be avoided by using a modified version of Dempster's rule that is more adequate when it comes to combine statistical evidence from independent observations.

Part II

Global warming and sea-level rise

1 Introduction

When conducting climate change impact assessments for coastal adaptation purposes, a "cascade of uncertainties" [Dessai 2007] from different levels arise and accumulates. Figure 2.1 describes schematically the integrated climate change impact assessment approach. Uncertainties are present in every step of the process. Roughly, they are associated to (1) climate process drivers (i.e., future emissions of GHG), (2) the response of the climate system to these changes (in terms of temperature, sea level, etc) and (3) the impact modelling.

This chapter is devoted to the description of the key uncertainties in climate projections, i.e., those related to (1) and (2). In the First section, we describe in detail the origins of the uncertainty in each of the future emissions and global warming assessment modules, and we review the literature on the methods and tools used to address these uncertainties. We then focus on the sea-level rise impact of climate change. We begin with a description of the key processes controlling it. Then, we discuss the sources of uncertainty in the published model-based projections and describe alternative approaches, namely, semi-empirical models and expert elicitation, developed in response to the limited predictive capacity of the process-based models.

2 A review of uncertainties in future global warming projections

2.1 Greenhouse gas emissions

GHGs include different gases including water vapour (H_2O), methane (CH_4), carbon dioxide (CO_2), ozone (O_3), etc. These gases, naturally present in the atmosphere, absorb heat and maintain the radiative balance of the atmosphere. Since the early 1800s, the proportion of GHGs in the atmosphere has been increasing due to human activities such as the production and combustion of fossil fuels or industrial processes. These synthetic GHGs disturb the atmosphere equilibrium and alter climate.

Man-made GHG emissions are the products of a very complex dynamic system, determined by driving forces that include population growth, technological and socio-economic developments [IPCC 2007]. The processes controlling the key driving forces, as well as the interaction between them, are multi-dimensional and very complex. This complexity makes impossible the accurate prediction of the evolution of the underlying drivers and leads to large uncertainties in the estimates of future levels of global GHG emissions.

The uncertainty surrounding future GHG emissions (also known as policy uncertainty) is multi-dimensional and does not itself to quantification. The IPCC proposed to characterise it qualitatively using scenarios – a set of different "images of the future" that qualify differently the trends of evolution of the driving forces and the interaction between them. In 1996, the IPCC commissioned a special re-

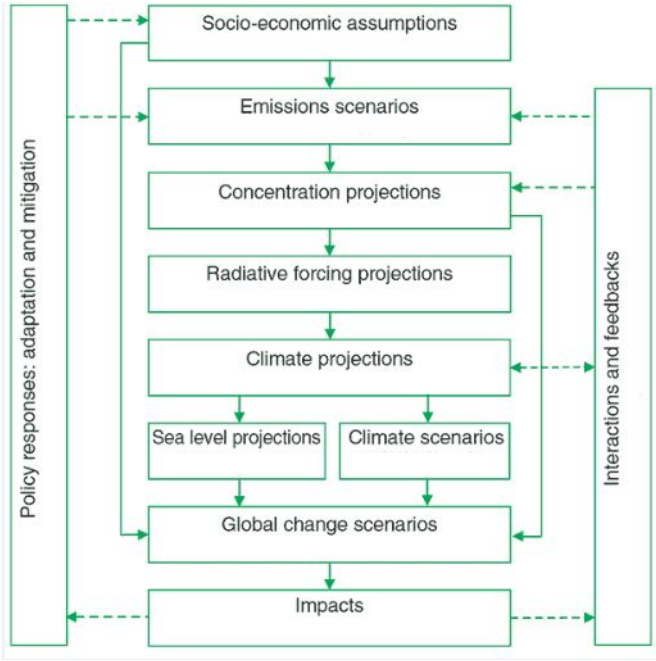

Figure 2.1: Schematic description of the integrated climate change impact assessment and adaptation. (source [IPCC 2007]).

port on emission scenarios (SRES), and four different storylines (A1, A2, B1 and B2) were defined. These storylines " are neither predictions nor forecasts, but rather stories...that describe range of possible futures" [IPCC 2007]. In the AR4, they were described as follows:

- "A1 storyline: describes a future of very rapid economic growth, global population that peaks in mid-century and declines thereafter, and the rapid introduction of new and more efficient technologies. Major underlying themes are convergence among regions, capacity building, and increased cultural and social interactions, with a substantial reduction in regional differences in per capita income. The A1 scenario family develops into three groups that describe alternative directions of technological change in the energy system: fossil intensive (A1FI), non-fossil energy sources (A1T), or a balance across all sources (A1B).

- A2 storyline: describes a very heterogeneous world. The underlying theme is self-reliance and preservation of local identities. Fertility patterns across regions converge very slowly, which results in continuously increasing global population. Economic development is primarily regionally oriented and per capita economic growth and technological change are more fragmented and slower than in other storylines.

- B1 storyline: describes a convergent world with the same global population that peaks in mid-century and declines thereafter, as in the A1 storyline, but

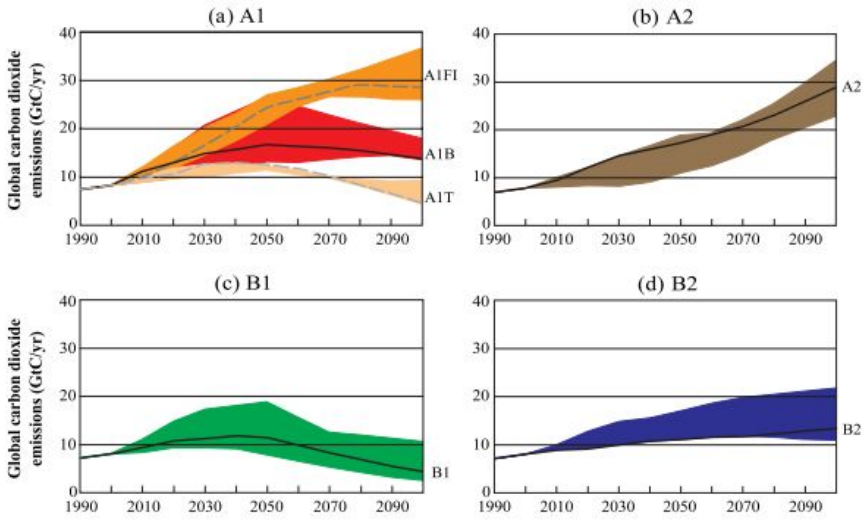

Figure 2.2: Projections of annual GHG emissions (in GtCO2 eq per year) from 1990 to 2000. Colored bands show the range of the scenarios within each family. Illustrative SRES marker scenarios for each family are highlighted in solid lines (source [IPCC 2007]).

with rapid changes in economic structures toward a service and information economy, with reductions in material intensity, and the introduction of clean and resource-efficient technologies. The emphasis is on global solutions to economic, social, and environmental sustainability, including improved equity, but without additional climate initiatives.

- B2 storyline: describes a world in which the emphasis is on local solutions to economic, social and environmental sustainability. It is a world with continuously increasing global population at a rate lower than A2, intermediate levels of economic development, and less rapid and more diverse technological change than in the B1 and A1 storylines. While the scenario is also oriented toward environmental protection and social equity, it focuses on local and regional levels."

The IPCC quantifies every storyline by different scenarios that make different assumptions for future driving forces. In total, 40 scenarios were defined, and they encompass the current range of uncertainties of future GHG emissions. The scenarios based on the same storyline form a *scenario family*. A scenario family is characterised by a *marker scenario* – a particular scenario selected in the scenario family by the SRES writing team as the most illustrative of the storyline. IPCC projections of the GHG emission in the coming century are reported in Figure 2.2.

It should be noted that the storylines are all considered possible, and no likelihood is attached to of any of them. Indeed, the IPCC refrained from specifying the most likely scenario and emphasised that none of them can be construed as a best guess since they are " built as descriptions of possible, rather than preferred, developments" [IPCC 2007].

Understanding and quantifying uncertainties in GHG emissions has attracted much attention in the last two decades. Some climate scientists believe these uncertainties do not lend themselves to quantification. For instance, Dessai and Hulme [Dessai 2004] argued that the quantification of uncertainty in emissions scenarios is problematic and that the scenario approach is the most suitable (and unique) way to tackle it because of the presence of what they call *human reflexive uncertainty* (human systems are reflexive to information about the future). In the last decade, there have been some attempts to explore the uncertainty in GHG emissions and their drivers in probabilistic terms [Webster 2002, Leggett 2003, Neill 2004]. For instance, Webster [Webster 2002] produced a probability density function of GHGs using a Monte Carlo (MC) analysis of a simple equilibrium model of the world economy based on the elicitation of expert opinions on the main forcing drivers (identified by a sensitivity analysis).

The probabilistic approach to quantify uncertainty in socio-economic scenarios is challenging because the lack of scientific evidence on all the key drivers and the relationships between them. In the last decade, alternative uncertainty frameworks have been investigated. Hall et al. [Hall 2007a] used the theory of imprecise probabilities to address the concerns in quantifying the uncertainty in emissions projections. The authors considered socio-economic scenarios to be fuzzy linguistic constructs, and they assigned every precise emission trajectory a degree of membership between 0 and 1 in a fuzzy scenario. In a second stage, they dealt with the aggregation of the fuzzy scenarios using non-additive measures, namely the Choquet integral. Ha-Duong [Ha-Duong 2003] proposed a method based on imprecise probabilities to bridge the gap between forecasts and scenarios. The author applied his method in a hypothetical study of global warming in the year 2100, defined by a simple model that links linearly the global atmospheric concentration of CO_2 in 2100 (the evidence is the IPCC SRES dataset) to climate sensitivity (the evidence is a set of subjective probability distributions provided by climate experts).

2.2 Future global warming

Global warming, which refers to the global temperature increase, is a direct response to GHGs emissions. Different climate models ranging from simple to coupled atmosphere-ocean global circulation models (AOGCMs) are used in the literature to estimate the future temperature rise. The key parameters of these models are climate sensitivity - defined as the increase in the global mean surface temperature that would result from a doubling of the atmospheric CO2 concentration relative to its preindustrial value - the heat uptake by oceans and aerosol forcings. Most of the works on quantifying uncertainties in future global temperatures focus on the quantification of the uncertainties in these variables.

To derive the results of the last IPCC report, 23 AOGCMs simulated climate change over the previous century and provided projections into the future. The different models accounted for uncertainty in key climate variables (climate sen-

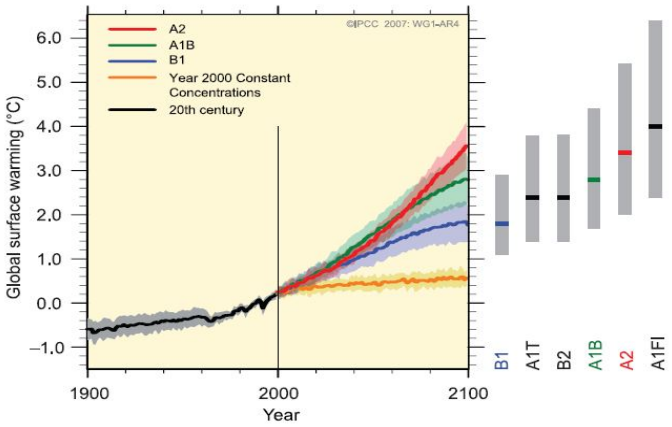

Figure 2.3: Projections of multi-models future global average surface temperature changes (relative to 1980-1990 average) for scenarios A2, B1 and A1B. Yellow color corresponds to the scenario where GHGs emissions remain constant (at year 2000 values). Solid colored lines represent "most likely" trends. Shaded regions represent "probable regions". On the right, vertical gray bars represent "likely ranges" of year 2100 temperatures and the horizontal bold lines indicates the best estimates (source [IPCC 2007]).

sitivity, ocean vertical diffusivity and aerosol forcing) and uncertainty in carbon cycle-climate feedback (i.e., the fact that ocean and terrestrial carbon uptake depends on the climatic state). The IPCC presented the results as a multi-model mean and a likely range enclosing the projections of all models. The temperature projections in the AR4 for the six illustrative scenarios are shown in Figure 2.3. The large uncertainty bands in the predictions underline the complexity involved in deriving temperature projections.

No likelihood is attached to IPCC projections of global warming. Several attempts to describe global temperature increase using probability distribution functions have been reported in the literature. Several methods, such as expert elicitation and various uncertainty analysis techniques, have been used to tackle uncertainty in the key climate variables. In short, Wigley and Raper [Wigley 2001] drew probability distributions for the main climate variables from a subjective expert elicitation [Wigley 2001] and produced PDFs of future global temperatures using a simple 1-D upwelling diffusion model. PDFs of the model parameters can also be derived from a comparison of the model behaviour and observational data [Andronova 2001, Forest 2002, Knutti 2002, Murphy 2000] (a likelihood function constructed by minimising the residuals between model response and data is updated with a specific prior via Bayes' rule) or purely from observations [Gregory 2002]. Then, using models of different levels of complexity, PDFs of global temperatures can be derived. A comprehensive review of the literature of the probabilistic projections of future global temperatures can be found in [Knutti 2008].

The use of probabilities to represent the scientific evidence on future global warming is debatable because, often, the information at hand is poor and does not justify the choice of a particular probability distribution. Recently, Millner

[Millner 2012] proved empirically that subjective probabilities can not adequately describe experts' beliefs on climate variables.

Lately, an intensive body of studies has explored the uncertainties in the future projections using alternative uncertainty frameworks. In particular, Kriegler [Kriegler 2005] and Hall [Hall 2007b] studied the influence of parameter uncertainty in energy balance and radiative forcing models on the estimation of the global mean temperature increase. Knowledge about key climate parameters, such as climate sensitivity and aerosol forcing, was represented by a p-box that encloses all the relevant probability distributions published in the literature on each of the parameters of interest. These p-boxes were then propagated through dynamical models using different dependence assumptions, and distribution bands on the global temperature change in 2050 and 2100 were derived for each of the emission storylines. In [Ha-Duong 2008], Ha-Duong modelled expert opinions on climate sensitivity using Bayesian belief and consonant belief functions. The latters were obtained by transforming expert's elicited distributions into a corresponding consonant belief functions. He then used different combination rules to combine expert opinions.

3 Sea-level rise

Given a particular emissions scenario, changes in GHGs concentrations and the associated global warming can be modelled with some confidence due to the improvement in the predictive capacity of the models. However, in regard to climate impacts, such as the elevation of sea levels, there is less confidence in the process-based projections because the processes controlling them are often ill-understood and too complex to be modeled with an acceptable level of confidence.

The scientific understanding of past and current sea-level changes has significantly improved since the early 1990s due to the significant development of tide gauge measurement techniques and the availability of accurate satellite observations. Coastal tide gauges measurements from coastlines around the world as well as the satellite altimetry data indicate that the global sea-level has been increasing at a rate of 1.7 mm/yr during the previous century, and that this rate moved to 3.3 mm/yr since 1993 [Church 2006]. Global sea-level is expected to keep increasing during the 21st century.

There are three major processes by which global warming directly affects sea level: (1) the thermal expansion of oceans, (2) the melting of mountain glaciers and ice caps and (3) the melting of ice sheets (Greenland and Antarctica). In the following, we briefly describe these processes as well as the models used to assess their contribution to future SLR.

3.1 Controlling processes

3.1.1 Thermal expansion of oceans

When temperatures increase, ocean water heats up, increasing the volume of the global ocean and rising sea levels. Thermal expansion is modelled using three-dimensional ocean circulation models, a component of coupled climate models [IPCC 2007]. Model-based simulations indicate that half of the sea-level rise over the last century was induced by this factor. The average rate of the sea-level rise due to thermal expansion estimated from these models is 0.3 to 0.7 mm/yr for the first decades to 0.6 to 1.1 mm/yr for recent decades. These results are consistent with the observational estimates. The agreement between the historical observations and the simulation results suggests a relative confidence in the models used to estimate the contribution of the thermal expansion to the global sea-level rise and, thus, confidence in their future projections.

To gain an idea about the order of magnitude of the contribution of the thermal expansion to the future sea-level rise, the best estimate for a moderate warming (A1B) scenario is an approximately 20 cm rise by 2100 [IPCC 2007].

3.1.2 Melting of mountain ice and glaciers

When temperatures increase, mountain glaciers and polar ice caps melt. The resulting water flows to the seas and leads to an increase of global sea levels.

With approximately 123,000 glaciers of different natures worldwide [Radič 2010], the melting of land ice is difficult to calculate from physical models. This component is rather computed from a simple empirical formula that links global mean temperature to mass loss (equivalent to a rate of sea-level rise) based on observed data from 1963 to 2003. According to this model, the best estimate of the contribution of the land ice melting to sea-level rise by the end of the century is approximately 10 cm for moderate global warming (A1B scenario)[IPCC 2007].

3.1.3 Ice sheet dynamics

There are two main ice sheets on Earth: Antarctica and Greenland. Antarctica, located in the southern hemisphere, is split between two ice sheets, separated by the Transantarctic Mountains. They are known as East Antarctica ice sheet (EAIS) and West Antarctica ice sheet (WAIS). The Greenland ice sheet (GrIS) is located in the northern hemisphere and is the smallest in volume (Figure 2.4).

The Greenland and Antarctica, which were assumed to be stable, have been showing since the end of the previous century unexpected dynamics. Evidence on the instability of both ice sheets was provided by satellite observations. The latter indicated that, over the last two decades, both ice sheets have been losing more mass than usual (their contribution to sea-level rise exceeded their average contribution in the twentieth century) and faster than expected. If they persist, such dynamics may cause a substantial increase of the sea-level rise. Indeed, Greenland and Antarctica

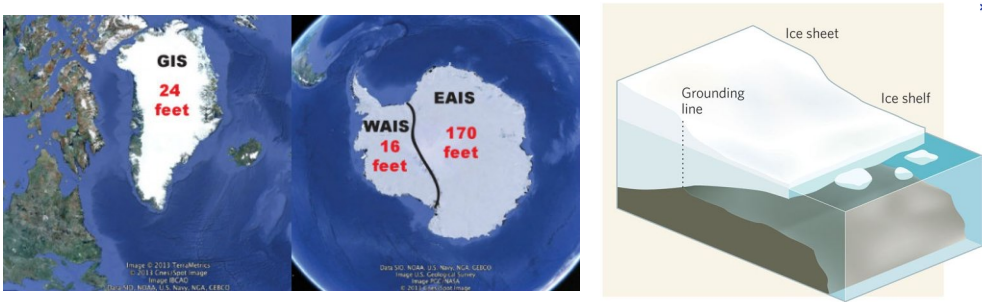

(a) (b)

Figure 2.4: (a) Earth's ice sheets: Greenland and Antarctica ice sheets. In red is the sea-level rise that would result from complete melting of ice sheet (1foot= 0.305m) (source: Google Earth). (b) A simplified depiction of the west Antarctica ice sheet. To the left, the grounded marine ice sits upon bedrock or sediment on the sea floor. To the right, floating ice shelf separated from the grounded ice sheet by the grounding line (source www.nature.com).

ice sheets store 99% of the earth glacier ice, and if they melt entirely, global sea-level would raise by 65 meters [IPCC 2007]. Fortunately, this extreme climatic scenario is not expected to happen for soon. However, even a small release of ice should be considered carefully.

The Greenland and Antarctica ice sheets lose mass via two processes with different underlying mechanisms. The first, surface melting, affects the mass balance – the difference between snow accumulation and melting – at the ice surface. This effect is controlled by air temperature and snowfall, and is approximated using an ice sheet surface mass balance model. The mass balance is expected to be positive for Antarctica (i.e., accumulation of snowfall exceeds losses from melting) and negative for Greenland. According to the AR4, the estimated sea-level contribution from the ice sheets by the end of the century is zero. The second process involved in SLR is dynamic flow. Dynamic flow consists of the thinning of the floating ice shelves due to the increase of ocean temperature, and affects Antarctica to a higher extent (see a simplified depiction of this process in Figure 2.4). Ice dynamics cannot yet be properly modelled because the controlling processes are extremely complex and ill-understood, and projections of their contribution to SLR can not yet be assessed with confidence. The difficulty in providing estimates of the ice dynamics contribution to SLR was highlighted by the IPCC, which concluded in its last report that "*understanding of these effects is too limited* [...] *to provide a best estimate or an upper bound for sea-level rise in the twenty-first century*". The IPCC projections of the sea-level rise in the coming century excluded future rapid dynamical changes in ice flow and assume that this contribution simply remains constant to the observed rate during the period $1993 - 2003$ ($0 - 0.7$ mm/yr) until the end of this century (Figure 2.5).

3.2 Future projections

3.2.1 Process-based projections

The IPCC provided in the AR4 projections of sea-level rise at 2095 relative to 1990 (the difference between the average sea level over 2090-2099 and over 1980-1999). The rise projected by climate models for this period was 0.18 to 0.59 m covering the different emission scenarios and different modelling approaches. The IPCC recommended to add 0.2 m to the upper limits of the projections to take account of dynamic ice-sheets processes (referred to scaled-up ice sheet discharge) that have not been integrated in their models .

IPCC projections of future SLR raise a number of issues. First, the contribution due to ice dynamics from Greenland and Antarctica ice sheets was estimated under the assumption that future flow rates remain constant (equal to the rate measured in 1993-2003). This assumption is in contradiction with the recent evidence (satellite observations, glaciological studies) that suggests a significant increase in ice flow rate since 2003. A second issue with IPCC range is that they do not include the contribution of all components involved in SLR such as small scale dynamics. Finally, the $[0.18, 0.59]$ interval does not account for uncertainty in climate-carbon cycle feedback, which is major source of uncertainty in future temperature projections [Rahmstorf 2007b].

After the release of the AR4, different studies confirmed that IPCC projections are conservative. Pfeffer and al. [Pfeffer 2008] performed a deep glaciological study of the movements and constraints of glaciers. The study showed that values exceeding one meter are absolutely possible with an upper bound of 2 meters, above which the values become "physically untenable ". Recent observations indicate that sea level is currently rising near the upper end of the AR4 projections [Vermeer 2009], which suggests that the IPCC projections, expected to be accurate for the first two decade of the 21st century, are underestimated.

The lack of understanding of the complete processes involved in the SLR has led researchers to resort to alternative approaches in assessing the contribution of the sea-level rise components and, mainly, the two major glaciers. Two approaches have been proposed: the semi-empirical approach and climate expert elicitation. The semi-empirical approach was initiated by Rahmstorf [Rahmstorf 2007a, Vermeer 2009, Rahmstorf 2012], who used the relationship between historical temperature and sea-level to project the sea-level in the 21st century based on the IPCC temperature projections (which are among the best assessed variables in the CGCM). The second approach is expert elicitation, which has been investigated recently by Bamber and Aspinall [Bamber 2013]. By performing a formalised pooling of 13 climate expert assessments of future ice-sheet contributions, they derived, among other results, a probability distribution of the global sea-level rise rate induced by both ice sheets in 2100. Both methods are described in what follows.

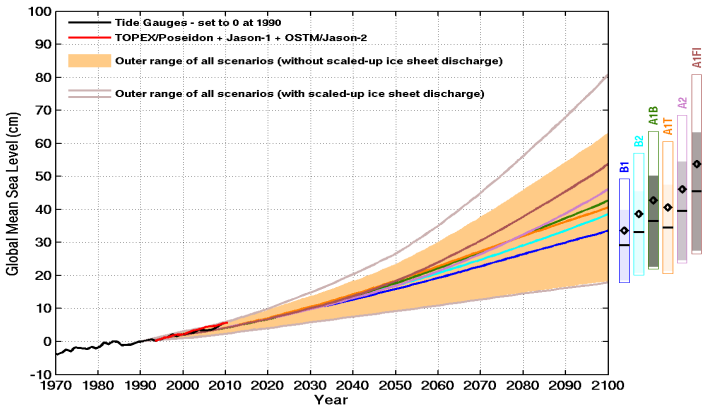

Figure 2.5: Projections of global averaged SLR from 1990 to 2100 and the observational estimates of global-averaged sea-level (based on tide-gauge measurements (black) and satellite-altimeter data (red)). The shaded region (respectively the region delimited by the upper and lower curves) represents the full range of projections without (respectively, with) scaled-up ice sheet discharge. Continuous colored lines represent the central value of the projections including the ice flow acceleration. The vertical bars indicate the range of the projections at year 2100, with the horizontal lines (diamonds) showing the central values without (with) the ice dynamics (source [IPCC 2007]).

3.2.2 Past observations to predict the future: the semi-empirical approach

The semi-empirical approach is based on linking, via a simple model, a standard diagnostic used to describe global warming (e.g., temperature, CO_2 projections) to the response of interest, here, the mean sea-level or the rate of sea-level rise.

With the second-most-cited paper of the 10,000 sea-level rise papers published since 2007 [Rahmstorf 2013], Rahmstorf is the pioneer of this approach. He proposed, in [Rahmstorf 2007a], relating the global temperature (one of the more accurate and best assessed variables in the CGCM) to the sea level through the following differential equation:

$$\frac{dH}{dt} = a(T - T_0), \tag{2.1}$$

where H represents the sea level, a is a proportionality coefficient, T represents the global average near-surface air temperature deviation (anomaly) from the 1950-1980 average and T_0 is the base equilibrium temperature (a baseline temperature at which the sea level is in equilibrium with climate). In 2009, he revisited the initial model in [Vermeer 2009] by including an instantaneous response:

$$\frac{dH}{dt} = a(T - T_0) + b\frac{dT}{dt}, \tag{2.2}$$

where b is the instantaneous response proportionality coefficient. The first term in the right part of Equation (2.2) describes the long-term response of climate com-

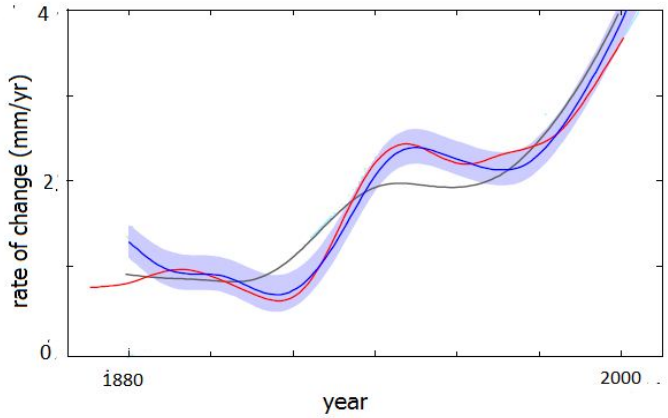

Figure 2.6: Observed rate of sea-level rise (red) compared with reconstructed sea level calculated from global temperature (dark blue with light blue uncertainty range). The grey line is reconstructed sea level from an earlier, simpler relationship between sea level and temperature (source [Vermeer 2009]).

ponents. The second term in Equation (2.2) describes the instantaneous response of climate components that adjust quickly to temperature rise, such as the oceanic surface mixed layer. The latter model will be denoted RV09 for the remainder of the dissertation.

By comparing the historical records of sea-level rise from 1880 to 2000 with the simulation results using Equation (2.2), the authors showed that the proposed relationship between sea-level and global temperature is robust. Figure 2.6 shows a satisfactory correlation between the observed (red line) and the reconstructed (dark blue line with light blue uncertainty range) sea-level rate. Global temperature projections, which are calculated with greater confidence, can be used to simulate sea-levels in the future for different emissions scenarios. Figure 2.7 shows the projected sea level-rise for three different SRES scenarios. The semi-empirical method predicts a sea-level rise roughly three times greater than the IPCC predictions, indicated by the vertical bars in the bottom right. The sea level is expected to rise by approximately one meter by 2100 for the lowest emission rate by approximately 1.4 meters for the highest emission rate.

The semi-empirical models provide higher sea-level projections than the process-based models. Higher projections than the process-based ones are consistent with recent estimates published since the release of the last IPCC report in 2007, such as, for instance, its last Draft Report [IPCC 2013] that revises upward the projections of 2007, the Antarctic report [Turner 2009a] or the US National Climate Assessment (projections ranging from 40 cm to 2 m). Higher projections are also consistent with the observational records in the latest two decades, which are underestimated by the process-based models. Another argument in favour of the semi-empirical method is the kinematic study of glacier movements by Pfeffer [Pfeffer 2008].

The climate community is quite reluctant to use the semi-empirical approaches.

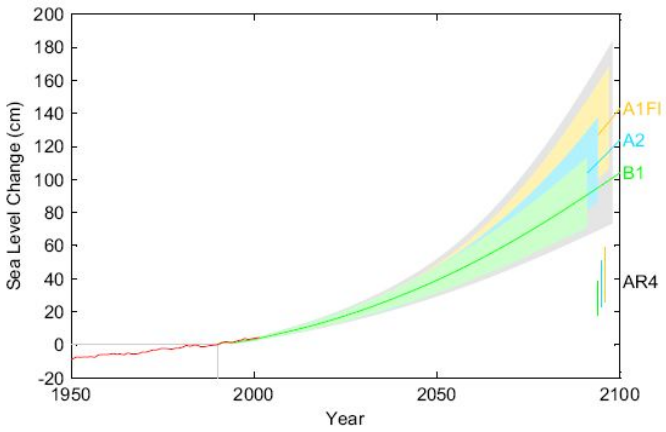

Figure 2.7: Projection of sea-level rise from 1990 to 2100, based on IPCC temperature projections for three different emissions scenarios (labeled on right). The sea-level range projected in the IPCC AR4 (2) for these scenarios is shown for comparison in the bars on the bottom right. Also shown in red the observations-based annual global sea-level data (source [Vermeer 2009]).

Rahmstorf's model has attracted some controversy mainly because of the lack of physics behind it, and a number of issues have been raised about the statistical analysis [Schmith 2007, Holgate 2007] (this point will be discussed in further detail in the next Chapter). However, the empirical method should be seen as an interesting alternative for modelling climate components that lack physical understanding. As noted out by Rahmstorf [Rahmstorf 2013], semi-empirical models are not better than the process-based approach, but by providing higher projections, they only show that "the uncertainty in future sea-level-rise is probably larger than previously estimated ".

Together with the semi-empirical approach, climate expert elicitation has been investigated starting from the last decade as a second alternative to tackle the immaturity of the physical models in representing some climate aspects.

3.2.3 Climate expert elicitation

In many engineering and environmental applications, when the available information about a variable of interest is very poor (due to poor empirical evidence, unobservability, or a limited understanding, etc.), soliciting experts and gathering their judgments on the uncertain quantities may be the only way to get a body of evidence [O'Hagan 2006]. This is held by a formally structured, protocol-based process called Expert Elicitation (EE), which is recognized as a particular form of scientific data. This method has been investigated in climate-related assessments to gain additional insight into poorly known climate variables [Morgan 1995, Kriegler 2005, Zickfeld 2010, Morgan 2006, Reilly 2001].

Bamber and Aspinall [Bamber 2013] carried out an expert elicitation to address the uncertainty induced by the least consensual component: the melting of the

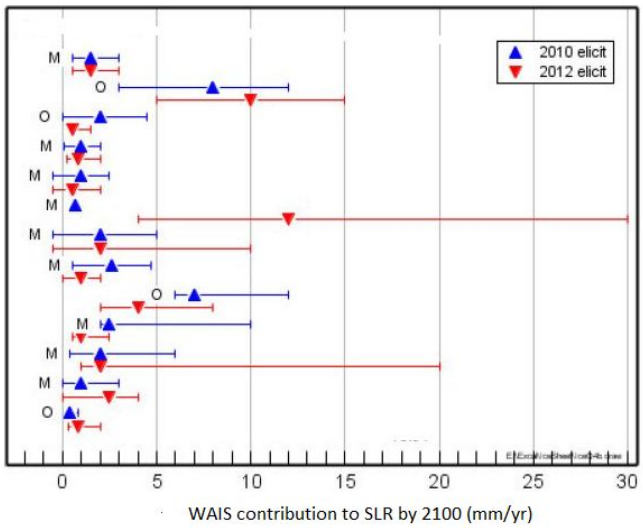

Figure 2.8: Range graph plots showing the individual responses by experts (modelers (M) and observers (O)) to the key quantitative question about the contribution of the WAIS to the total sea-level rise rate by 2100 in the 2010 survey (blue) and repeat 2012 survey (red) (source [Bamber 2013]).

ice sheets. They conducted a survey with 13 leading climate experts, classified as observational scientists (4) and modellers (9), who have informed opinions on the behaviours of the ice sheets. The experts answered 11 questions focused on the behaviour of each of the ice sheets in the coming centuries as well as two questions on the ice sheets' global sea-level rise rate in the previous century and in the last decade. The responses to these two questions, of which the true answers are known, were used to evaluate the performance of the experts. The survey was first conducted in 2010 and then repeated in 2012 for two purposes: (1) to assess the evolution of experts' knowledge and (2) to measure the stability of their answers.

The experts were solicited to assess the projections of the contribution of the ice sheets to the global sea-level rise rate by the end of the century. The answers were requested for the EAIS, WAIS and GrIS individually because the controlling processes are different for each ice sheet. For each qualitative question, each expert described his belief about the parameter of inquiry using a best estimate value and the upper and lower bounds of the 90% credible range. The lower 5th and upper 95th percentiles are equivalent to the qualitative statements *"virtually certain not to fall above this value "* and *"virtually certain not to fall below this value"*. The results collected for the question related to the sea-level rise rate induced by the West Antarctica ice sheet (WAIS) by 2100 are shown in Figure 2.8. Are reported in this range graph plot the lower, upper and best estimate values of the WAIS contribution to SLR rate by 2100, by each of the experts in 2010 survey (blue) and 2012 survey (red). Similar responses on the contribution of the eastern part of the Antarctica and the Greenland ice sheets were collected.

These quantiles were used to construct individual elementary probability distri-

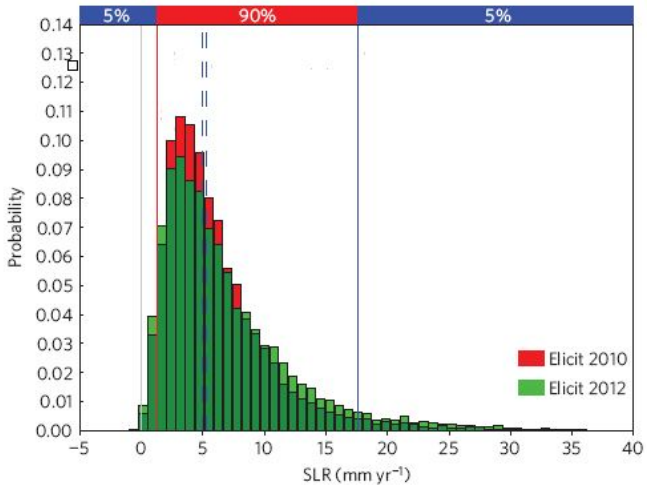

Figure 2.9: PDF of the rate of SLR due to ice-sheet contributions by year 2100. Red is the PDF for the 2010 elicitation, and green is the PDF for 2012 elicitation (source [Bamber 2013]).

butions for each question, and these distributions were then combined with different combination modes (equal weights and differential expert pooling weights). For the total SLR contribution, the estimates for the three ice sheets were aggregated using Monte-Carlo re-sampling to produce a single overall rate. The resulting PDF for the rate of SLR due to ice-sheet contributions by the year 2100 is represented in Figure 2.9, which shows that the median total SLR rate in the year 2100, indicated by the discontinuous blue line, is 5.4 mm/yr. The 90% probability range indicated by the vertical red and blue lines indicates a 90% confidence range of $1.35 - 17.6$ mm/yr. The rate was then integrated assuming a linear increase of the SLR rate from 2000 and the overall contribution of the ice sheets to the total SLR by 2100 was estimated. The authors found that the median estimate of the contribution of the ice sheets in the future sea-level rise is 29 cm larger than that in the AR4, while the upper 95th percentile has a value of 84 cm. These results, when combined with the median estimates of the thermal expansion and land ice melting contribution, imply a conceivable risk of sea-level rise greater than one meter by the end of the century.

4 Conclusion

In this chapter, we described the main approaches to assessing the future sea-level rise in the next several decades. The three methods lead to quite different projections based on specific assumptions. The process-based models provide the smallest projections, ranging from 0.18 to 0.79 m, under the assumption of a stable mass loss rate of the Greenland and Antarctica ice sheets during the next century. Kinematic

studies of glacier movements confirm that the IPCC projections are too conservative and suggest that the sea-level rise could reach two meters by the end of the century. A higher contribution of the major ice sheets to the global rate of sea-level rise has also been confirmed by expert elicitation assessment and by semi-empirical models performed by Rahmstorf that calculate the likely range of values for SLR by the end of the century to be $[0.3, 1.3]$ and $[0.5, 1.4]$ m, respectively.

The three methods for assessing future climate impacts lead to different results, which suggests that uncertainty in future projections is very large. It is essential to recognise and account for this uncertainty in policy and risk analyses.

Part III

Quantifying uncertainty in future sea-level projections

This chapter is concerned with the assessment of future sea-level rise (in particular, projections by 2100) using belief functions. Projections are derived based on the three approaches described in the previous chapter, i.e., the process-based, the semi-empirical and the expert elicitation methods. Each of these methods involves different types of evidence (statistical evidence, expert evidence, or both), and requires different tools to represent, combine, and propagate them. The objective of this chapter is to describe and illustrate how the belief functions formalism can be used in the assessment of uncertain climate quantities from incomplete information.

1 Process-based projections

Future SLR projections as reported in the AR4 by the IPCC are obtained using multi-dimensional climate models that depend on many poorly known parameters (climate sensitivity, aerosol forcing, GHGs, etc.). Assessing the likelihood of the sea-level response to the global warming given the deep uncertainty on some of the models key inputs and the model themselves is a challenging question. Several authors tackled the issue and used different methods to assign probabilities to future SLR projections. Titus and Narayanan [Titus 1995] were the first to provide probability based projections. They used simple a one-dimensional climate model and quantified uncertainty on the key model parameters based on subjective probability distributions supplied by a cross-section of climate experts who were mostly authors of the previous versions of the IPCC assessment reports. The probabilistic assessment suggests that a sea-level rise ranging between 10 and 65 cm by 2100 has a 80% probability of occurrence, while there is a 99% chance that it will not exceed 104m.

We propose to use belief functions to assess future SLR projections provided by process-based models. A principled approach would be to quantify available knowledge about climate parameters by belief functions constructed using elicitation methods as described in [Ha-Duong 2008], and to propagate these belief functions in numerical models as done in [Kriegler 2005]. An alternative approach is to directly represent final conclusions on the SLR parameter, as reported in the recent literature, in the form of a belief function.

The process-based projections of the SLR in the coming century can be summarised by the IPCC estimates and the upper bound based on kinematic constraints of glacier outlet velocities reported by Pfeffer [Pfeffer 2008]. According to these two sources, the likely range of values for SLR over the $1990-2095$ period is $[0.18, 0.79]$ meters (not excluding higher values), and the upper limit is two meters. These estimates cover the range of the different scenarios of future greenhouse gas emissions. As it was mentioned previously, no likelihood degrees are attached to the sea-level rise trajectories as the panel refrained from assigning probabilities to the emissions scenarios and to the climate models used to calculate the projections.

The information provided by both sources may be represented by any belief function verifying $Bel([0, 2]) = 1$ (values outside the range $[0, 2]$ are impossible) and $Pl([0.18, 0.79]) = 1$ (the interval $[0.18, 0.79]$ is entirely plausible). In the absence of

more precise information, the most reasonable approach is to carry out some form of sensitivity analysis by considering different belief functions satisfying these two constraints.

Here, we will consider three types of random intervals:

1. Consonant random intervals with core $[0.18, 0.79]$, support $[0, 2]$ and contour plausibility function π defined by

$$\pi(x) = \begin{cases} \phi\left(x/0.18\right) & 0 < x \leq 0.18 \\ 1 & 0.18 < x \leq 0.79 \\ \phi\left(\dfrac{2-x}{2-0.79}\right) & 0.79 < x \leq 2 \\ 0 & \textit{otherwise}, \end{cases} \tag{3.1}$$

   where ϕ is a continuous, non decreasing function from $[0, 1]$ to $[0, 1]$ such that $\phi(0) = 0$ and $\phi(1) = 1$ (see Figure 3.1(a)).

2. P-boxes with upper and lower bounding functions defined, respectively, as follows:

$$\overline{F}(x) = \begin{cases} 0 & x \leq 0 \\ \phi\left(\frac{x}{0.18}\right) & 0.18 \leq x \\ 1 & x > 0.18, \end{cases} \tag{3.2}$$

   and

$$\underline{F}(x) = \begin{cases} 0 & x \leq 0.79 \\ 1 - \phi\left(\frac{2-x}{2-0.79}\right) & 0.79 < x \leq 2 \\ 1 & x > 2, \end{cases} \tag{3.3}$$

   as shown in Figure 3.1(b).

3. Random closed intervals $[U, V]$, such that U and V are independent and have cumulative distribution function (CDF)s $\overline{F}$ and $\underline{F}$ defined, respectively, by equations (3.2) and (3.3).

For given ϕ, the bounds of all these random intervals have all the same marginal distributions $\overline{F}$ and $\underline{F}$. Consequently, their plausibility and belief functions coincide on all intervals of the form $(-\infty, x]$, since

$$bel((-\infty, x]) = P(V \leq x) = \underline{F}(x) \tag{3.4}$$

and

$$Pl((-\infty, x]) = P(U \leq x) = \overline{F}(x). \tag{3.5}$$

More generally, their plausibility functions coincide on all closed intervals since, for all $x \leq y$,

$$Pl([x, y]) = 1 - P(V < x) - P(U > y); \tag{3.6}$$

which only depends on the marginal distributions of U ad V. In particular, they have identical contour function $pl(x) = Pl([x, x])$. In contrast, degrees of belief $Bel([x, y])$ depend on the joint distribution of U and V as:

$$Bel([x, y]) = P((V < y)\&(U > x)). \tag{3.7}$$

These quantities have the folloing expressions:

$$Pl_\pi([x,y]) = Pl_{[\underline{F},\overline{F}]}([x,y]) = Pl_{[U,V]}([x,y]) = \max(0, \overline{F}(y) - \underline{F}(x)); \tag{3.8}$$

$$\begin{aligned} Bel_\pi([x,y]) &= \min(1 - \sup_{t<x} \pi(t), 1 - \sup_{t>y} \pi(t)) \\ &= \min(1 - \overline{F}(x), \underline{F}(y)); \end{aligned} \tag{3.9}$$

$$Bel_{[\underline{F},\overline{F}]}([x,y]) = \max(0, \underline{F}(y) - \overline{F}(x)); \tag{3.10}$$

and

$$Bel_{[U,V]}([x,y]) = \underline{F}(y)(1 - \overline{F}(x)). \tag{3.11}$$

Let's compare the precision of these three representations. For given ϕ and for every interval $[x,y]$ such that $0 \leq x \leq y \leq 2$, it is clear that:

$$\max(0, \underline{F}(y) - \overline{F}(x)) \leq \underline{F}(y) - \underline{F}(y)\overline{F}(x) \leq \min(\underline{F}(y), 1 - \overline{F}(x)), \tag{3.12}$$

Thereby:

$$Bel_{[\underline{F},\overline{F}]}([x,y]) \leq Bel_{[U,V]}([x,y]) \leq Bel_\pi([x,y]). \tag{3.13}$$

This inequality suggests that the most precise representation is the consonant belief function, followed by the random closed interval, and then by the P-box. Precision here refers to the size of the set of probability measures $\mathcal{P}$ that a belief function encodes:

$$\mathcal{P} = \{P | Bel(A) \leq P(A) \leq Pl(A)\} \tag{3.14}$$

for every set A in the σ-algebra $\mathcal{A}$. Given that the upper measure (Pl) is the same for the three sets, inequality (3.13) leads to the following relation:

$$\mathcal{P}_{[\underline{F},\overline{F}]} \subseteq \mathcal{P}_{[U,V]} \subseteq \mathcal{P}_\pi. \tag{3.15}$$

For this particular case, the inclusions are strict. Baudrit [Baudrit 2005] conducted a formal comparison of the expressitivity of some imprecise probabilities models. He demonstrated in particular that the set of probabilities induced by a consonant belief function (i.e., a possibility measure) is a strict subset of the set of probabilities encoded by the P-box generated by this belief function (i.e., the P-box defined by: $\underline{F}(x) = Bel(]-\infty, x])$, and $\overline{F} = Pl(]-\infty, x]))$.

In the following, we considered three different functions ϕ: linear ($\phi(x) = x$), convex ($\phi(x) = x^2$) and concave ($\phi(x) = \sqrt{(}x)$). The corresponding contour functions and cumulative distributions (via Equations (3.5) and (3.4)) are shown, respectively, in the left and right panels of Figure 3.1. Figures 3.3 and 3.2 show, respectively, a contour plot of $Pl([x,y])$ and $Bel([x,y])$ for $-0.5 \leq x \leq y \leq 2.5$ (for the particular case of a linear ϕ).

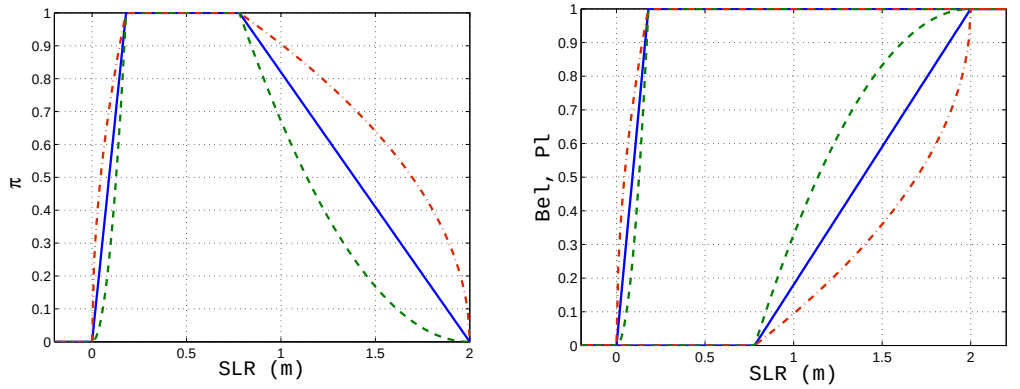

(a) (b)

Figure 3.1: Contour functions (a) and upper and lower cdfs (b) of random sets on SLR in 2100 with respect to 1990 for different forms of function ϕ ($\phi(x) = x$ (–), $\phi(x) = x^2$ (-) and $\phi(x) = \sqrt(x)$ (-.).)

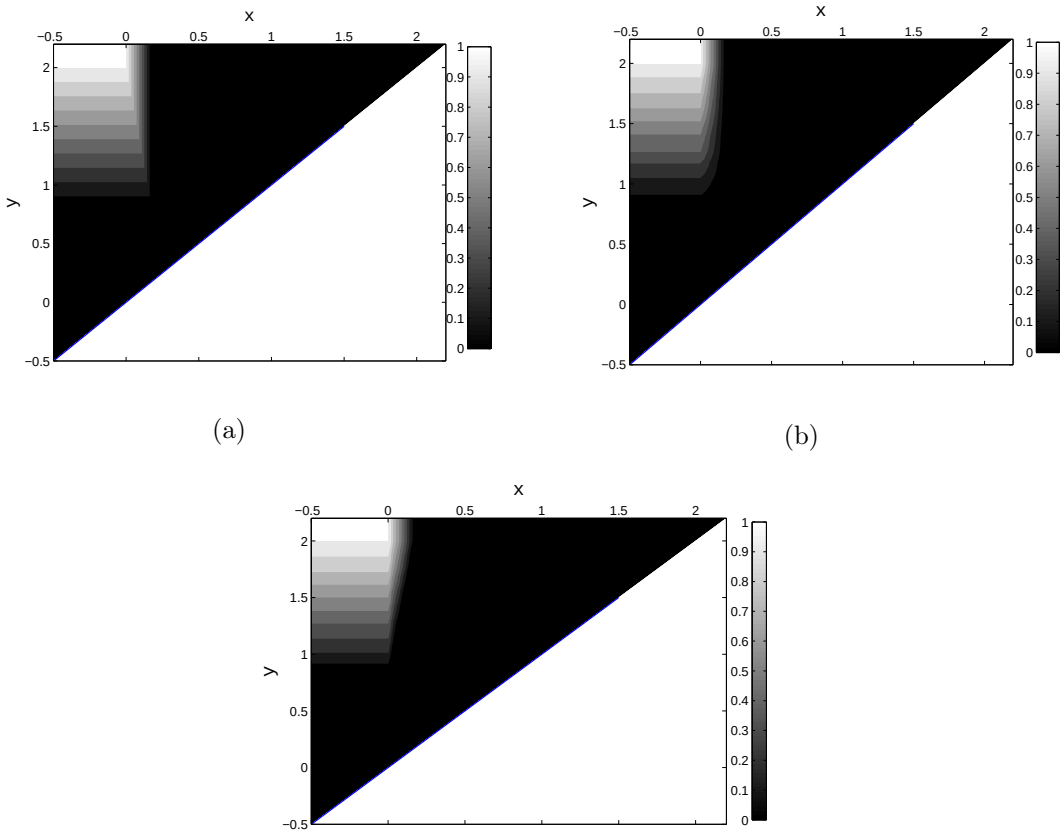

(a) (b)

(c)

Figure 3.2: Contour plot of beliefs $Bel(SLR \in [x, y])$ for the consonant belief function (a), closed random interval (b) and p-box (c) on SLR by 2100 (wrt 1990) $\phi(x) = x$.

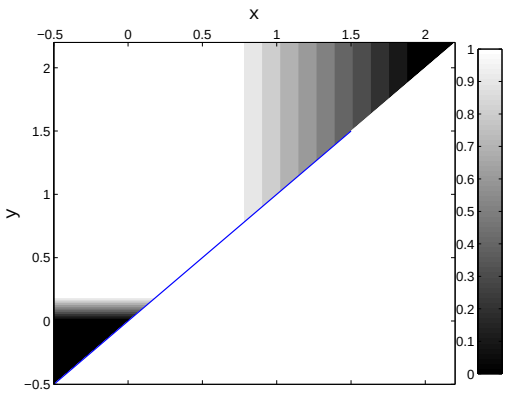

Figure 3.3: Contour plot of plausibilities $Pl(SLR \in [x, y])$ for the three types of random intervals on SLR by 2100 with respect to 1990 for $\phi(x) = x$.

We can see from the last figures that the results are very similar for the three types of random intervals, which confirms that the particular choice of random interval has a minor influence on the results, provided that the core and the support are the same. The cumulative probability of the SLR in 2100 is bounded by the upper (plausibility) and lower (belief) distributions. If we infer a probability distribution over the SLR projections by the IPCC and Pfeffer, the resulting cumulative distribution (i.e., the probability of non-exceeding) will be bounded by the belief and plausibility distributions. According to Figure 3.1, for a linear ϕ, the probability that the SLR by 2100 wll be less than one meter by 2100 is between 0.2 and 1 .

2 Projections derived from statistical fit to historical data

Since the release of the AR4, many authors have investigated the semi-empirical approach to address the prediction gap of the process-based models. In 2009, Rahmstorf and Vermeer [Vermeer 2009] proposed a model that linearly links the rate of global sea-level rise to global temperature. According to this model, the sea-level rise can be described by Equation (2.2) or, equivalently, by a discretised version of the differential expression:

$$\frac{\Delta H}{\Delta t} = a(T - T_0) + b\frac{\Delta T}{\Delta t}, \tag{3.16}$$

where T is the temperature anomaly relative to the $1950 - 1880$ average, and a, b, and T_0 are the model parameters. In the following, we consider, as in [Vermeer 2009], a yearly incrementation, i.e., $\Delta t = 1$ year.

The model is partially empirical as it describes a simple physically-motivated relation that is then calibrated statistically with historical data of both global temperature and sea level. Assuming that this relationship will still hold in the coming

century, future temperatures are injected into the model, and projections of the sea-level rise (rate) can be estimated.

Two sources of uncertainty are involved in these SLR projections. The first is statistical and stems from the model parameters a, b and T_0. The second is epistemic and pervades the model drivers, i.e., the (imprecise) temperature projections. We propose in the following to quantify both uncertainties, combine them and estimate the model response in the DS framework.

2.1 Analysis method

We begin by conducting a statistical calibration of the model, using the same data as in [Vermeer 2009], to estimate the model parameters a, b and T_0. The model calibration is based on a time series analysis. Basic concepts are briefly recalled in an informal way in the Appendices, section 2.

The relationship proposed by Rahmstorf was calibrated with observed data sets of global sea-level and temperature for an overlapping period for both series ranging from 1880 to 2001. For temperature, we used the best global coverage data available in the literature, i.e., the National Aeronautics and Space Administration (NASA) Goddard Institute for Space Studies (GISS) dataset, which is a monthly time series from 1880 to 2010 (the datafile is accessible and can be downloaded from the GISS Internet website). The GISS analysis uses 1951-1980 as the base period. For global mean sea-level, we used the 2006 version of the data by Church and White [Church 2006]. Church and White used a combination of local tide-gauge records from around the world and satellite-altimeter data to reconstruct the global sea level from 1870 to 2001 (the data file is accessible and can be downloaded from the permanent service for mean sea level (PSMSL) Internet website (http://www.psmsl.org/products/reconstructions/church.php). Again, the time series is monthly. The global data were processed as annual means. The sea-level data were corrected by including water volumes impounded in the world's artificial reservoirs [Chao 2008]. The authors derived from Chao's results on artificial reservoir storage an analytical expression of the reservoir correction effects:

$$\Delta H = 1.65 + (\frac{3.7}{3.14}) \arctan(\frac{t - 1978}{13}), \tag{3.17}$$

where ΔH is the increase of the sea level (in cm) induced by the reservoir storage effects and t is the year of observation.

The annual temperature anomaly relative to the 1950-1980 average and the corrected sea-level data (reconstructed and corrected versions) are represented, respectively, in the right and left panels of Figure 3.4.

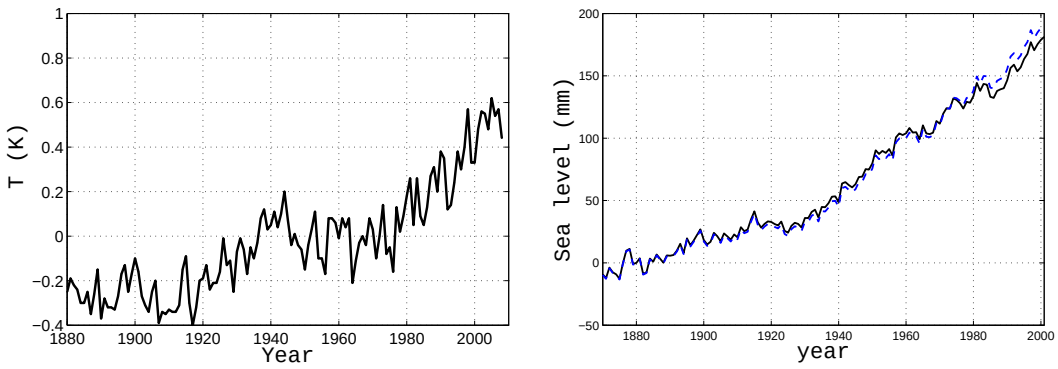

(a) (b)

Figure 3.4: (a) GISS annual temperature anomaly relative to 1950-1980 average. (b) Church and White annual sea-level data (-) and corrected data (- -) from 1870 to 2001 (relative to 1880 estimate).

To remove the short-term noise, which is unrelated to the climate signal, the time series need to be smoothed. Rahmstorf suggests smoothing the time series with a 15-year smoothing period using the singular spectrum analysis (SSA) decomposition [Moore 2005]. This filter was developed to analysing geophysical time series, such as tide gauge records. The authors' choice to use a 15-year embedding period was based on a sensitivity analysis to the smoothing period. The analysis showed that periods less than 10 years would fit the parameters to variability noise, whereas values higher than 20 years would lead to a smoothing of important anthropogenic parts of the signal [Rahmstorf 2007a]. We adopted this smoothing technique to filter both the annual temperature and annual sea-level datasets. The smoothed time series along with the raw data (marked by stars), are plotted in Figures 3.5 and 3.6.

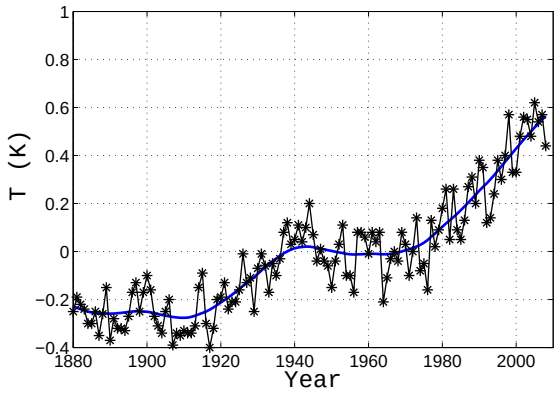

Figure 3.5: GISS annual temperature anomaly (marked by stars) and smoothed data (-) from 1880 to 2010.

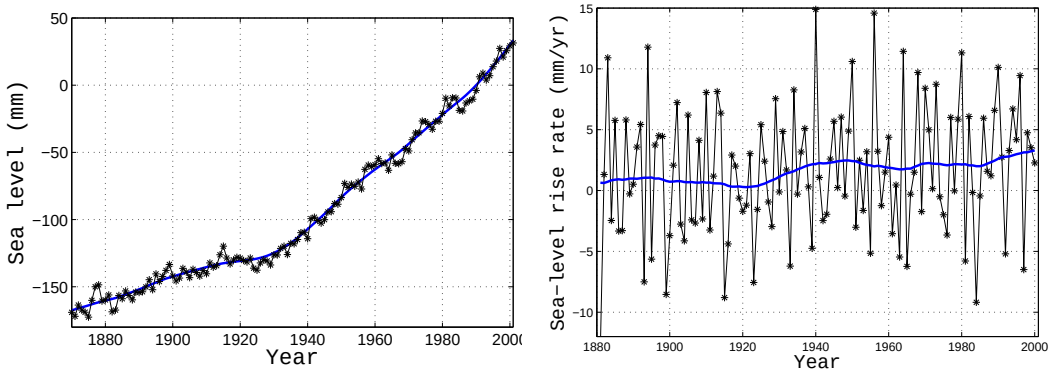

(a) (b)

Figure 3.6: Church and White annual sea-level (relative to 1990 estimate) (a) and sea-level rate (b) from 1870 to 2001: raw data (stars) and smoothed data (-).

After preparation of the data, the second step is to fit the differential Equation (2.2). As the regression is performed on time series data, the errors may not be independent. Autocorrelation of the errors is problematic and particular attention should be paid to it.

Rahmstorf used two different methods for fitting the differential equation. In a first analysis [Vermeer 2009], he proposed a binned fit, i.e., he binned both (smoothed) time series using a 15-year window. The objective behind binning data is to remove correlation between residuals, a residual being the difference between the observed sea-level rates and the fitted values. Then, he performed a linear regression without taking into account the residuals time series structure.

Many statisticians, including Schmith [Schmith 2007], Holgate [Holgate 2007] and Guttorp [Guttorp 2012], have discussed and challenged certain aspects of the statistical approach. Guttorp detected a "poor statistical practice in fitting" the model. Holgate and Schmith argued against binning data and suggested including a time series analysis for a thorough analysis of the problem of projected sea-level rise.

In a revisited version of the first paper [Rahmstorf 2012], the authors took into account the criticisms and provided a more robust method for fitting the differential equation. Instead of using binned fit, they accounted for the residuals' time series structure. They performed a generalised least squares fit assuming the residuals to have an first order autoregressive process (AR1) correlation structure.

In this study, we adopted the second approach, i.e., we fitted the RV09 equation using annual rather than binned data. Working with non-binned data involves the difficulty of characterising the residuals' time series structure, which tends to be complex. A time series analysis of the residuals (plotted in Figure 3.7) from an ordinary least squares fit of the regression was performed. Visual analysis of the empirical auto-correlation function (ACF) and partial auto-correlation function (PACF) in correlogram 3.8 confirms that the correlation structure can not be described by a

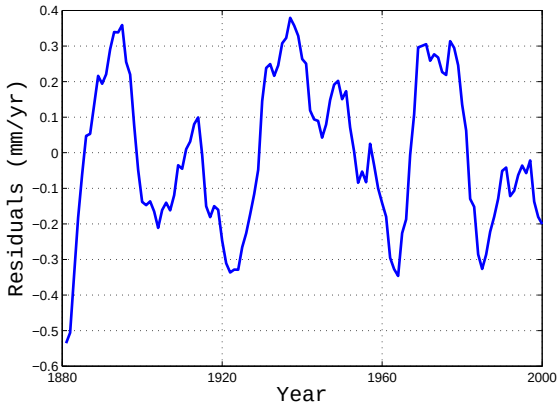

Figure 3.7: Residuals plot.

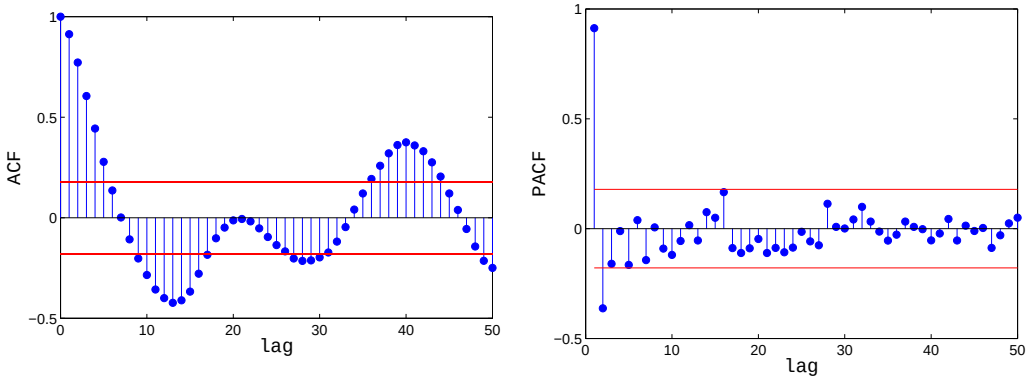

(a) (b)

Figure 3.8: Correlation (a) and partial autocorrelation (b) functions for the residuals from the ordinary least squares fit. Dotted horizontal line is the approximate confidence interval $\pm 2/\sqrt{n}$.

simple model (e.g., white noise, AR(p)). Recently, Guttorp [Guttorp 2012] published a paper in which he throughly analyzed the residuals time series structure of Rahmstorf's initial model (2.1). He suggested an autoregressive moving average (ARMA) process of order $(2, 2)$ to describe the correlation between the errors.

In this analysis, we assumed the model residuals $r = (r_1, ...r_n; n = 120)$ to be a Gaussian white-noise. We are conscious that not taking the dependence structure into account over-estimates the uncertainty, and that a thorough analysis requires a more proper residual analysis. This issue is beyond the scope of this work.

Based on this hypothesis, we performed an ordinary least squares regression. The best-fit in the least-squares sense minimises the sum of the squared residuals S:

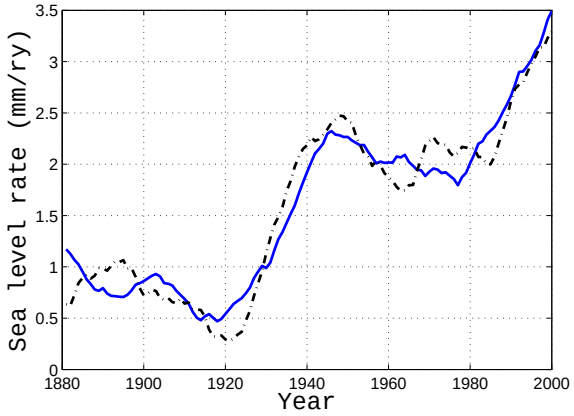

Figure 3.9: Observation-based rate of sea-level (-) compared with that predicted by RV09 (- -).

$$S = \sum_{i=1}^{n} r_i^2 = \sum_{i=1}^{120} (\Delta H(i) - (a(T(i) - T_0) + b\Delta T(i)))^2, \tag{3.18}$$

where $\Delta H(i)$ and $T(i)$ $(i = 1, ..., 120)$ are, respectively the observed sea-level rate and temperature anomaly at year $i + 1980$.

It is known that ordinary least-squares and maximum likelihood estimates are identical for normally-distributed residuals [Charnes 1976]. Thus, minimising S in Equation (3.18) is equivalent to maximising the likelihood function of the residuals' statistical model, defined on the joint parameter space by:

$$L(a, b, T_0; r) = \frac{1}{(2\pi\sigma^2)^{\frac{n}{2}}} \exp\left(-\frac{\sum_{i=1}^{n} r_i^2}{2\sigma^2} \right) \tag{3.19}$$

with σ being the variance of the Gaussian noise signal.

Maximising Equation (3.19) gave the following maximum likelihood estimate (MLE)s: $\hat{a} = 5.2$ $(mm/yr \cdot K)$, $\hat{b} = -45$ (mm/K) and $\hat{T}_0 = -0.4$ (K), which are very close to the results by Rahmstorf ($\hat{a} = 5.6$, $\hat{b} = -49$ and $\hat{T}_0 = -0.41$). Figures 3.9 and 3.10 show the fit by plotting the annual observed sea level and sea-level rate with the predicted results. The result suggests a good fit with an overestimation for the period 1920-1940.

The results yield a negative value for the b parameter, which may seem surprising. Indeed, one expects that an increase in the temperature would cause an instantaneous increase in the sea level, rather than a decrease. The authors explained this counter-intuitive result by certain physical mechanisms that result in a time lag between the temperature rise and the sea-level response. They refrained from giving a more robust argumentation and description of these phenomena: "*Thus, the most plausible physical interpretation of our statistical fit is that the negative*

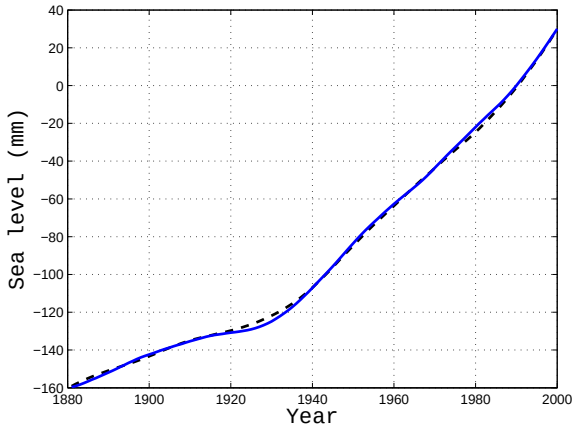

Figure 3.10: Observations-based sea level (-) and integrated fit of RV09 (- -).

value of b results from a positive ocean mixed layer response combined with a lag of over a decade in the response of the ocean-cryosphere system. Several mechanisms could be envisaged for a delayed onset of sea-level rise after warming. For example mass loss of ice sheets can be caused by warm water penetrating underneath ice shelves, triggering their collapse and subsequent speed-up of outlet glaciers banked up behind the ice shelf. We can not explore causes of delay in more details here, but note statistical result is robust irrespective to its causes" [Vermeer 2009]. Regarding the T_0 parameter, the results also yield a negative estimate. Note that this result is not counter-intuitive because all temperature measures in the model, including T_0, are estimated relative to a reference base period.

The objective of this section was to estimate the model parameters using the same data and broadly following the method described by Rahmstorf and Vermeer in their original paper. Because of our minor expertise in climate modelling and the opacity of the statistical analysis in [Vermeer 2009], we encountered certain difficulties in understanding some ideas underlying the original analysis. Because the objective of this thesis is to describe a methodology for uncertainty quantification in climate assessment rather than the fitting aspect, we allowed ourselves, for the sake of simplicity, to make some simplifying hypotheses when estimating the model parameters.

2.2 Quantifying uncertainty of the model statistical fit

The classical approach to uncertainty when estimating statistically parameters is based on the confidence intervals. We propose in the following to quantify the uncertainty in RV09 model parameters that stems from statistical fitting in the DS framework.

By normalising the joint likelihood function of the errors, we derive the corre-

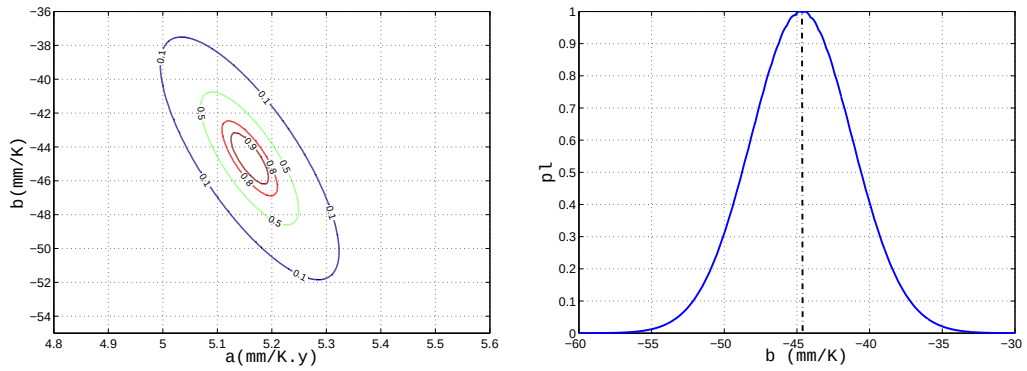

(a) (b)

Figure 3.11: (a): joint contour plausibility pl(a, b, $\hat{T}_0$). (b): Marginal contour plausibility $pl(\hat{a}, b, \hat{T}_0)$.

sponding joint contour plausibility according to Equation (1.54):

$$pl(a, b, T_0; r) = \frac{L(a, b, T_0; r)}{\sup\limits_{a,b,T_0} L(a, b, T_0; r)}. \tag{3.20}$$

The joint contour plausibility function has an ellipsoidal shape. By marginalising it according to T_0, we obtain the contour plausibility function of the joint random set on a and b :

$$pl(a, b; r) = \frac{L(a, b, \hat{T}_0; r)}{L(\hat{a}, \hat{b}, \hat{T}_0; r)}, \tag{3.21}$$

where $\hat{a}$, $\hat{b}$ and $\hat{T}_0$ are the MLEs. Again, by marginalising out a in $pl(a, b; r)$, we obtain the marginal contour plausibility for the b parameter. Figure 3.20 represents the respective results of the two marginalisation steps. The membership function for the b parameter has a Gaussian form and defines a consonant belief function. The maximum plausibility ($pl = 1$) is reached at the MLE of b. With the two-step marginalisation of the normalised joint likelihood, we can approximate the joint random set on (a, b, T_0), and we end up with three random intervals encoding evidence on each of the model parameters with the contour plausibilities plotted in Figures 3.20 and 3.12.

2.3 Representing evidence on future temperature projections

The IPCC last assessment report used 19 AOGCMs which differently formulate the physical processes controlling the climate components. Projections are represented by a central estimate and upper and lower bounds corresponding to the envelope over the circulations models and the carbon cycles. Figure 3.13 reproduces the IPCC

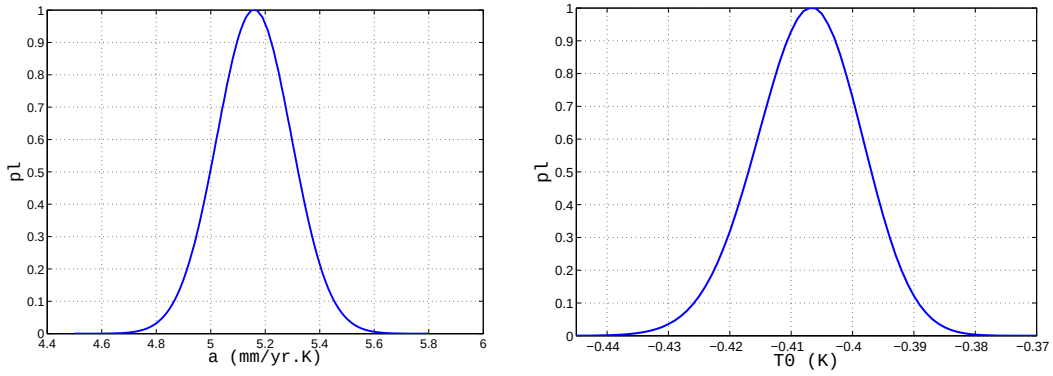

(a) (b)

Figure 3.12: Contour plausibility of the random set on the a (a) and T_0 (b) parameters.

temperature projections, shifted with respect to 1950-1980, for the particular A1B emission scenario.

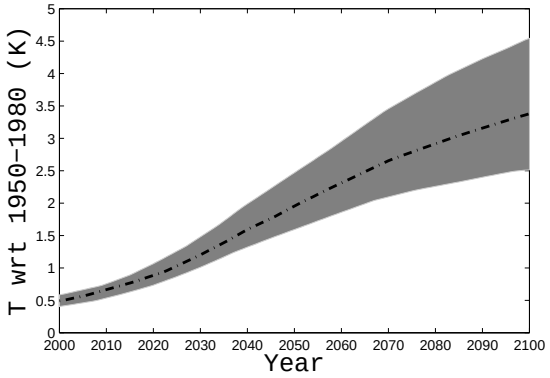

Figure 3.13: Reproduction of IPCC temperature anomaly projections relative to the 1950-1980 period for the A1B scenario: bold line represents central estimate whereas shaded region represents the full uncertainty range.

For each year t in the 2000-2100 time span, the available evidence thus consists in central (T_t), lower ($\underline{T}_t$) and upper ($\overline{T}_t$) estimates. Because no information is available on the likelihood of each of the AOGCMs, characterising a scenario in a deterministic way by selecting a specific trajectory, or doing so statistically by inferring a subjective probability distribution that would describe the likelihood of the trajectories lying in the outer envelope, would not be justified. In the DS framework, the available evidence can, however, be represented in a more natural way. The central estimate is assigned the maximum plausibility (or possibility) degree in the scenario, whereas values outside the outer envelope are viewed as impossible and assigned a null plausibility. The available evidence suggests representing the annual temperature projections at year t by a random interval Γ^t with core T_t, support

$[\overline{T}_t, \underline{T}_t]$ and contour function π defined by

$$\pi(x) = \begin{cases} \phi(\frac{x-\underline{T}_t}{T_t-\underline{T}_t}) & \underline{T}_t \leq x \leq T_t \\ 1 & x = T_t \\ \phi(\frac{\overline{T}_t-x}{\overline{T}_t-T_t}) & T_t < x \leq \overline{T}_t \\ 0 & \textit{otherwise}, \end{cases} \tag{3.22}$$

where ϕ is a continuous, non-decreasing function from $[0,1]$ to $[0,1]$ such that $\phi(0) = 0$ and $\phi(1) = 1$. In this analysis, we considered a linear membership function ϕ (i.e., $\phi(x) = x$, Figure 3.14). As discussed in the previous section, the choice of the form of ϕ is not crucial, and it does not need to be linear. In Figure 3.14, we represent the membership function π of random sets on the IPCC temperature anomaly in 2000, 2060 and 2100, as well as the ω-level cuts (according to Equation (1.19)), $\Gamma^t(\omega)$, for a random $\omega \in [0,1]$.

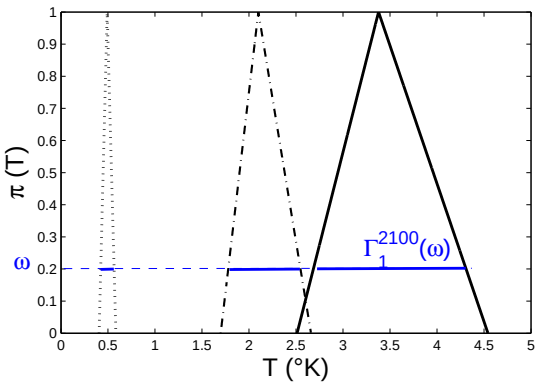

Figure 3.14: Contour functions and ω-level cuts of random sets on IPCC projected temperature anomalies in 2000 (..), 2060 (- -) and 2100 (-).

2.4 Propagation results: SLR projections

We constructed two independent random intervals, one encoding evidence on the RV09 model parameters and one encoding evidence on the temperature inputs. These random intervals were propagated through RV09. The combined evidence on the SLR model response was obtained by combining both random intervals according to the following scheme:

1. Pick at random ω in $[0,1]$. For every year $t \in [2000, 2100]$, derive the corresponding ω-cut from the contour plausibility associated with Γ^t: the ω-cut is an interval $[U_t^T(\omega), V_t^T(\omega)]$. Figure 3.15 (a) represents the consecutive cuts for $\omega = 0.167$.

2. Pick at random ω' in $[0,1]$. Obtain from the joint contour plausibility on the RV09 parameter space the corresponding ω'-cut. The joint ω'-cut can be

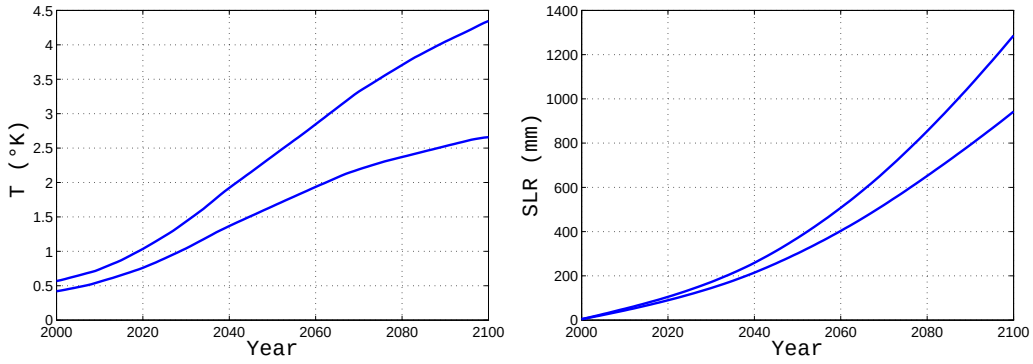

(a) (b)

Figure 3.15: (a) Consecutive ω-cuts of the random intervals on the annual temperature from 2000 to 2100. (b) Projected sea-level change in 2100 relative to 2000 (mm).

approximated by the product of three ω'-cuts on the marginal random intervals on a, b and T_0: $[U^a(\omega'), V^a(\omega')]$, $[U^b(\omega'), V^b(\omega')]$ and $[U^{T_0}(\omega'), V^{T_0}(\omega')]$.

3. Propagate the focal elements through RV09 and derive the upper and lower sea-level rise responses. The results of the propagation for $\omega = 0.167$ and $\omega' = 0.85$ are represented in the right panel of Figure 3.15.

This three-step process was repeated N (N=1,000) times. We obtained N intervals $[U_i, V_i]$ $(i = 1, ..., N)$ on the SLR by 2100. Belief and plausibility measures on the SLR at the end of the century can be approximated by

$$\hat{Bel}(I) = \frac{1}{N} \# \{1 \leq i \leq N | [U_i, V_i] \subseteq I\} \tag{3.23}$$

and

$$\hat{Pl}(I) = \frac{1}{N} \# \{1 \leq i \leq N | [U_i, V_i] \cap I \neq \emptyset\}. \tag{3.24}$$

For $I = (-\infty, x]$, the cumulative belief and plausibility functions were estimated and are plotted in Figure 3.16. The results of the three cases are compared: the curves in dashed-dotted blue lines correspond to the case where only the uncertainty in the model parameters is propagated and where the temperature was fixed to the best estimate values (i.e., T_t for every $t \in [2000, 2100]$). The green dashed curves are associated with the case where the projections are calculated with the MLEs of the RV09 parameters and random intervals on the temperatures. Continuous red represents the results when both uncertainties are combined. The dotted vertical line indicates the deterministic (mean temperature, best estimates parameters) results. We can see from these plots that the uncertainty in the SLR in 2100 is mainly due to the uncertainty in the future temperature projections.

For the A1B scenario, which reflects a medium to high emissions trajectory, the most plausible value for the sea level in 2100 is 109 cm. This is two times higher than the upper projections by the IPCC, including all emissions scenarios.

In this study, we illustrated the use of the DS theory in quantification and propagation through a model of statistical and expert evidence. Additional sources of uncertainty should be considered when deriving climate projections from semi-empirical models. Particularly, historical data used to fit the models, which are often subject to important errors.

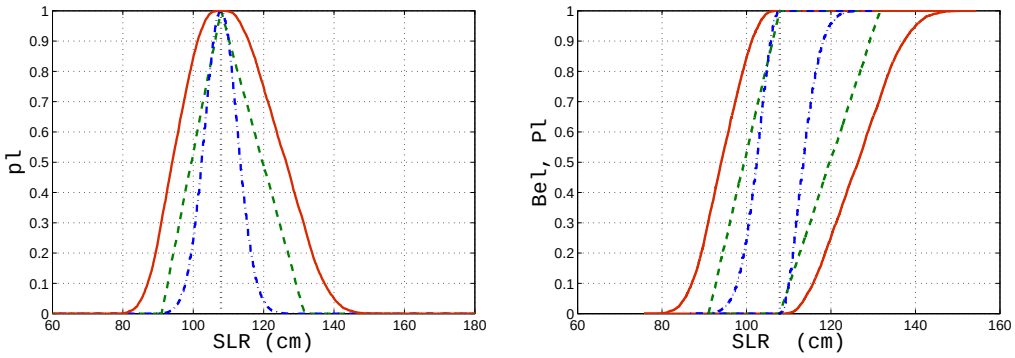

Figure 3.16: Contour plausibility (a) and cumulative plausibility and belief (b) of the SLR at the end of the century relative to 2000. Uncertainty induced only by IPCC temperature projections (green –), by statistical fit (blue .-) and by both model inputs and statistical fit (red -). Deterministic results are indicated by a dotted vertical line.

The semi-empirical approach raised controversy within the climate community because it resumes the very complex interactions between the climate components and the different time scales of the system response in a unique and simple relationship. Holgate [Holgate 2007] expresses scepticism to this approach: "we do not agree that simplistic projections of the nature presented contribute any understanding of the uncertainties in the non-linear relationships of the climate systems". This approach, by assuming that the future behaviour is entirely conditioned by the past behaviour, can not account for SLR components that have not been observed in the historical data. In particular, it can not reflect the acceleration of ice sheet dynamics observed in the last decade. While scientific research is ongoing to better understand and model physical processes controlling changes in ice sheets behaviour, experts' opinions can be thought of as a valuable source of scientific evidence.

3 Projections derived from climate expert judgments

Because of the absence of mature physical models that account for the ice dynamics and the scarcity of observational records (observations of the ice sheet mass balance go back to 1992), Bamber and Aspisnall [Bamber 2013] resorted to expert judgments to obtain qualitative and quantitative information about the contribution of both the Greenland and Antarctica ice sheets to global sea-level rise by 2100.

The quantitative questions had the following form: "What do you consider will be the lower/upper and best estimate contribution of the EAIS (WAIS and GrIS)

to SLR (in mm/yr) by 2100 ". Range graph plots of the individual responses by the experts to the question relative to each component in the 2010 survey (blue) and the 2012 repeat survey (red) are reproduced in Figure 3.17.

The authors used the setting of probability theory in assessing and pooling experts' opinions about the future contribution of the ice sheets to the total sea-level rise rate by the end of the century. The adequacy of probability theory in modelling subjective judgments, particularly in the climate field, has been challenged. For instance, Millner et al. [Millner 2012] conducted an empirical experiment to answer the question "*Do probabilistic expert elicitations capture scientist's uncertainty about climate change?*". They were particularly interested in assessing whether experts' knowledge about a poorly known climate parameter, climate sensitivity, can be captured by subjective probabilities elicited from the experts' beliefs. By comparing the elicited subjective probabilities with choices over bets with uncertain outcomes, they detected the existence of ambiguity in the experts' beliefs which made them violate axioms that must be satisfied for subjective probabilities to adequately describe their knowledge. They showed that existing elicitation studies, by automatically presupposing the existence of subjective probabilities, may qualitatively understate the extent of experts' uncertainty about climate change. The authors of the study recommended using alternative frameworks to represent experts' imprecision.

In this study, we proposed modelling expert opinions by means of belief functions, as they better reflect the lack of precision of expert knowledge than probabilities do. Different combination modes were then used to combine the individual assessments and the overall sea-level rise is finally estimated.

3.1 Representing expert judgments with belief functions

The first step of the analysis is to model the experts' knowledge. In the following, θ denotes the contribution of one amongst WAIS, EAIS and GrIS ice sheets to the global sea-level rise rate by the end of the century.

When asked about his belief regarding θ, each expert e_i $(i = 1, ..., 13)$ provided a median estimate as well as the lower and upper bounds of the 90% credible range denoted by $\theta^i_{50\%}$, $\theta^i_{5\%}$ and $\theta^i_{95\%}$, respectively.

The use of probabilities to represent this type of evidence is debatable. First, as there is no a unique probability distribution that is compatible with the evidence at hand (i.e., the group of three quantiles), the choice of a particular probability model in the set of the compatible models is arbitrary. Second, because it assigns an exact degree of belief to every single value, a probability model does not reflect the lack of precision of the expert knowledge. Alternative uncertainty models that better describe the imprecision in expert opinions without making subjective assumptions are preferable. Dubois et al. investigated in [Sandri 1995] the possibility theory to represent expert's knowledge. The authors formulated a model of expert opinions using possibility distributions derived from probabilistic estimates. Baudrit [Baudrit 2005] described different imprecise probabilities models to represent

imprecise information provided by experts (confidence intervals, quantiles).

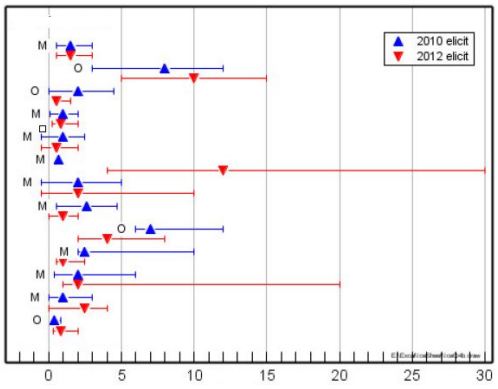

(a)

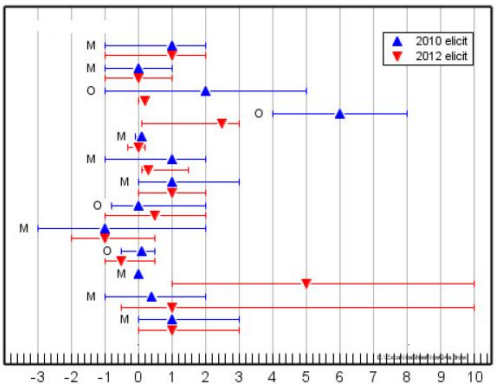

(b)

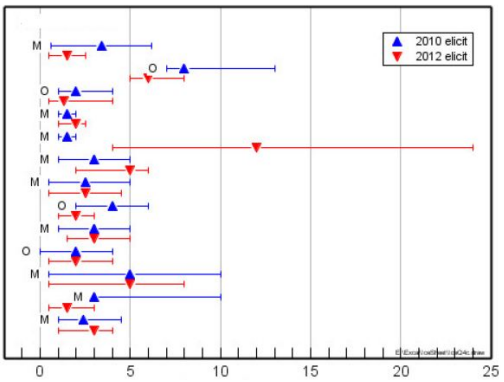

(c)

Figure 3.17: Range graph plots showing the individual responses by experts (modellers (M) and observers (O)) to the key quantitative question about the contribution of the WAIS (a), EAIS (b) and GrIS (c) (mm/yr) to the total sea-level rise rate by 2100 in the 2010 survey (blue) and the 2012 repeat survey (red). The triangular symbol indicates the best estimate, vertical bars delimit the 90% credible range (source [Bamber 2013]).

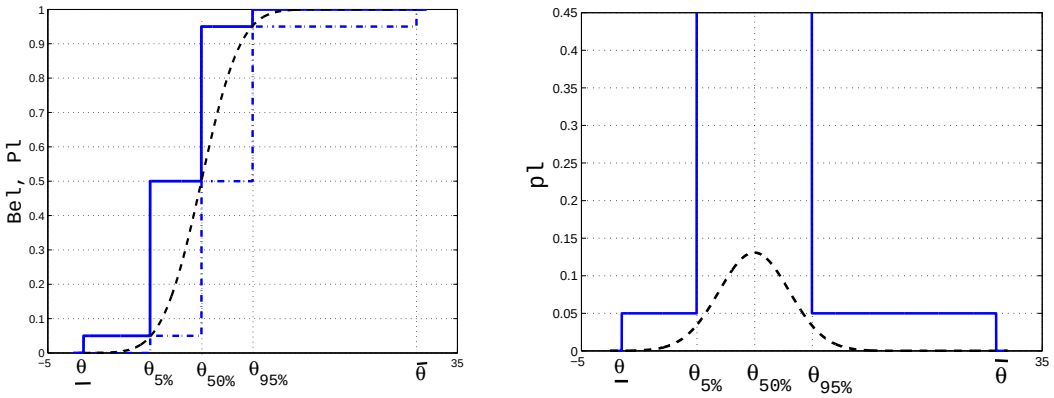

(a) (b)

Figure 3.18: Cumulative belief (-.-) and plausibility (-) (a), and contour plausibility (b) induced by the DS structure on θ. The dashed curves correspond to a probabilistic (Gaussian) description of the same information.

The frame of discernment of θ is $\Theta = [\overline{\theta}, \underline{\theta}] =]-\infty, +\infty[$. The information supplied by an expert e_i can be reformulated by the following: by giving the median estimate of θ, he distributes his belief on Θ equally between $]-\infty, \theta_{50\%}]$ and $[\theta_{50\%}, +\infty[$. By providing the upper (lower) bound of the 90% credible range, he refines his belief on every sub-interval by assigning a 5% chance that the true value of θ exceeds (falls behind) the $\theta_{95\%}$ ($\theta_{5\%}$) bound. Without making any assumption, these beliefs are described within the DST with the body of evidence:

$$(\mathcal{F}_i, m_i) = \left\{([\underline{\theta}, \theta^i_{5\%}], 0.05),]\theta^i_{5\%}, \theta^i_{50\%}], 0.45), (]\theta^i_{50\%}, \theta^i_{95\%}], 0.45), (]\theta^i_{95\%}, \overline{\theta}], 0.05)\right\}. \tag{3.25}$$

Figure 3.18 plots the cumulative belief and plausibility (left panel) and contour plausibility (right panel) induced by such a body of evidence on Θ.

We represented every expert's judgment by a DS structure. We ended up with 13 belief functions for every ice sheet contribution. The next step was aggregating of the individual judgments into an overall assessment.

3.2 Pooling expert judgments

There is no general consensus about what is the best combination mode when aggregating multiple pieces of evidence provided by several experts. In this study, we tested several combination rules: Dempster's rule, discounting and averaging rules. We discuss the appropriateness of each rule and analyse the sensitivity of the overall result to the choice of the combination mode. We provide the details of the calculations and the intermediate results for the WAIS variable. The results for the EAIS and GrIS variables were derived in a similar way.

Expert	Conflict	Conflict on discounted masses
2	0.9	0.3
3	0.75	0.29
4	0.34	0.15
5	0.54	0.23
6	0.9	0.31
7	0.34	0.14
8	0.34	0.15
9	0.7	0.24
10	0.36	0.15
11	0.34	0.14
12	0.34	0.14
13	0.34	0.15

Table 3.1: Conflict (in the sense of Dempster) between expert 1 and expert i ($i = 2...13$) calculated between the original (second column) and discounted (third column) masses.

- **Dempster's rule of combination**

Before proceeding to the combination via Dempster's rule, we evaluated the conflict among experts. Recall the definition of the conflict (K) between an expert e_i and an expert e_j, whose judgments on a given quantity are described by two bodies of evidence $(\mathcal{F}_i, m_i)$ and $(\mathcal{F}_j, m_j)$:

$$K = \sum_{A \in \mathcal{F}_i, B \in \mathcal{F}_j | A \cap B = \emptyset} m_i(A) m_j(B). \tag{3.26}$$

Conflict between experts was calculated using expression (3.26). The degrees of conflict between expert e_1 and expert e_j ($j = 2, ..., 13$) are reported in the second column of Table 3.1. The conflict matrix with the degrees of conflict for every two experts (e_i, e_j) is reported in Table 6.2 in the Appendices.

The 13 belief functions were then combined using the normalised Dempster's rule. Dempster's rule reinforces the agreement between experts and assigns higher evidential weight to items of evidence on which the majority of experts agree. Such results are confirmed by the visualisation of the contour plausibility of the combined assessment represented in Figure 3.19. The graphic reveals that Dempster's rule produces very focused beliefs around the value of 1.5 mm/yr and excludes values exceeding 2 mm/yr because it assigns to them a null plausibility.

Because the conflict is relatively high between some experts (e.g., experts 1 and 2), Dempster's rule of combination, which ignores the conflict, is not a good candidate for pooling the highly conflicting individual assessments. Another obstacle to the use of this rule is that the independence requirement is hardly satisfied because the climate experts certainly share common knowledge on which they base their judgments, and can not, consequently, be considered independent sources of information.

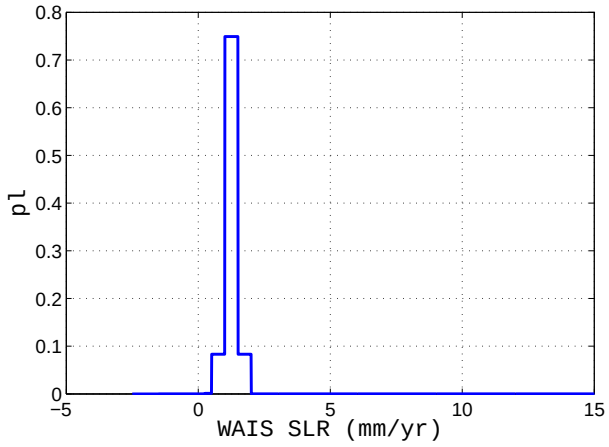

Figure 3.19: Contour plausibility of the belief function on the combined WAIS contribution using Dempster's rule of combination.

- **Discounting-based combination**

Given the high conflict among experts, it may be more appropriate to discount the beliefs before combining them with Dempster's rule. Individual assessments were aggregated via the discounting mode with a *Jousselme*'s distance-based discount factor. First, the disagreement between an expert i and the group of the other (n-1) experts was evaluated using Equation (1.25):

$$Diss(m_i) = \frac{1}{n-1} \sum_{\substack{j=1...n \\ j \neq i}} d_J(m_i, m_j) = \alpha_i,$$

where n is the number of experts, i.e., $n = 13$. The values are reported in Table 3.2. Before combining the discounted masses (calculated via equation (1.22)) using Dempster's rule, we re-evaluated the conflict. The results are reported in the third column of Table 3.1 (the conflict matrix that summarises the degree of conflict for every pair (e_i, e_j) after discounting can be found in Table 6.3, Section 4 in the Appendices). The comparison shows a significant reduction of the conflict after discounting. The discounted elemental masses were finally aggregated using Dempster's rule of combination. In Figure 3.20, we plot the contour plausibility of the pooled assessment of the contribution of WAIS using Dempster's rule, before and after discounting. The figure shows that discounting reduces the focus and extends the range of possible values.

- **Averaging rule**

In addition to their forecasts about the ice sheets' future behaviours, the scientists were solicited to give their estimates of the combined ice sheets contribution to SLR for the 20th century and over the last decade. Because the survey was

Expert	Disagreement	Disagreement-based weights	Stability-based weights
1	0.36	0.64	0.96
2	0.48	0.52	0.56
3	0.39	0.60	0.47
4	0.33	0.67	0.66
5	0.35	0.65	0.58
6	0.47	0.54	0.37
7	0.35	0.65	0.66
8	0.32	0.68	0.49
9	0.46	0.54	0.44
10	0.35	0.65	0.43
11	0.36	0.64	0.54
12	0.38	0.62	0.57
13	0.31	0.69	0.55

Table 3.2: Disagreement between one expert and the others (second column) and weights used in the averaging rule to combine experts' judgments on the WAIS contribution: weights derived from the reliability measure (third column) and from the stability in the answers in the 2010 and 2012 surveys (fourth column).

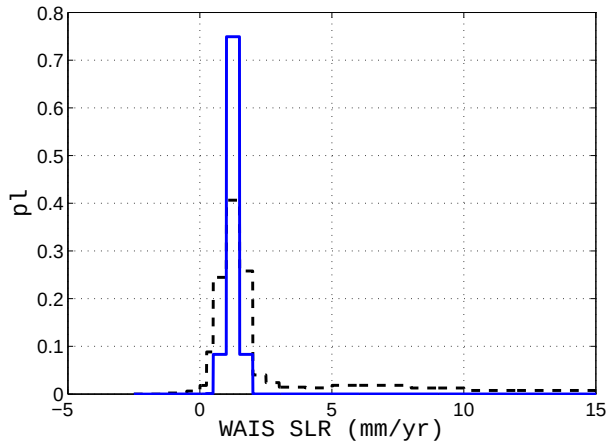

Figure 3.20: Effect of discounting: contour plausibility on the aggregated WAIS contribution to SLR using Dempster's rule on the original masses (blue -) and on discounted masses (black - -).

conducted twice, each expert answered four seed questions. It would have been interesting to score the experts according to their responses to these seed questions, and to later combine the individual assessments using the performance weight-based averaging rule as described in Subsection 2.4.3 in the first chapter. In the original paper, however, the authors mixed up the order of experts, making it impossible to match the experts with the assessments. Despite our attempts, we could not, unfortunately, obtain this information from the authors.

Given the lack of relevant information regarding the performance of the experts, we used alternative weights for averaging their judgments. We thought of three different ways to weight the scientists. The first is to suppose that all of them have the same contribution in the final assessment, in which case they are assigned equal weights. We also viewed the dissimilarity (in the sense of *Jousselme*'s distance for instance) between one expert and the others as a measure of the reliability (Equations (1.26) and (1.27)) of the expert, and assigned it as a weight to the expert of interest. The higher the dissimilarity between the assessment of an expert and the average assessment of the remaining group, the smaller his contribution to the overall assessment. The third way to weight the expert according to the stability of his assessments in the 2010 and 2012 surveys. We considered that the more stable the expert's answer, the higher the confidence in his assessment and the higher the weight assigned to him in the global assessment. The stability can be defined as a decreasing function of the distance (in the sense of *Jousselme*, for instance) between the assessments in 2010 and 2012. We used the same function as in (1.27). The values of weights derived from the dissimilarity and the stability of the assessments for the WAIS variable are reported in the third and fourth columns of Table 3.2.

The resulting combined assessments for the three averaging rules are depicted in Figure 3.21. The overlapping contour plausibilities suggest that the discriminative power of the scores based on *Jousselme*'s distance or the stability is not strong. This result is expected because the evaluation was made for only one variable.

The results on the overall sea-level rise rate induced by the WAIS by 2100 are very sensitive to the way experts' judgments are combined. As explained previously, one requirement for the use of Dempster's rule is not fulfilled, namely the independence between experts. In the absence of segregative scores based on the evaluation of the performance of each expert, the averaging rule based on equal weights seems to be the most natural and appropriate in this analysis and will be used for the remainder of the analysis.

In Figure 3.22, we plot the contour plausibility of each ice sheet's contribution to SLR by the end of the century. The most plausible values for the WAIS, EAIS and GrIS SLR rates by 2100 suggest that the experts believe the GrIS to have the highest rate, followed by the WAIS and then the EAIS, which is consistent with the recent observations [Bamber 2013]. We can also read from this graph that the EAIS is the only ice sheet likely to gain non negligible mass (i.e., has a negative rate) and that the WAIS has the longest upper tail. These statements are also consistent with the scientific intuition.

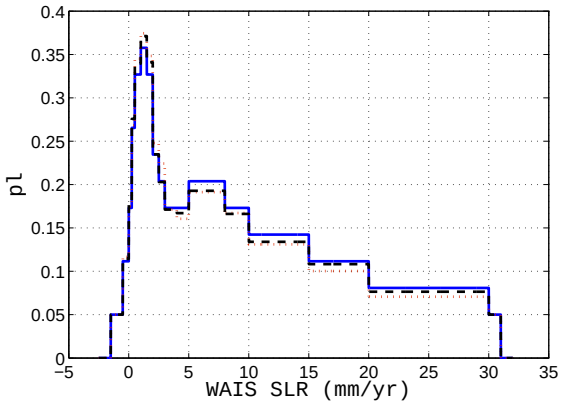

Figure 3.21: Contour plausibility of the combined WAIS contribution to SLR by 2100 using the weight and average rule: equal weights (blue-), discounting-based weight (black –) and stability weight (red ...).

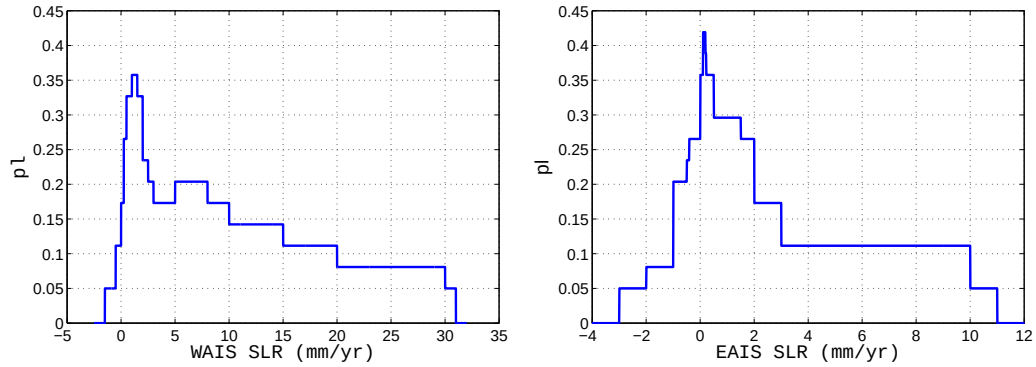

(a) (b)

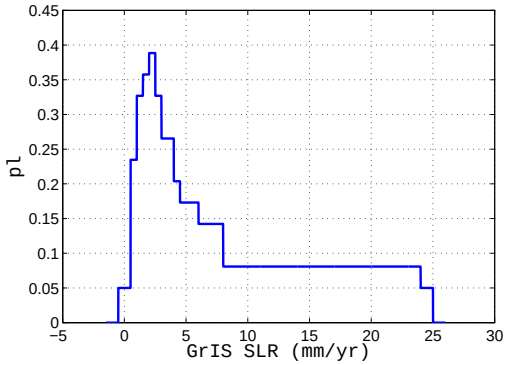

(c)

Figure 3.22: Contour plausibility on the overall (using the averaging rule with equal weights) sea-level rise rates of the WAIS (a), EAIS (b) and GrIS (c).

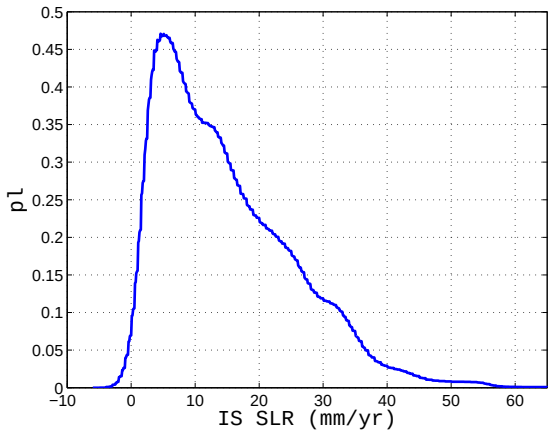

Figure 3.23: Contour plausibility on the contribution of the ice sheets to the sea-level rise rate by the end of the century.

3.3 Propagation results: combined ice sheets contribution and global sea-level rise projections

We represented the evidence on the contribution of each ice sheet to the sea-level rise rate by the end of the century using a belief function. The total sea-level rise rate induced by both the Antarctica and Greenland ice sheets was derived by summing the three contributions. In the absence of relevant evidence about the structure of dependence between the elemental contributions, we assumed independence between them. Because the sum operator is strictly increasing, we used the vertex method to approximate the overall contribution of the ice sheets to the sea level. First, we calculated the Antarctica ice sheets (AIS) contribution by summing the WAIS and EAIS contributions as explained in the example in the last section of the first chapter. Then, the resulting belief function was summed with that on the GrIS contribution. The contour plausibility on the overall ice sheets contribution to SLR by 2100 is plotted in Figure 3.23. In Figure 3.24, we give the results of the probabilistic analysis as published in [Bamber 2013]. The central tendency of both measures suggests that the overall sea-level rise rate induced by ice sheets at the end of the century is approximately 5 mm/yr.

To derive the global sea-level induced by the ice sheets at the end of the century, the annual SLR rate is integrated by assuming a linear trend from 2010 to 2100, with an estimated rate of 0.9 mm/yr by 2010. We can read from the plot of the resulting contour plausibility (Figure 3.25) that the most plausible value for the sea-level rise induced by the ice sheets is 26 cm (the median estimate is 29 cm in [Bamber 2013]). This level is twice as high as the upper projections of the IPCC in the AR4 (between -10 and 12 cm).

In addition to their judgments about the contributions of the ice sheets to the global sea-level rise by 2100, the experts were solicited to express their opinion on

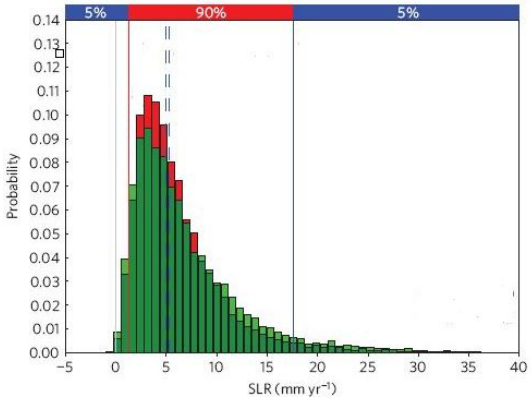

Figure 3.24: PDF for the rate of SLR due to ice sheets contributions by 2100 (2010 elicitation is plotted in red, and 2012 is plotted in green). Vertical lines indicate the 90% probability range.

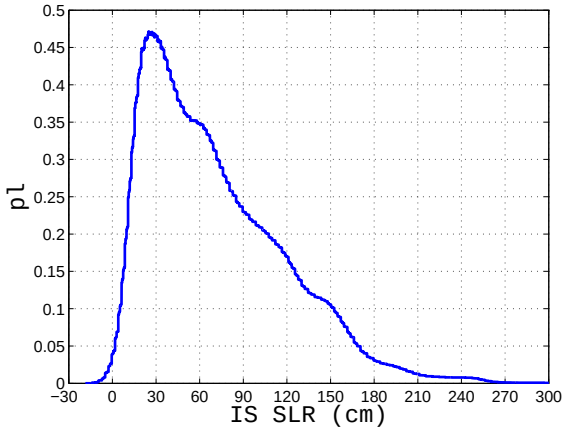

Figure 3.25: Contour plausibility on the contribution of the ice sheets to the sea-level rise by the end of the century.

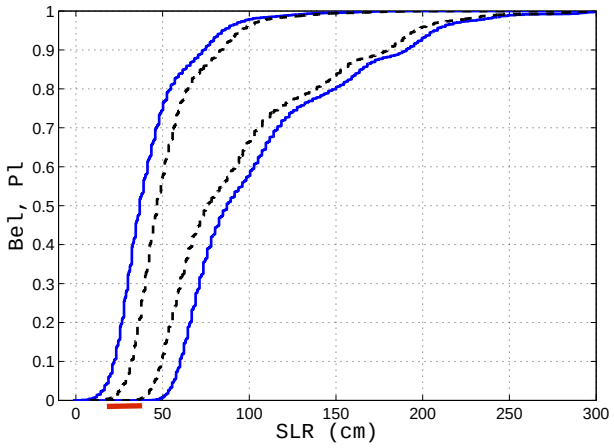

Figure 3.26: Cumulative belief and plausibility on the global SLR by 2100 derived from experts' judgments considering uncertainty in the three physical components (-) and only in the ice sheets components (- -). IPCC projections in bold horizontal line.

the temperature increase by the end of the century. Their pooled prediction of temperature rise at 2100 was shown in [Bamber 2013] to be close to the B1 scenario warming by the IPCC (3.5 degrees Celsius over pre-industrial levels or 2.8 degrees Celsius over 1980-1999 average).

The total sea-level rise by 2100 was obtained by simply combining the projections estimated above with the estimates of thermal expansion and glaciers melting contributions that correspond to the B1 scenario. The estimates reported in the last assessment report [IPCC 2007] are, respectively, [10, 24] cm and [7, 14] cm for the thermal expansion and melting of the glaciers. We represented the evidence on these contributions using a vacuous belief function, and then we summed the three belief functions. In Figure 3.26, we represent the cumulative uncertainty measures on the global sea-level rise by 2100. In dashed line, we plot the uncertainty measures with the thermal expansion and glaciers fixed to the best estimates (17 cm for the thermal expansion and 10 cm for the glaciers and ice sheets), and in continuous lines, we plot the same measures when the uncertainty in these components is accounted for. Clearly, most of the uncertainty in future projections pertains to the ice sheets contribution. The figure also shows the important prediction gap between the physical models used in the AR4 (the projected interval is indicated by a horizontal bold line on the x-axis) and the experts' judgments about the contribution of the ice sheets to the global sea level rise.

4 Comparative analysis and conclusion

In this chapter, we investigated three methods to assess future sea-level rise projections: process-based models, statistical fit to historical data and expert elicitation.

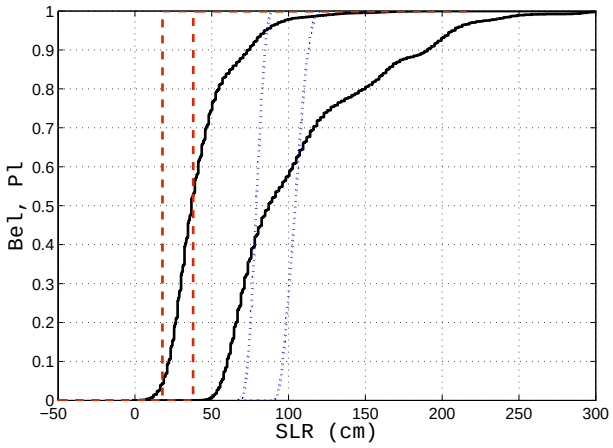

Figure 3.27: Upper and lower cdfs on the SLR projection by 2100 (wrt 2000) for the B1 SRES scenario derived from IPCC projections (- -), Rahmstorf's model (...) and expert elicitation (-).

The process-based projections accounted for the uncertainty in the emissions scenarios and the physical models. The projections based on the semi-empirical approach included uncertainty on temperature projections and the model statistical fit. Finally, the projections derived from expert elicitation included uncertainty in experts' opinions about the contribution of the different components of the sea-level rise.

We compared the projections by the three approaches for the particular B1 emissions scenario. The IPCC projections for this scenario are the interval $[0.18, 0.38]$ m. For the semi-empirical projections, the RV09 model is applied to the B1 temperature projections as in Subsection 2. We superimpose on Figure 3.27 the lower and upper cdfs of the SLR by 2100 induced by the three methods.

The three methods lead to different results. Expert elicitation yields higher projections in terms of central tendency and extreme values (i.e., the upper tail) than the physical models by the IPCC, reflecting the gap between the process-based and expert elicitation approaches in assessing future ice sheets contribution. Statistical fit to historical data gives higher projections (nearly two times) than the climate models. If we consider the 1 meter threshold, the probability that this level will not be exceeded by 2100 is 1 if we believe the IPCC projections, between 0.3 and 1 according to the semi-empirical approach, and between 0.58 and 0.98 according to expert elicitation.

It should be emphasised that providing numerical assessment of the sea-level rise is not the first objective of this work, which is instead focused on providing a methodology based on DST to tackle the uncertainties that are involved in climate change assessment. These uncertainties may have different sources, and accordingly, they need specific treatment. This analysis demonstrates the applicability and value of belief functions and their ability to model evidence from different sources (statistical, expert opinion) and combine them in climate related applications.

The paper by Bamber and Aspinall was published in January 2013, as were the results of the expert elicitation. The work reported in this section is only preliminary and two aspects require deeper investigation. The first aspect is physical and is related to certain assumptions we made, e.g., the independence between the ice sheets responses. This assumption needs to be constrained by physical arguments, and closer interaction with climate experts would be beneficial for this purpose. Moreover, the analysis could be refined if we further exploit the information provided by the survey. For instance, pooling experts' views can be performed through more informative aggregation techniques. We could consider, in addition to the performance-based weighting rule mentioned above, the hierarchical fusion introduced by Ha-Duong [Ha-Duong 2008]. The hierarchical fusion in this study would be based on the partition of experts into two groups: observers and modellers.

In mid of 2013, the IPCC released a draft of the fifth assessment report (a final version of the report is foreseen by January 2014), with a special report dedicated to the sea-level rise impact. Twenty pages of this report were dedicated to the description of the ice sheets future behaviour and their dynamical changes, reflecting a significant improvement in the physical understanding and modelling of these components (ice sheets dynamical models that were unavailable for the AR4 are now available). This new evidence can be used to update evidence provided by experts on the contribution of ice sheets to the sea-level rise.

Part IV

Coastal design and adaptation to climate change

Extreme sea condition events, such as a high water levels, high waves, or the conjunctions of both, can lead to functional and structural failures of the existing defence assets, and cause human and economic damages in the coastal areas. In the coming decades, because of global warming, extreme sea events are expected to increase, which will result in more frequent and severe hazards.

To limit future hazards, such as storm-surges, caused by long-term sea-level-rise, coastal adaptation involves the construction of new defence structures or the reinforcement of existing ones. Coastal engineers design the structures so that they withstand a certain level of admissible damage estimated through a comprehensive risk and vulnerability analysis.

This chapter is intended to provide some basic elements of coastal design. In the first section, we describe the main sea condition variables as well as the failure mechanisms that a typical defence structure can be subjected to. Then, we define some design criteria and describe the common techniques used to estimate them. In particular, the (joint) return period and design levels notions are introduced, as well as the main statistical tools of the extreme value theory (EVT). Afterwards, we make an inventory of the relevant sources of uncertainty when estimating coastal design and adaptation levels, and report a brief review of the literature on the common ways to integrate SLR projections in coastal risk and design analyses.

1 Coastal defence structures and hydrographic loading

1.1 Defence structures

Coastal defences can be natural (reefs, dunes, etc.) or artificial (foreshore, dikes, rock-armour, sea-walls, etc. [Allsop 2007]). Dikes are among the most effective defences and are predominant in coastal countries. An inventory analysis performed within the SAO POLO project [POLO 2012] showed that this type of assets is by far the predominant in France, with 180 km of the coasts being protected by such structures.

Figure 4.1 shows a schematic depiction of a typical dike. In this figure, R_c denotes the crest freeboard defined as the distance between the still water level (indicated by the horizontal blue line) and the crest level (i.e., the top of the dike). Both levels are measured with respect to a same reference. If the reference is the toe of the structure indicated by O, then $R_c = C_r - h$, where h is the water depth at the toe of the structure and C_r is the distance between O and the crest level.

Dikes are designed to meet functional and structural requirements. The former is related to the crest height, whereas the latter is related to the stability of the structure. The main hydraulic conditions involved in the design are the waves and the water level.

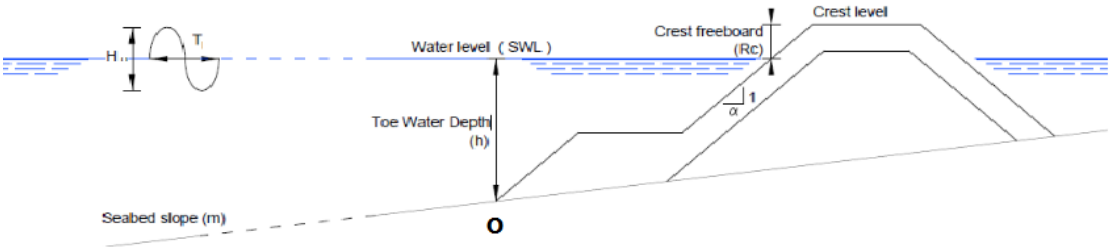

Figure 4.1: A generic dike and the main hydrographic loads (source [POLO 2012]).

1.2 Hydrographic loads

1.2.1 Still water level

Dikes are subjected to two hydrographic loads: sea-level and waves. The sea-water level (SWL) is the sum of three components represented in Figure 4.2: the mean sea-level, a deterministic astronomical tidal component, and a stochastic meteorologically induced surge component. The mean sea water is related to the mean sea-level of oceans and is site-specific. Tides are an astronomical component related to the rise and fall of sea-levels caused by the joint effects of the gravitational forces (by the moon, the sun and the rotation of the earth). Tides are entirely predictable over a nodal cycle of 18.6 years. In many shorelines, they may have well-defined periods. For instance, for most of the French coasts, tide behavior is semi-diurnal, i.e., it consists of two almost equal high tides per day, or equivalently, 706 high tides yearly. Storm surges define the rising of sea level due to wind and barometric pressure changes. This component is aleatory and is estimated as the difference between the measured water levels (using tide gauges) and the predicted tides. Extreme sea water levels that are of principal concern in coastal design correspond to conjunctions of positive surges and high tides.

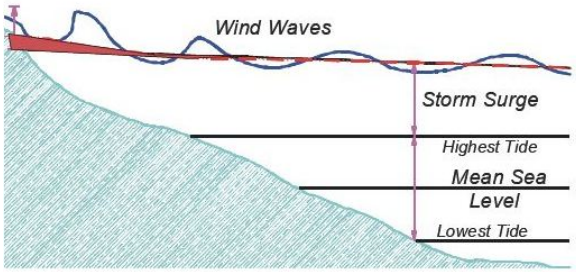

Figure 4.2: The components of still sea-level (source: [Turner 2009b]).

1.2.2 Waves

In addition to surges, meteorological storms cause waves. Waves are generated offshore and propagate inshore. Offshore, they are characterized by their height H_0 – the vertical distance between the wave crest and trough –, their period T_0 and their direction [Pullen 2004]. The significant wave height – defined as the average of the highest third of the waves and denoted H_s – is more used than H_0 to characterize wave heightsin coastal engineering. Wave data are collected either by measurements, or mostly by numerical wave prediction.

When waves propagate nearshore, their characteristics (height, period) change according to some depth limited effects that depend on the sea steepness, the slope of the bathymetry, etc. Numerical (such as SWAN, REEF 2000, BEACH, etc.) or empirical (Goda model [Goda 2000]) wave transformation models are used to propagate the offshore wave characteristics at the toe of the structure. The empirical model by Goda is often used in coastal engineering. It propagates high waves in shallow water as follows [POLO 2012]:

$$H_{Toe} = min(\beta_0 H_s + \beta_1 h, K_s H_s, \beta_{max} H_s) \tag{4.1}$$

and

$$T_{Toe} = T_0 = 5.3(H_s)^{0.3}. \tag{4.2}$$

Coefficients in equation (4.1) are defined by:

- $\beta_0 = 0.028(\frac{H_s}{L_0})^{-0.38} exp(20m^{1.5})$,
- $\beta_1 = 0.52.exp(4.2m)$,
- $\beta_{max} = max(0.92, 0.32(\frac{H_s}{L_0})^{-0.29} exp(2m))$,
- $L_0 = \frac{gT_0^2}{2\pi}$,

where m is the seabed slope (see Figure 4.1), h is the toe water depth, and k_s is the shoaling coefficient (defined as the ratio of shallow water to deep water wave height). In this formula, H_{Toe} stands for the significant wave height (an alternative notation is $H_{1/3}$). Finally, T_{Toe} is the wave period at the toe of the structure.

For mild sea bed slope (i.e., for small values of m), the formula (4.1) can be simplified [POLO 2012] into:

$$H_{Toe} = \beta_0 H_0 + \beta_1 h. \tag{4.3}$$

The correlation between waves and total still water level is not very significant because, contrary to the wave component, the predominant component of water level (astronomical tide) is not related to the local weather conditions [Hawkes 2002]. However, the correlation is expected to be more significant between surges and waves. As coastal design is concerned with extreme events, dependence is commonly analyzed at high water (i.e., when tides are high) extreme sea conditions.

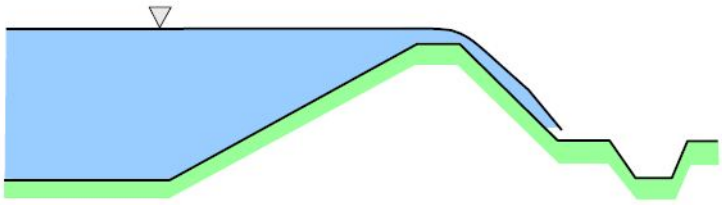

Figure 4.3: Overflowing process on a dike (source: Floodsite report [Allsop 2007]).

1.3 Functional failure mechanisms

Extreme sea conditions at the toe of the structure lead to different functional or structural failure mechanisms (erosion, overflowing, etc.) on the structure. A comprehensive listing of the most common failure modes for generic flood defence assets can be found in the report prepared within the sixth framework program for European Research and technological Development [Allsop 2007]. In this work, we focus on two particular functional failure mechanisms: the overflowing and the overtopping. Both are of principal concern in coastal design as they can, individually or jointly, cause flooding.

1.3.1 Overflowing

The overflow of a dike is a major functional failure that occurs when the volume of water that overflows the defence asset exceeds a critical admissible volume beyond which damage is significant.This failure mode is schematically depicted in Figure 4.3.

The overflowing mean discharge (i.e., the total volume of overflowing water per unit of length per second, expressed in $m^3/s/m$) is a reliable indicator of the of water is calculated based on the following formula:

$$q_{overflow} = A\sqrt{(R_c)_+}^3, \tag{4.4}$$

where $x_+ = \max(x, 0)$ and R_c is the crest freeboard defined previously.

1.3.2 Wave overtopping

Wave overtopping occurs when waves run up the crest of the structure as illustrated in Figure 4.4. There are several analytical models based on empirical methods that relate the mean overtopping discharge q to the main sea conditions. EurOtop Manual [Pullen 2007], a reference guideline in coastal engineering, suggests the following model:

$$q = 0.21\sqrt{gH_{Toe}{}^3}exp[-\frac{R_c}{H_{Toe}\gamma_f\gamma_\beta(0.33 + 0.022\xi_0)}], \tag{4.5}$$

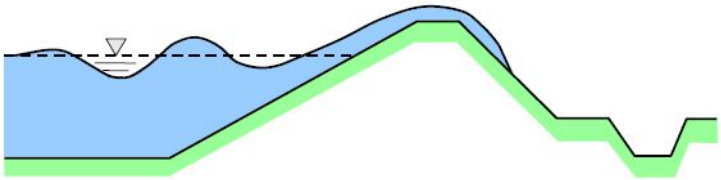

Figure 4.4: Wave overtopping process on a dike (source: Floodsite report [Allsop 2007]).

with

$$\xi_0 = tan(\alpha)\sqrt{\frac{gT_{Toe}^2}{2\pi H_{Toe}}}. \tag{4.6}$$

The breaker parameter ξ_0 (or Iribarren number) characterizes the breaking wave behavior nearshore. Small values of ξ ($\xi < 2.5$) indicate that the waves will mostly break on the dike, whereas for higher values, they do not. The coefficient α is the slope of the dike (see Figure 4.1). The coefficient γ_β is the reduction factor for oblique wave attack. The angle of the wave attack β is defined as the angle of the propagation direction with respect to the normal of the alignment axis of the dike. The coefficient γ_f is the slope roughness and g is the gravitational constant ($g = 9.8$ m/s^2).

Critical discharge values beyond which significant damages occur can be found in table 4.1. These limits were derived from tests and measurements made within the European Crest Level Assessment of coastal Structures by full scale monitoring, neural network prediction and Hazard analysis on permissible wave overtopping (CLASH) project in 2007 on a real dike in the Netherlands, and are often adopted in coastal engineering design.

Hazard type	**Mean discharge** $q(l/m/s)$
People on the crest of the structure	3.10^{-5}
Aware pedestrian, clear view of the sea, able to tolerate getting wet	0.1
Trained staff, well protected pedestrian, expecting to get wet, overtopping flows at lower levels only, low danger	0.03
Driving at low speed, overtopping by pulsating flows at low flow depths, no falling jets, vehicle not immersed	10-50
Driving at moderate or high speed, impulsive overtopping, giving falling or high velocity jets	0.01-0.05

Table 4.1: Tolerable limits of mean overtopping discharge corresponding to some hazards on pedestrians and vehicles (source: EurOtop manual [Pullen 2007]).

2 Coastal design

The level of admissible damage (overflowing or overtopping) that the defence asset is designed to withstand can alternatively be expressed in terms of the sea conditions that cause the specified damage, termed as the design events.

The common criterion used in coastal design to characterize the design event is the return period of extreme conditions. The return period of an event is defined as the time that separates two successive occurrences of the event. In statistical parlance, it is the inverse of the probability of exceedance (see details in Section 2.1). Therefore, when the event is described by a random variable X, the return period of the event "$X \geq x$" is:

$$T(x) = \frac{1}{NP(X \geq x)} \tag{4.7}$$

where N is the average number of observations per year. If the return period of a certain magnitude x of the event is $T(x)$, it means that this value will be experienced once every $T(x)$ years on average. A level that has a probability of being exceeded once in hundred years is called the $100-$*year return level* or the centennial return level. Coastal defences are usually built to a centennial design standard.

In the following, we'll be describing the statistical tools to estimate the return period of an event given some observations. We'll distinguish two cases: (1) the univariate case, i.e., when the event of interest involves a unique random variable (such as the overtopping response solely induced by the still-water level), and (2) the multivariate case, that involves more than two variables (such as the overtopping response) partially dependent.

2.1 Univariate design variable: the level of overflowing

As overflowing is solely induced by the still sea-level, the response and the driver have the same return period. The design overflowing level can thereby be estimated directly from the design still sea-level (referred to as the extreme flood level).

Several methods based on the analysis of extremes have been proposed in the literature to estimate the probability of occurrence of extreme sea-levels and derive from it the return periods. These methods can be categorized into two approaches. Within the first approach, the still sea-level is treated statistically as a unique component using the annual maxima method. Roughly speaking, this approach fits an appropriate frequency distribution to the ranked annual extremes, and uses this distribution to estimate, by extrapolation, the return level associated to a given return period. The extreme value theory (EVT) [Gumbel 1958] provides a family of probability distributions that are suitable for describing the frequency of the maximum (or minimum) values. Assume we have observed a sample of n annual maxima $z = (z_1, z_2, ...z_n)$ of a variable Z over n years. If these observations are a realization of an independent and identically distributed (i.i.d.) random sample $Z_1, ..., Z_n$, then, according to the EVT, z has asymptotically a generalized extreme

value (GEV) distribution with cumulative distribution function given by:

$$F(z,\mu,\sigma,\xi) = \begin{cases} exp(-[1-\xi\frac{z-\mu}{\sigma}]^{\frac{1}{\xi}}) & \text{for } \xi \neq 0, \\ exp(-(exp[-\frac{z-\mu}{\sigma}])) & \text{for } \xi = 0, \end{cases} \tag{4.8}$$

where μ, $\sigma > 0$ and ξ are, respectively, location, scale and shape parameters. According to the sign of ξ, the distribution is called Frechet ($\xi > 0$), Weibull ($\xi < 0$) or Gumbel ($\xi = 0$).

The return level z_T that is exceeded in average once in a return period T is the quantile of the distribution of Z at the probability of non-exceeding $1 - \frac{1}{T}$. When Z has a GEV distribution, z_T has the following expression:

$$z_T = \begin{cases} \mu - \frac{\sigma}{\xi}[1-(-Log(1-\frac{1}{T}))^{-\xi}] & \xi \neq 0, \\ \mu - \sigma Log(-Log(1-\frac{1}{T})) & \xi = 0. \end{cases} \tag{4.9}$$

The Annual maxima method is suitable when many years of data exist as it keeps a single observation per year. When the available span of data is short, it's preferable to use the r-largest values method, which is an extension of the annual-maxima method and consists of fitting a probability distribution to the r-largest values rather than the largest value.

The peak over threshold (POT) [Davison 1990] is an alternative sampling method. It consists on extracting the peak values that exceed a fixed threshold. According to the EVT, the generalised Pareto distribution (GPD) can be used for describing the frequency of the top few percent of data. Hence, the Generalised Pareto cumulative frequency distribution of a level z exceeding the threshold μ (i.e., $z > z_0 = \mu$) is given by:

$$F(z,\mu,\sigma,\xi) = \begin{cases} 1-(1+\frac{\xi(z-\mu)}{\sigma})^{\frac{-1}{\xi}} & \xi \neq 0, \\ 1-exp(-(\frac{z-\mu}{\sigma})) & \xi = 0. \end{cases} \tag{4.10}$$

The second approach for estimating probabilities of extreme sea-levels separates the still sea-level into its different components (mean sea-level, surges and tides), estimates the probability distribution of each component, analyses the dependence between them, and then combines them taking into account the possible interactions. The method has been first suggested and investigated by Pugh and Vessie [Pugh 2003]. They proposed the *joint probability method* based on the separation of the deterministic (tidal) and stochastic (surges) contributions. They used the annual maxima method to estimate the asymptotic distribution of the storm surges and then combined it with the known distribution of tides to provide estimates of the extreme sea levels. Tawn [Tawn 1989] revisited this method so that it can handle short span of data by fitting the r-largest values of storm surges to a probability distribution instead of the annual maxima. This method was referred to as *Revised Joint Probability Method*.

The joint tide-surge probability approach has many advantages comparing to the first approach as it uses higher amount of data, does not require long periods

of data, and does not involve large extrapolations. The extreme sea level estimates obtained with this method are expected to be more reliable because the method exploits the knowledge of the exact deterministic tidal distribution. However, this method requires high degree of analytical skill mainly in the selection and analysis of the data that need to have timing accuracy to better than few minutes. The method also involves extra computational effort [Pugh 2003].

2.2 Multiple design variables: the level of overtopping

Wave overtopping is induced by the conjunction of high waves and high water levels, which are partially dependent, because waves and the surge component of the sea level are related to the same local conditions. For such events, the univariate procedure described above is no more appropriate, and multivariate modelling that captures the dependence structure among the variables is required.

Multivariate modelling approaches in hydrological applications were rare until the 1980s. The common procedure to estimate the joint probability of a conjunction of two variables was based on an independence hypothesis. For example, the centennial wave-sea level conjunction was commonly defined as the conjunction of the centennial sea water level and the centennial wave height. In the last two decades, an intensive body of literature investigated the joint probability in hydrological and hydraulic studies, and more practical and rigorous methods [Hawkes 2002, Coles 1991] to deal with multiple events were developed. In particular, Hawkes [Hawkes 2002] proposed a rigorous joint probability method that has been widely used in flood management analyses [Hawkes 2005a]. The method was originally applied for the joint probability analysis of water level, wave height and wave steepness. It is a five step process summarized in [Hawkes 2002] as follows:

1. Preparation of input data: input data consist of a set of independent and simultaneous records of the source variables.

2. Fitting of marginal distributions:

3. Fitting of a statistical model to the dependence between the conjunctions: with the marginal distributions defined, the joint distribution between the marginals can be determined.

4. Long-term simulation: generate a large sample of synthetic conjunction records based on the statistical distributions defined and the correlation between the marginal distributions.

5. Analysis of extremes on the source variables and the (synthesized) structure response: derive extreme estimates that can be used in design.

The dependence between the random sea condition variables in the third step was modeled using a bivariate normal (BVN) model – a model for which the

dependence and extreme characteristics are well understood. The BVN method requires the variables involved in the joint analysis to have the same statistical distribution. When this hypothesis does not held, more flexible multivariate models are needed. Amongst the alternative multivariate models that offer the desired flexibility, copulas [Sklar 1959] are increasingly investigated in the hydrological literature related to the description of multidimensional phenomena [Salvadori 2004b, Michele 2005, Genest 2007]. The computational advantage of copulas in the estimation of joint return period in hydrological applications has been demonstrated in [Salvadori 2004b].

2.2.1 Copulas: a multivariate model

The mathematical basis for the analysis of copulas was founded by Sklar [Sklar 1959] in the fifties. In the bivariate case, copulas are functions that relate the univariate marginal CDFs F_X and F_X of any pair of random variables (X, Y) to their bivariate cumulative distribution F_{XY} by:

$$F_{XY}(x, y) = P(X \leq x, Y \leq y) = C(F_X(x), F_Y(y)) \quad \forall x, y \in \mathbb{R}. \tag{4.11}$$

This definition can be extended to the higher dimension case. According to Sklar theorem, C is unique when the marginals are continuous. The copula density is given by:

$$c(u, v) = \frac{\partial^2 C(u, v)}{\partial u \partial v} \quad \forall (u, v) \in [0, 1]^2. \tag{4.12}$$

The joint density of an observation (x, y) is expressed by:

$$f_{X,Y}(x, y) = c(F_X(x), F_Y(y)) f_X(x) f_Y(y). \tag{4.13}$$

For exhaustive and general introduction to copulas, one can refer to [Joe 1996, Nelsen 2006].

Archimedean copulas are particular models which are widely used in practical applications (finance [McNeil 2005], hydrology [Salvadori 2004b, Wahl 2012], etc). Archimedean copulas find a wide range of applications because (1) copulas within this class have a relatively simple explicit parametric expression and (2) this class allows a great variety of dependence structures among variables.

Examples of Archimedean copulas include Gumbel, Clayton and Franck families. Each of these families captures a particular dependence structure. Gumbel copula exhibits upper tail dependence, whereas Clayton family models lower tail dependence. Frank family models positive dependences as well as negative ones. Expressions of these copulas can be found in the Appendices, Section 3.

The joint return period in the bivariate case considers the random variables jointly and can be defined using several combinations of the two random variables [Salvadori 2004a, Shiau 2003]. Two particular definitions are commonly used in

hydrology [Shiau 2003]:

$$\begin{aligned} T_{XY}(x,y) =& \frac{1}{NP(X \geq x \text{ and } Y \geq y)} \\ =& \frac{x}{1 - F_X(x) - F_Y(y) + F_{X,Y}(x,y)} \end{aligned} \tag{4.14}$$

and

$$\begin{aligned} T'_{XY}(x,y) =& \frac{1}{NP(X \geq x \text{ or } Y \geq y)} \\ =& \frac{x}{N(1 - F_{X,Y}(x,y))} \end{aligned} \tag{4.15}$$

where N is the average number of observations per year.

2.3 Impact of climate change

2.3.1 Impact of climate change on sea conditions

The magnitude and frequency of extreme sea-water levels in the future can be influenced by several factors that affect each of the components: the elevation of the mean sea-level, the increase of the tidal range [McInnes 2009], or the change in the variability of storm surges (storms will become more intense and frequent). Amongst the three, the rise in mean sea-level contributes the most at the observed increase in the frequency of extreme sea-level events [Bindoff 2007, Hunter 2010]. In particular, a recent study performed by the Centre d'Etudes Techniques Maritimes et Fluviales (CETMEF) in 2010 [Morellato 2010] showed that the impact of climate change on the waves climate (i.e., wave height and period) is very moderate in the North East Atlantic zones. According to this study, the increase of offshore extreme waves will not exceed 30 cm if we consider all the emissions scenarios defined by the IPCC. This effect is negligible comparing to the variations induced by the rise of the mean sea-level.

Taking into account the results of the cited studies, the analysis of the impacts of the climate change on extreme events and design levels performed in our application will be based on the assumption of the stationarity of storms and tides in the Havre site (the study area considered in the application). Hence, the climate change impacts on sea condition variables considered in this work are twofold. First, the mean sea-level will be shifted by the SLR and so will be h (i.e., $\Delta h = SLR$). Second, the wave height at the toe of the structure will increase according to equation (4.3), and the variation is mainly induced by the second term in this equation, i.e., the factor related to the mean sea-level. Hence, the variation of the nearshore wave height is:

$$\Delta H_{Toe} = \beta_1 \Delta h. \tag{4.16}$$

2.3.2 Adapting to climate change: an analytical approach

By impacting the hydrographic loads, the climate change affects directly the occurrence of overtopping events and hence the defence levels. To maintain the performance of a dike, its crest need to be elevated. The required elevation of the crest can be estimated using a simple analytical method [POLO 2012]. Consider a given admissible discharge levels q_0: in shallow water and for small values of q_0 ($q_0 \leq 510^{-2}$ m^3/s), a limited development of order one of equation (4.5) leads to a simple relation between the the crest freeboard elevation and the mean sea level [POLO 2012]:

$$\Delta R_c = -(0.33 + 0.22\xi)\gamma_f\gamma_\beta \ln q_0 \Delta H_{Toe}. \tag{4.17}$$

For small Iribarren numbers and in shallow waters, combining the previous equation with the simplified (for breaking waves) Goda formula yields to:

$$\Delta R_c = -0.33\gamma_f\gamma_\beta \ln q_0(\Delta\beta_0 H_s + \beta_1 \Delta h). \tag{4.18}$$

Given that the effect of climate change on the offshore wave height comparing to the mean seal-level rise,

$$\Delta R_c = -0.33\beta_1\gamma_f\gamma_\beta \ln q_0 \Delta h. \tag{4.19}$$

The increase of the crest level required to maintain the hydraulic performance is obtained by shifting the increase in the crest freeboard with the mean global sea-level rise:

$$\Delta D = \Delta h + \Delta R_c. \tag{4.20}$$

2.3.3 Uncertainty in coastal adaptation

Efficient coastal design requires the estimates of the hydraulic risks to be as accurate as possible. However, coastal engineer is confronted when estimating design levels to different uncertainties that fall into four main categories:

- Statistical uncertainties: include uncertainties in the extrapolated extreme statistics, in the description of the dependence between variables in the bivariate case, etc.
- Data uncertainty: includes heterogeneity of data, measurement errors, etc.
- Model uncertainty: reflects the inaccuracy of the empirical and numerical models in the description of the physical processes such as wave overtopping or wave propagation.
- Parameter uncertainty: includes uncertainties in the structure, geotechnical and geometrical parameters of the defence asset, etc.

These uncertainties make the estimation of the design variables inaccurate and may result in an unsafe under-design or an expensive over-design. Coastal engineering design under uncertainties has gained a lot of attention in the last two

decades. The main approach used to address this topic is probability. Probabilistic design has been widely applied in coastal risk analyses and design applications [Apel 2004, Oumeraci 2004]. This approach does not make distinction among the different sources and types of uncertainty as it treats all uncertain quantities (stochastic loads, models, parameters, etc.) as random variables. When a probability model can not be inferred from the available evidence on a given quantity, the common practice is to represent the latter by a normal distribution with a fixed standard deviation [Pullen 2007]. In 2008, Shuttrumpf [Schuttrumpf 2008] tried to get additional information on some poorly known variables involved in coastal design using expert elicitation. In this study, experts in coastal engineering were asked to provide their best estimates, and the uncertainty band of some geometrical, hydraulic and geotechnical parameters.

In the recent dacades, alternative uncertainty frameworks for dealing with uncertainty in flood risk and coastal design analyses were investigated. In particular, the fuzzy set theory is gaining ground in recent literature [Komatina 2005, Beraldi 2011].

In a context of changing climate, coastal engineers are faced to an additional source of uncertainty related to the magnitude of the climate change impacts, particularly the magnitude of the sea-level rise. Indeed, the current wide range of projections of future sea-level rise is challenging for adaptation. Indeed, because of this uncertainty, coastal engineers, planners and decision makers can not have an accurate estimate of the climate change risk and can not develop reliable adaptation strategies.

The common practice in the integration of the SLR in quantitative hydrological climate climate change studies for adaptation is to ignore the pervasive uncertainty and to consider a unique particular scenario. Often, the mean or worst case scenario is selected when estimating future risk and exposure [Dawson 2005]. The scenario approach was adopted within the SAO POLO project to evaluate the impact of the sea-level rise on the performance of a typical defence structures. Purvis [Purvis 2008] showed that undertaking a flood risk assessment using the most plausible sea level scenario may "significantly underestimate monetary losses as it fails to account for the impact of low probability, high occurrence events" [Purvis 2008]. To estimate future flood risk due to uncertain sea-level rise, the author suggested a probabilistic methodology. He took as SLR projections the last IPCC range and described it probabilistically by inferring a simple triangular probability distribution over the 3 values range (best estimate and the upper and lower bound).

The probabilistic approach in integrating the uncertain projections of the sea-level rise in climate related assessments is subject to some criticism mainly related to the particular choice of a probability distribution and a specific range of projections in the literature.

3 Conclusion

The objective of this chapter was to present the main concepts and models used in coastal engineering. First, we described the hydraulic loads (tides, surges, waves) and the main mechanisms of the functional failure of a typical typical defence asset (overflowing and overtopping). Then, we reported a literature review of the commonly used methods to estimate some risk indicators (return period, joint return period) used in coastal design. In particular, we made an inventory of the statistical methods used to estimate extreme hydraulic loads and extreme hazards (EVT, copulas). Finally, we addressed the issue of coastal adaptation to climate change. First, we identified sea conditions that are mostly affected by the rise of the sea level and described an analytical method to evaluate the required reinforcement of a dike so that its hydraulic performance is maintained. We ended this chapter with a brief review of the sources of uncertainty encountered in coastal design and adaptation, and the common methods to cope with uncertainty.

Part V

Adapting under uncertainty: a methodologically-oriented case study

Assessing the impact of climate change on the performance and the vulnerability of a typical defence structure protecting different sites along the French coasts was among the main objectives of the SAO POLO project. The authors of the final report of the project [POLO 2012] provided a global methodology for assessing the global warming impacts on a typical defence structure, but did not conduct a formal uncertainty analysis when integrating future projections (it only provided a set of sensitivity analysis results).

We propose here to address the problem of adapting under uncertainty by presenting a methodologically-oriented case study that develops a full uncertainty analysis based on DST. The proposed approach was applied to estimate two design criteria and to assess their evolution when climate changes. The first design criterion we were interested in is the centennial sea level. The second design criterion is the centennial overtopping hazard caused by conjunctions of storm waves and high water levels. In particular, we were interested in evaluating the required elevation of a defence asset to maintain its current level of protection from (centennial) overtopping at future sea levels.

As mentioned in the end of the previous chapter, there are several sources of uncertainty when estimating risk indicators for design. In this study, we addressed two of them. The first stems from the statistical analysis of hydrographic inputs when estimating these quantities. In particular, for the centennial sea level, uncertainty arises from the fitting and extrapolation of the extreme value model. For the second criterion, it arises from the dependence estimate between the hydraulic variables. The second uncertainty we considered in this study is epistemic and is related to the magnitude of future-sea level rise to be integrated for adaptation purposes.

A recorded hydrographic data from the Havre site is used as a case study to illustrate the proposed methodology.

1 Description of the study site

The analysis was held using data recorded in Havre site. The Havre is a coastal urban city in the north-western France (see location in Figure 5.1). Its harbour, the largest in France after that of Marseille, is on the Atlantic coast. The port was amongst the candidate sites that have been studied within the SAO POLO project.

For this study site, the available hydrographic data are:

- tide records: hourly measures calculated by the *PREDIT* software, developed by the Service Hydrographique et Océanographique de la Marine (SHOM);
- sea level records (tides+surges): hourly measures from 1994 to 2009 provided by the Réseau d'Observation du Niveau de la Mer (RONIN);
- wave records: 7.1 years of hourly measures from 1997 to 2008 provided by the Centre d'Archivage National de Données de Houle in Situ (CANDHIS);

Figure 5.1: The Havre location (source: http://www.enviro2b.com).

- 21 years of wave-surge simulated conjunctions at high water: the simulations are provided by the atlas numérique des états de Mer céaniques et côtiers (ANEMOC).

We conducted the analysis on a typical dike (the type of structures used in harbors), for which the design formulas presented in the previous section apply. The dike has the following characteristics:

- located in shallow waters;
- mild sea slope: $m = 1\%$;
- crest height $C_r = 14$ m;
- a roughness factor $\gamma_f = 0.6$;
- $\gamma_\beta = 1$ (perpendicular waves);
- an outer slope α such that $tg(\alpha) = 0.4$.

The heights are indicated in meter Cote Marine du Havre (CMH). They are measured with respect to the hydrographic zero, which is close to the lowest level that the still sea water can reach.

2 Extreme sea-level analysis

2.1 Models and assumptions

2.1.1 Extreme value statistics for present-day conditions from statistical evidence

Assume that we need to estimate the sea level z_T associated to some return period T from a historical dataset of n years of sea-level records. Among the candidate methods to estimate the probability of extreme events, we adopted the annual maxima

method which implies fitting a GEV distribution to the observed annual-maxima sample $\mathbf{z} = (z_1, ...z_n)$ and the extrapolation of the GEV fit to a domain outside the range of the available records.

Different parametric or non-parametric GEV distributions can be used to estimate high return levels, as long as they fit well to the observed data. If the n annual maxima are fitted to a Gumbel distribution, a widely used GEV model in hydrology, the pdf of each z_i is

$$f(z_i; \mu, \sigma) = \frac{1}{\sigma} \exp\left(-\frac{z_i - \mu}{\sigma}\right) \exp[-\exp\left(-\frac{zi - \mu}{\sigma}\right)]. \tag{5.1}$$

Different inference methods can be used to determine the model parameters μ and σ that provide the best fitting to the observed data. The method of maximum likelihood is commonly adopted in hydrology. According to this method, the model best fits the observed sample $\mathbf{z}$ for values $\hat{\mu}$ and $\hat{\sigma}$ that maximize the joint likelihood:

$$\begin{aligned} L(\mu, \sigma; \mathbf{z}) &= \prod_{i=1}^{n} f(z_i; \mu, \sigma) \\ &= \left(\frac{1}{\sigma}\right)^n exp\left(-\sum_{i=1}^{n} \frac{z_i - \mu}{\sigma}\right) exp[-\sum_{i=1}^{n} exp\left(-\frac{z_i - \mu}{\sigma}\right)]. \end{aligned} \tag{5.2}$$

The best estimate of the return level z_T that occurs once in every T years in average is therefore:

$$z_T = \hat{\mu} - \hat{\sigma} Log(-Log\left(1 - \frac{1}{T}\right)).$$

and the statistical uncertainty in this estimate is described by error bounds.

As mentioned in the first chapter, the performance of ML inference can be erratic for small samples. Therefore, its use in extreme values analyses, which often involve small samples, is challenging. Martins and Stedinger [Martins 2000] showed that the ML inference can generate absurd and irrelevant values when estimating extreme quantiles of the GEV distribution. They provided an example that illustrates the instability of the method: they generated a random sample of size $n = 15$ from a GEV distribution with shape parameter $\xi = 0.2$ and showed that the ML gives $\xi = 2.48$. They conclude that the use of alternative methods that do not rely on sample size properties is preferable when estimating extreme quantiles.

We propose to use the likelihood-based-inference described in the first chapter to infer extreme quantiles of sea-level from the statistical evidence.

As the parameter of interest is z_T, the pdf can be re-parametrized as a function of μ and z_T. Using the quantile function (4.9), we get $\sigma = (\mu - z_T)/c$ with

$$c = log[-log(1 - \frac{1}{T})], \tag{5.3}$$

from which we obtain

$$f(z_i; \mu, z_T) = \frac{c}{\mu - z_T} \exp\left(c\frac{z_i - \mu}{z_T - \mu}\right) \exp\left[-\exp\left(c\frac{z_i - \mu}{z_T - \mu}\right)\right]. \tag{5.4}$$

The re-parametrized likelihood function is thus:

$$L(\mu, z_T; \mathbf{z}) = \prod_{i=1}^{n} f(z_i; \mu, z_T)$$
$$= \left(\frac{c}{\mu - z_T}\right)^n \exp\left(\frac{c}{z_T - \mu}\sum_{i=1}^{n}(z_i - \mu)\right) \exp\left[-\sum_{i=1}^{n}\exp\left(c\frac{z_i - \mu}{z_T - \mu}\right)\right]. \tag{5.5}$$

Using (1.54), the corresponding contour function is the normalized likelihood function:

$$pl(\mu, z_T; \mathbf{z}) = \frac{L(\mu, z_T; \mathbf{z})}{\sup\limits_{\mu, z_T} L(\mu, z_T; \mathbf{z})}. \tag{5.6}$$

Here, the parameter of interest z_T and μ is a nuisance parameter, which can be marginalized out by considering the normalized profile likelihood. We finally get

$$pl(z_T; \mathbf{z}) = \sup_{\mu} pl(\mu, z_T; \mathbf{z}). \tag{5.7}$$

We have hence encoded the statistical evidence about z_T with a random interval, denoted $(\Omega_1, P_1, \Gamma_1)$ which induces $pl(z_T; \mathbf{z})$ as a contour plausibility.

2.1.2 Impact of climate change on extreme sea levels

The impact of global warming on extreme events can be assessed through analyzing the evolution of their extreme quantiles or return periods comparing to current climate conditions. To evaluate the evolution of an extreme sea level after a given period P in a context of changing climate, its present-day climate conditions estimate needs to be combined with projections of the sea-level rise during the same period P. Assuming that sea-level rise will have little effect on the variability of the still sea level, i.e., on tide heights and on the variability of surges, the evolution is described by simply shifting to the right the sea-level return level (estimated under current climate conditions) by the relevant estimate of sea-level rise. Therefore, the quantile z_T becomes in P years:

$$z'_T = z_T + SLR, \tag{5.8}$$

where SLR is the magnitude of the sea-level rise over the period P.

We performed the impact assessment using the most relevant projections of SLR adopted in coastal planning, i.e. projections by the IPCC, Rahmstorf and Pfeffer.

IPCC projections, even if they underestimate the overall sea-level rise and can be judged too low for safe adaptation, are based on the best state of knowledge about the evolution of the climate and are agreed on by the climate scientific community. For impact assessment and adaptation planning, the IPCC recommends the use of the range of the four scenarios groups to capture the range of uncertainties associated to driving forces and emissions. Taking into account this recommendation,

Source	2030			2050			2100		
	min	mid	max	min	mid	max	min	mid	max
IPCC	0.06	0.1	0.14	0.1	0.18	0.27	0.18	0.43	0.79
RV09	0.08	0.17	0.23	0.18	0.28	0.48	0.5	0.83	1.4

Table 5.1: Lower, mid and upper sea-level rise projections (in meter) by the IPCC and Rahmstorf in 2030, 2050 and 2100.

we considered projections provided by the IPCC that cover the range of emissions scenarios. The semi-empirical approach by Rahmstorf is increasingly supported because it provides projections that are consistent with the latest observations of the increase of the sea-level in the latest decades and with recent expert elicitation. The mid scenario of 1 meter elevation by 2100 projected by this approach is often adopted as a careful scenario in many impact analysis in coastal adaptation. Finally, we considered the upper bound of 2 meters elevation by 2100 justified physically by Pfeffer. The highest, lowest and mid estimates of the considered sources are recalled in Table 5.1.

2.2 Application to the Havre data

2.2.1 Extreme sea-level statistics under present-day conditions

We applied the method described in Section 2.1.1 to the Havre data, i.e., to $n = 15$ years-length dataset of still sea-level records (in cm) from 1994 to 2009. The ML estimates of the fitting Gumbel distribution were found to be $\hat{\mu} = 853.4$ and $\hat{\sigma} = 12.07$. The empirical CDF of the 15 annual maxima is plotted together with the fitted distribution in the left panel of Figure 5.2. There is a close match between both curves, which indicates that the statistical fit is reasonably adequate. The right panel of the same figure shows the model prediction of extreme sea-levels for return periods up to 1000 years as well as the upper and lower bounds of the 90% confidence interval.

For the centennial sea-level (i.e., sea level associated to a $T = 100$ years return period), the joint contour plausibility and the marginal contour plausibility of Z_T, calculated according to equations (5.6) and (5.7), are plotted in Figure 5.3.

In Figure 5.4, we plot together the contour plausibility of the return levels z_T associated to 25, 100 and 1000 year return periods. We can see from the extent of the contour functions that the statistical uncertainty associated to the fitting and extrapolation increases when the return period increases.

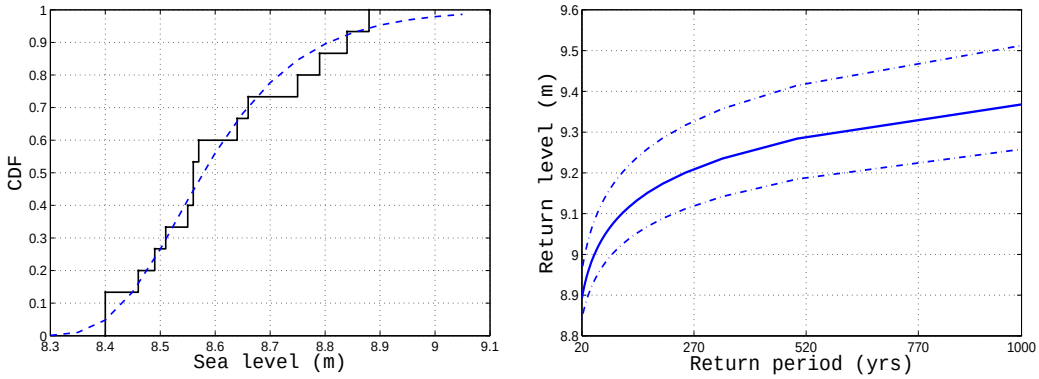

(a) (b)

Figure 5.2: (a) Empirical CDF (black line) of 15 annual maxima of sea-level together with the Gumbel fitting distribution (blue line). (b) Sea-level return period curve (continuous line) and the 90% confidence interval (dotted line) (from 20 to 1000 years) predicted from the Gumbel model.

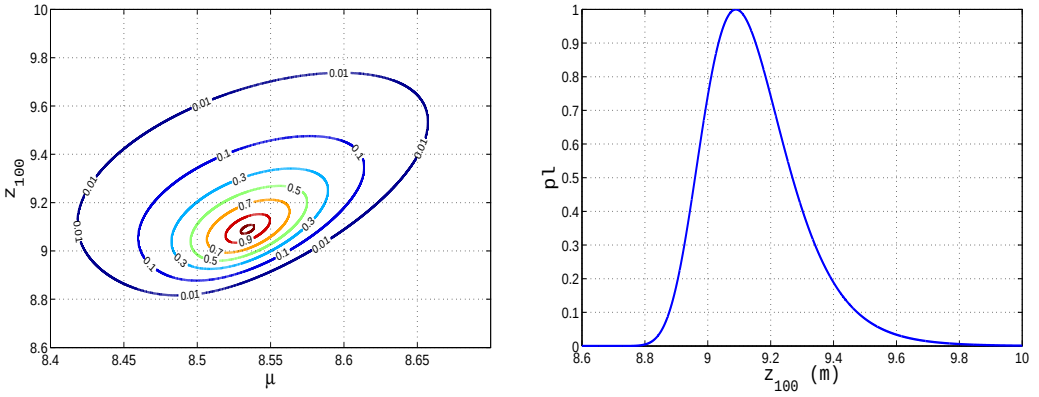

(a) (b)

Figure 5.3: (a) Joint contour plausibility function $pl(\mu, z_T)$ and (b) marginal contour plausibility $pl(z_T)$ for $T = 100$.

2.2.2 The impact of climate change

To analyze the impact of climate change on the return periods of extreme sea-levels in the coming decades, we shifted the return levels estimated under the current climate conditions with the SLR over the period of interest according to equation (5.8). We present the results of the analysis for two cases. First, we did not account for the uncertainty in both the statistical quantity (z_T) and the imprecise SLR. For this purely deterministic analysis that acts as a reference case, we analyzed the sensitivity of the future return level z'_T to the sea level rise scenario by the end of the century. This analysis is useful because it gives a primary idea about the weight and

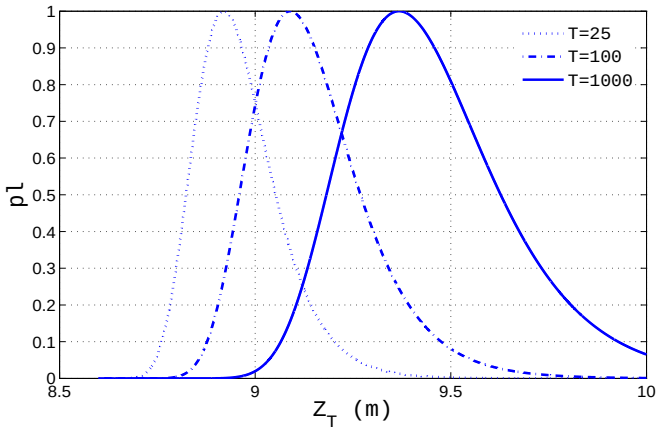

Figure 5.4: Contour plausibility of Z_T for $T = 25$ years (dotted), $T = 100$ years (dashed) and $T = 1000$ years (continuous).

contribution of each of the uncertain SLR in the overall output uncertainty. Then, we performed an uncertainty analysis by combining z_T and the SLR expressed in the DS framework to assess z'_T.

2.2.2.1 Sensitivity analysis

The changes in extreme sea-levels z_{25}, z_{50}, z_{100} and z_{1000}, considering the upper projections of the cited sources (i.e., 1.4 m for Rahmstorf and 0.79 m for IPCC projections) in 2030, 2050 and 2100 are reported, respectively, in the third, forth and fifth columns of Table 5.2. Figure 5.5 shows how the sea level return period curve estimated under present-day climate conditions (black curve) will evolve in coming decades (in 2030 (red), 2050 (blue) and 2100 (green)) when we integrate the sea-level rise (IPCC estimates (continuous) vs Rahmstorf estimates (dashed)).

From the graph, or equivalently the table, we can assess the relative contribution of the sea-level rise to changes in extreme sea-levels in the coming decades. We can see in particular how sea-levels currently experienced on a given return period will be much more frequent in the future. For instance, the level of 9.09 m that occurs once every 100 years under current climate conditions will occur once every 20 years on average by 2030 if we believe the IPCC most pessimist projections, and once every 10 years if we commit to Rahmstorf's projections. A sea-level of 9.37 m, the current 1000-year return level, may become a 1 in 100 year event by 2030, under Rahmstorf's projections, or a 1 in 100 year event by 2070, under IPCC projections.

2.2.2.2 Uncertainty analysis

In what follows, we propose to estimate the return period under climate change z'_T by accounting for the statistical uncertainty in the extreme value statistics z_T, as well as in the SLR. In particular, we focus on assessing the impact of the climate

Return Period	**Return level**	**2030**		**2050**		**2100**		
		IPCC	**RV09**	**IPCC**	**RV09**	**IPCC**	**RV09**	**Pfeffer**
25	8.92	9.06	9.15	9.19	9.42	9.71	10.32	10.92
50	9	9.14	9.23	9.27	9.5	9.79	10.4	11
100	9.09	9.23	9.32	9.36	9.59	9.88	10.49	11.09
1000	9.37	9.5	9.63	9.6	9.86	10.16	10.76	11.37

Table 5.2: Return levels under current climate conditions and three sea-level rise scenarios (IPCC, Rahmstorf and Pfeffer). Values (in meter) relative to late 20th century mean sea-level.

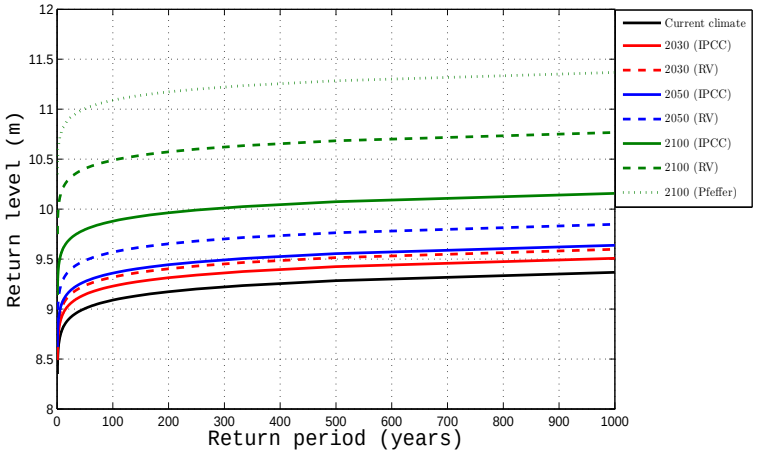

Figure 5.5: Sea-level return period curves for the Havre site under current climate conditions (black curve) and three scenarios of future climate change based on IPCC projections (continuous), RV09 projections (dashed) and Pfeffer estimates (dotted). Different colors indicate three periods of interest: 2030 (red), 2050 (blue) and 2100 (green).

change on the centennial return period by the end of the century, i.e., $z_T = z_{100}$ and SLR is the sea-level rise by 2100.

An advantage of using Dempster–Shafer theory of belief functions in representing evidence on SLR is that it allows to combine the evidence on the SLR provided by different reliable sources in a natural and straightforward way. According to the three sources cited above, the interval $[0.5, 0.79] = [0.18, 0.79] \cap [0.5, 1.4]$ seems to be fully supported by the available evidence on the SLR by 2100, as it is considered highly plausible by all three sources, while values outside the interval $[0, 2]$ are impossible. This information is represented by a belief function verifying $Pl[0.5, 0.79] = 1$ and $Bel[0, 2] = 1$. We encoded the evidence on the selected SLR projections with a

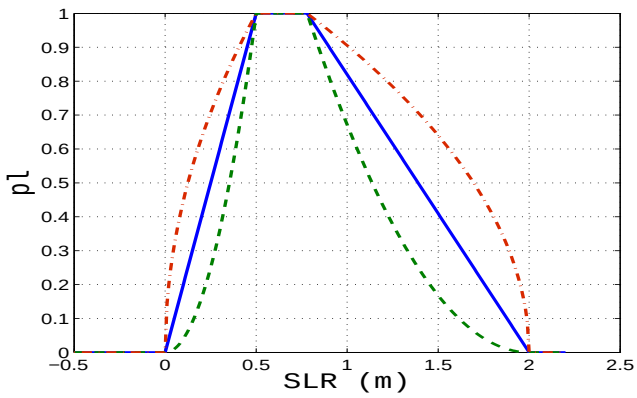

Figure 5.6: Contour plausibility induced by the random interval on the SLR in 2100 for $\phi(x) = x$ (–), $\phi(x) = x^2$ (-) and $\phi(x) = \sqrt{(x)}$ (-.).

consonant belief function whose contour plausibility function is

$$\pi(x) = \begin{cases} \phi\left(x/0.5\right) & 0 < x \leq 0.5 \\ 1 & 0.5 < x \leq 0.79 \\ \phi\left(\dfrac{2-x}{2-0.79}\right) & 0.79 < x \leq 2 \\ 0 & otherwise, \end{cases} \tag{5.9}$$

The belief function induces a random interval $(\Omega_2, P_2, \Gamma_2)$. We analyzed the sensitivity of the final results to the choice of the membership function ϕ so we considered three forms for the latter: linear, concave and convex functions. The contour plausibility induced by this random set is plotted, for the three different membership functions, in Figure 5.6.

Assuming independence between the sources of evidence (a natural hypothesis here, as the two pieces of evidence have completely different origins), the combined evidence on z'_T is simply the sum of the two random intervals on z_T and SLR, which is a random interval (Ω, P, Γ), with $\Omega = \Omega_1 \times \Omega_2$, $P = P_1 \times P_2$ and

$$\Gamma(\omega_1, \omega_2) = [U_1(\omega_1) + U_2(\omega_2), V_1(\omega_1) + V_2(\omega_2)] \quad \forall (\omega_1, \omega_2) \in \Omega, \tag{5.10}$$

where $\Gamma_1(\omega_1) = [U_1(\omega_1), V_1(\omega_1)]$ and $\Gamma_2(\omega_2) = [U_2(\omega_2), V_2(\omega_2)]$.

The plausibility and belief functions induced by (Ω, P, Γ) are difficult to derive analytically. They can however be easily approximated using Monte Carlo simulation. An i.i.d. random sample $(u_1, v_1), ..., (u_1, v_1)$ from (U, V) can be generated by sampling N elements $\omega_1, ..., \omega_N$ from (Ω, P) with replacement and computing $[u_i, v_i] = \Gamma(\omega_i)$, $i = 1, .., N$. For every interval I, quantities $Bel(I)$ and $Pl(I)$ can then be estimated by

$$\hat{Bel}(I) = \frac{1}{N} \# \left\{1 \leq i \leq N | [u_i, v_i] \subseteq I\right\} \tag{5.11}$$

and

$$\hat{Pl}(I) = \frac{1}{N}\#\left\{1 \leq i \leq N | [u_i, v_i] \cap I \neq \emptyset\right\}. \tag{5.12}$$

The corresponding contour functions and upper and lower CDFs are shown, respectively, in Figures 5.7 and 5.8. These functions depend on the choice of the function ϕ. The corresponding functions for the random interval obtained by adding a constant SLR value (the upper bound of the interval $[0.5, 0.79]$) to the random interval of z_T are also shown in Figures 5.7 and 5.8 for comparison. We can see that, among the two sources of uncertainty tackled here, uncertainty in future SLR dominates the one in extreme value statistics since it accounts for most of the uncertainty in z'_T, a conclusion that holds for all three choices of ϕ. The figures show also that ignoring uncertainty in SLR can lead to a net underestimation of the extreme sea-level quantiles, and therefore to an unadapted design.

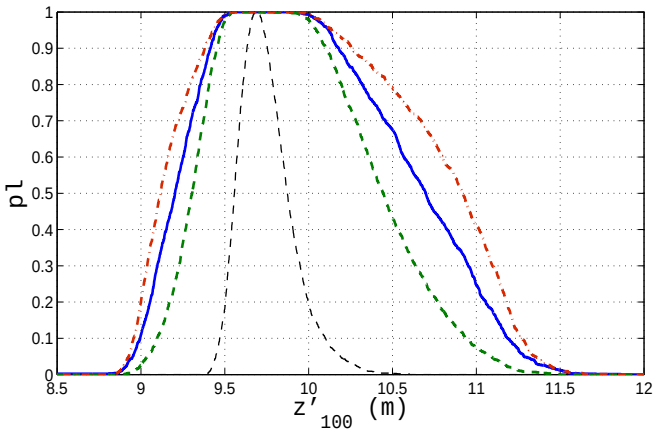

Figure 5.7: Contour plausibility induced by the random set on z'_{100} for three choices of function ϕ ($\phi(x) = x$ (–), $\phi(x) = x^2$ (-) and $\phi(x) = \sqrt{(}x)$ (-.)) and a constant prediction of SLR by 2100 (in a fine line).

In an analogous way, we were interested in assessing the impact of climate change on the performance of the defence asset by analyzing the sensitivity of its hydraulic performance (against overtopping) to the elevation of the mean sea level in 100 years. The methods and results are presented in the next section.

3 Overtopping hazard analysis

3.1 Models and assumptions

Records of wave overtopping are unlikely to be available. Overtopping records are rather derived by calculation on the hydrographic inputs, for which records exist. For the Havre site, characterized by important high tides, significant overtopping is likely to occur in stormy weather when tides are high. In our analysis, we restricted ourselves to (1) high water sea conditions (we consider only records representing

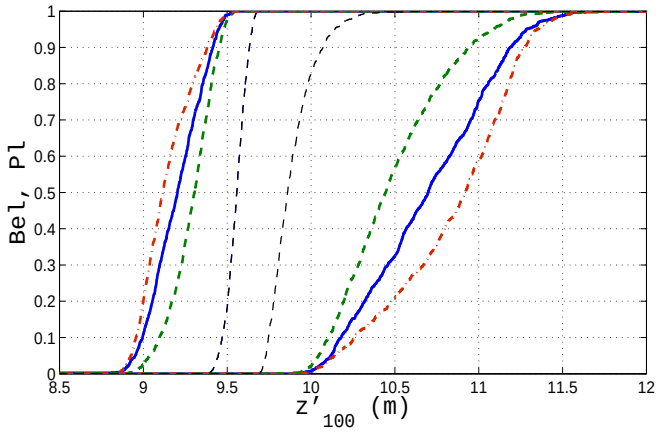

Figure 5.8: Cumulative belief and plausibility induced by the random set on z'_{100} for three choices of function ϕ ($\phi(x) = x$ (–), $\phi(x) = x^2$ (-) and $\phi(x) = \sqrt(x)$ (-.)) and a constant prediction of SLR by 2100 (in a fine line).

conditions at the peak of each tidal cycle, i.e., one record every 12 hours), for which surges can be assumed to be independent from the tidal component and to (2) storm events.

The estimation of the centennial overtopping hazard was conducted according to the following scheme:

1. Preparation of input data: select the records of storm events that correspond to wave-surge (offshore) conjunctions such that both variables exceed a storm threshold.

2. Perform a bivariate statistical analysis to characterize the partial dependence that exists between storm waves and surges. We propose to use copulas to model the joint behavior as they are expected to provide more accurate description of the dependence structure than the BVN model.

3. Enrich the recorded sample of storm events by sampling in the specified joint distribution.

4. Combine the simulated conjunctions with the remaining components of the still sea water-level, i.e., high tides and mean sea level to obtain a sample of wave-sea level conjunctions.

5. Propagate the sample at the toe of the structure using Goda equations (4.1) and (4.2) and calculate the overtopping response for every synthetic hydraulic conjunction.

6. Approximate the centennial overtopping discharge q_{100} from the empirical distribution.

Then, we were interested in evaluating the reinforcement of the dike so that it maintains the current level of protection from overtopping by the end of the century. We used the formula (4.19) to determine the crest level elevation ΔD required to maintain the same hydraulic performance of the dike against centennial overtopping. Therefore,

$$\Delta D = SLR(1 - 0.33 \times 0.52exp(4.2m)\gamma_f\gamma_\beta \ln q_{100}). \tag{5.13}$$

3.2 Application to the Havre site

We applied the method described previously to evaluate the reinforcement of a dike so that it maintains its hydraulic performance against the centennial overtopping. We began by estimating the hydraulic hazard (i.e. the centennial overtopping discharge) from the available records of sea condition.

3.2.1 Multivariate analysis of storm waves and surges

We conducted a multivariate statistical analysis to determine the dependence structure between the hydraulic variables that cause overtopping.

3.2.1.1 Data preparation

As it was explained in Subsection 3.1, overtopping will occur only under high water sea conditions. For the Havre site which is diurnal, i.e., high tides occur every 12.4 hours, the statistical analysis will be based on 706 high waters conditions per year.

A common hypothesis in hydrology is to suppose that the storm duration is inferior to 12.4 hours [POLO 2012]. This hypothesis implies that storm conditions at high waters are independent.

Storm waves (H) and surges (S) were sampled from wave and surge data sets. The technical report by the Department for Environment, Food and Rural Affairs (DEFRA) [Hawkes 2005b] on flood and coastal defence recommends defining the extreme events as the 10 % upper values of the observed sample. With our data, this corresponds to storm surges and waves exceeding, respectively, 0.27 and 2.25 m thresholds. 292 wave-surge conjunctions ((H_i, S_i) $i = 1..., n = 292$) that simultaneously exceed the storm thresholds were sampled in the bivariate records dataset. The sample is highlighted in blue in Figure 5.9.

Given the sampling method (POT), the EVT [Gumbel 1958] suggests the use of the GPD for modeling both marginals. The GP cumulative distribution function of a random variable X exceeding a threshold μ is given by:

$$F_X(x, \beta) = 1 - (1 + \frac{\xi(x - \mu)}{\sigma})^{-\frac{1}{\xi}}, \tag{5.14}$$

$\beta_X = (\xi, \sigma)$ is the set of, respectively, shape and scale parameters. The Q-Q plot, which is a heuristic test that compares empirical and theoretical quantiles, confirms the goodness of fit of both marginals (Figure 5.10).

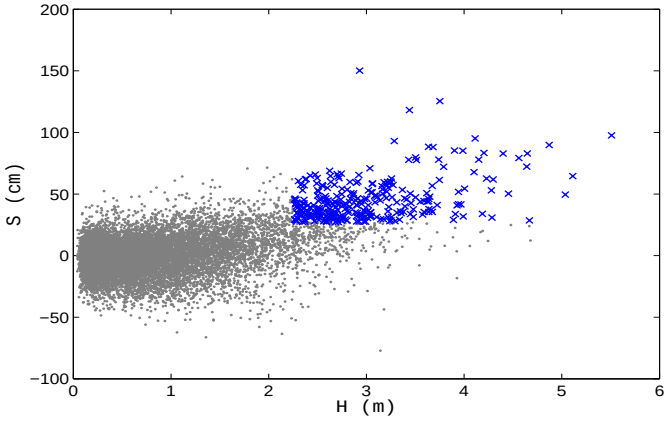

Figure 5.9: Offshore Wave-surge conjunctions (gray dots) and storm events (blue stars).

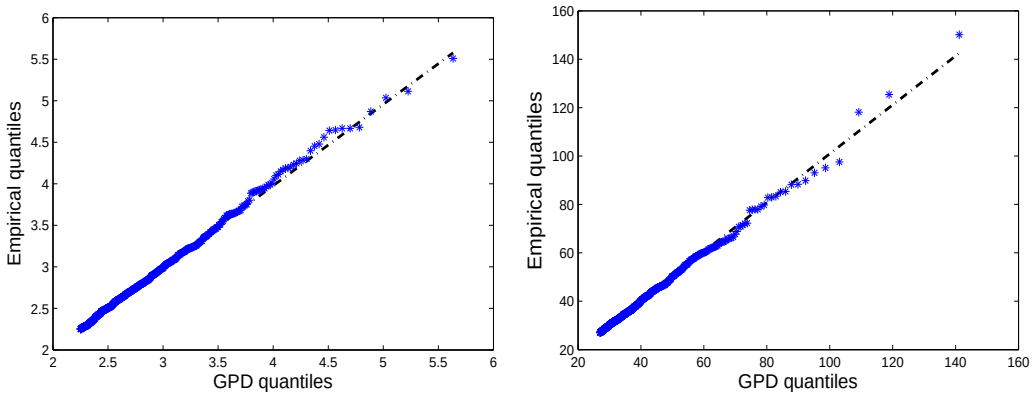

(a) (b)

Figure 5.10: QQ plot for storm waves (a) and surges (b) variables.

3.2.1.2 Modelling dependence with copulas

To characterize the dependence structure among storm waves and surges, we used Archimedean copulas as they allow for several dependence structures as well as for tractable calculations. Three families were tested: Gumbel, Clayton and Frank. Each of these families captures a particular dependence structure. Expressions of these basic families are given in Table 5.3.

The parameter α of the copula can be estimated by parametric or semi-parametric methods. The main parametric methods are the inference functions for margins (IFM) [Joe 1996] and the exact maximum likelihood (EML). The EML estimates the parameters of the marginals and those of the copula simultaneously by maximizing the joint likelihood with respect to all of them. The problem with this direct method is that it could be time-consuming in high-dimensional case. The IFM method is a two-stage parametric method that relies on the split of the parameters

	α	$C(u,v)$
Clayton	$[-1,+\infty[\setminus\{0\}$	$(\max\{u^{-\alpha}+v^{-\alpha}-1;0\})$
Gumbel	$[1,+\infty[$	$exp(-((-Ln(u))^{\alpha}+(-Ln(v))^{\alpha})^{\frac{1}{\alpha}})$
Frank	$\mathbb{R}\setminus\{0\}$	$-\frac{1}{\alpha}Ln\left(1+\frac{(\exp(-\alpha u)-1)(\exp(-\alpha v)-1)}{\exp(-\alpha)-1}\right)$
Independence	$-$	uv

Table 5.3: Expressions of basic families of multivariate Archimedean copulas and the product copula modelling independence.

into *specific* parameters for marginals and *common* (or association) parameters for the copula. First, the parameters of the marginals are estimated, then the parametric margins are plugged into the copula likelihood and the latter is maximized with respect to the copula parameters. Contrary to the EML approach, the IFM does not require costly computations in high dimensional case. Kim [Kim 2007] showed that the IFM performs well in case of goodness of marginal distributions. Since there is no mis-specification of the marginal distributions, we used the IFM technique for inferring the dependence parameter of the tested Archimedean copulas. The copula parameter best estimates were found to be $\hat{\alpha}=1.26$, $\hat{\alpha}=2.16$ and $\hat{\alpha}=0.45$ for, respectively, Gumbel, Frank and Clayton families.

After estimating α for the three families, we needed to check which class fits best the data. Different analytical and graphical goodness-of-fit (GOF) procedures exist to assess the relative quality of fitting. A comprehensive survey of these methods was given by De Metteis [Matteis 2001]. Among the available methods, we applied the graphical GOF procedure by Genest and Rivest [Genest 1993]. This approach is based on comparing the probability distribution $K(.)$ of (1) the empirical copula and (2) the parametric copula, and is easy to implement when the latter is Archimedean. A detailed description of the basis underlying this method is given in Section 3 of the Appendices.

In Figure 5.11, we compare the empirical and the parametric functions λ defined on $[0,1]$ by $\lambda(t)=t-K(t)$ (calculation details can be found in Section 3 in the Appendices). The GOF graphic shows that among Frank, Clayton and Gumbel copulas, the latter best matches the joint records as it's Kendall distribution is the closest to the empirical one. This conclusion was confirmed by an analytical GOF test based on the Akaike's information criterion (AIC):

$$AIC=-2Log(L)+2d, \tag{5.15}$$

with d is the number of the statistical model parameters (for the considered multivariate models, $d=1$) and L is the joint likelihood of the observations, calculated

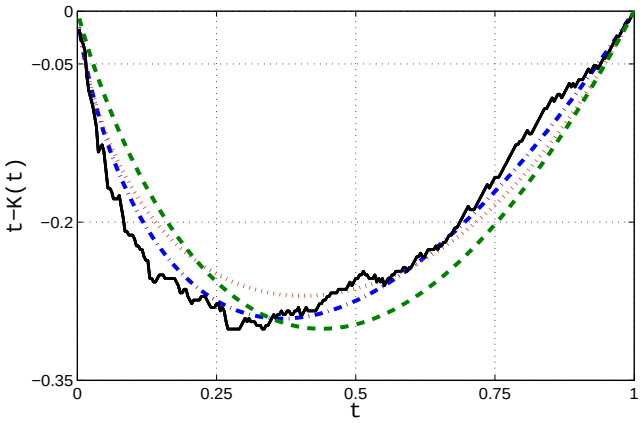

Figure 5.11: Genest and Rivest GOF graphical plot: parametric Kendall distribution (Gumbel (blue dash-dotted), Frank (green dashed) and Clayton (red dotted)) and its empirical estimator (continuous black).

for every multivariate model C by:

$$\begin{aligned} L &= \prod_{i=1}^{n} f_{H,S}(H_i, S_i) \\ &= \prod_{i=1}^{n} c(F_H(H_i), F_S(S_i)) f_H(H_i) f_S(S_i), \end{aligned} \tag{5.16}$$

with c is the copula density. This criterion was found to have the lowest value for Gumbel copula (-63 vs -20.5 for Clayton and -38 for Frank families), confirming thereby that it is the best fitting model.

The selected dependence model suggests that the bivariate sample exhibits upper tail dependence. This suggests that high waves induced by extreme weather conditions are accompanied with high surges, which is an expected result. The estimated coefficient of the dependence structure is relatively low, which means that dependence between storm waves and surges at upper tail is not very significant. To understand the effect on the copula parameter on the dependence structure in the upper tail, we plot in Figure 5.12 two random samples simulated in a Gumbel copula with (1) a relatively high value of the dependence parameter $\alpha = 3$ (left panel) and (2) the ML estimate of the dependence parameter inferred from the data, i.e., $\alpha = \hat{\alpha} = 1.26$ (right panel).

After inferring the ML margin parameters, the likelihood functions at the second

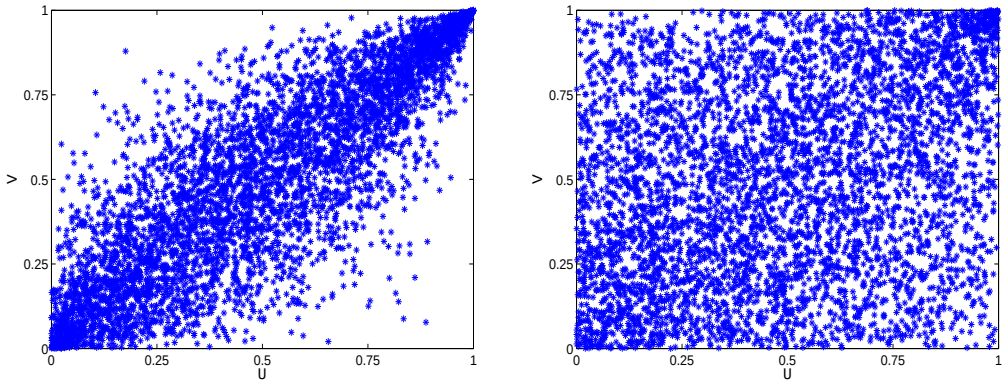

(a) (b)

Figure 5.12: Random sample (U, V) from Gumbel copula with parameter $\lambda = 3$ (a) and $\lambda = 1.26$ (b).

stage of the IFM becomes:

$$\begin{aligned} L(\theta, \hat{\beta}_H, \hat{\beta}_S, H_i, S_i) &= \prod_{i=1}^{n} f_{H,S}(H_i, S_i) \\ &= \prod_{i=1}^{n} c(F_H(H_i, \hat{\beta}_H), F_S(S_i, \hat{\beta}_S)).f_H(H_i, \hat{\beta}_H).f_S(S_i, \hat{\beta}_S) \end{aligned} \tag{5.17}$$

with c is the Gumbel copula density and $\hat{\beta}_H$ and $\hat{\beta}_S$ are the ML best estimates of, respectively, f_H and f_S parameters.

We applied the likelihood-based inference described above to infer the copula parameter α. By normalizing the likelihood in equation (5.17), we constrained the correlation coefficient with a consonant belief function whose contour plausibility is plotted in Figure 5.13.

In what follows, we propose to estimate some design criteria considering the upper tail dependency among hydrographic inputs.

3.2.2 Joint design conjunction

By replacing the bivariate model in (4.14) with the Gumbel copula, the joint return period of the event "$H \geq H*$ and $S \geq S*$" has the following expression:

$$\begin{aligned} T(H^*, S^*) &= \frac{1}{NP(H \geq H^*, S \geq S^*)} \\ &= \frac{1}{N(1 - F_H(H^*) - F_S(S^*) + C(F_H(H^*), F_S(S^*))}. \end{aligned} \tag{5.18}$$

Where N is the average number of observations per year.

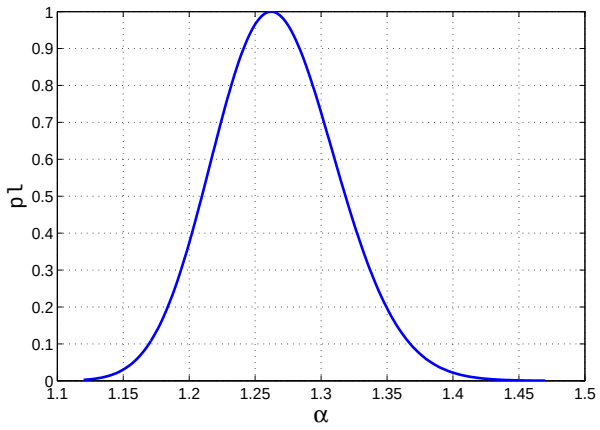

Figure 5.13: Contour plausibility induced by the consonant belief function on the dependence model parameter.

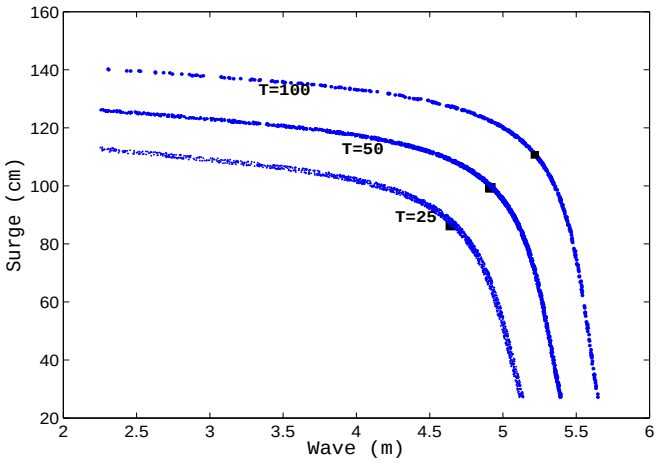

Figure 5.14: Iso-lines of the return periods of storm waves and surges events. Joint design levels are highlighted with squared markers.

We analyzed the impact of the statistical uncertainty on the dependence among both variables on the return period of a particular centennial wave-surge conjunction ($H = 5.2m$, $S = 111cm$) highlighted in black in the centennial iso-return period curve. The selected point has the highest joint probability of occurrence and is often termed as the *design joint conjunction*. To estimate the joint return period, we propagated the random interval on α through expression (5.18). It is easy to check that the function expressing the joint return period is increasing in α, a property that simplifies the calculations as it reduces the propagation algorithm to the vertices method. Figure 5.15 depicts the upper and lower cumulative bounds (respectively plausibility and belief) of the estimated joint return period derived from the belief functions-based representation of the statistical evidence on the dependence parameter. The return period best estimate is 100 (years). When the statistical uncertainty in the dependence parameter is accounted for, the return period estimate remains relatively narrow as it ranges between 70 and 180 years. Assuming absolute dependence and independence between extreme waves and surges would have led respectively to 25 and 10^4 years return period for the conjunction of interest. The huge gap between those values confirms the necessity of rigorously characterizing the dependence structure among hydrographic variables.

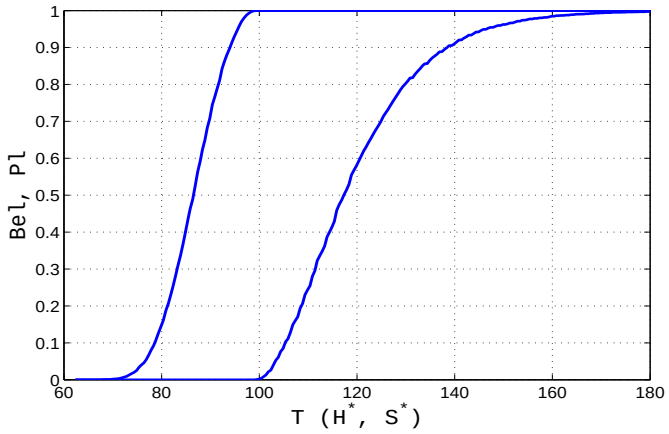

Figure 5.15: Cumulative plausibility and belief on the joint return period of the design storm wave-surge conjunction.

3.2.3 Centennial overtopping

In the synthetic sample of storm events, we combined the surge component with the tidal component. The tide level was sampled in the density function of high tides, constructed over a tidal cycle of 18.6 years (the empirical Kernel density was estimated using tide values predicted by the *PREDIT* software and plotted in Figure 5.16).

The hydrographic sample was then propagated through Goda formula and the overtopping model. The centennial overtopping discharge was then approximated

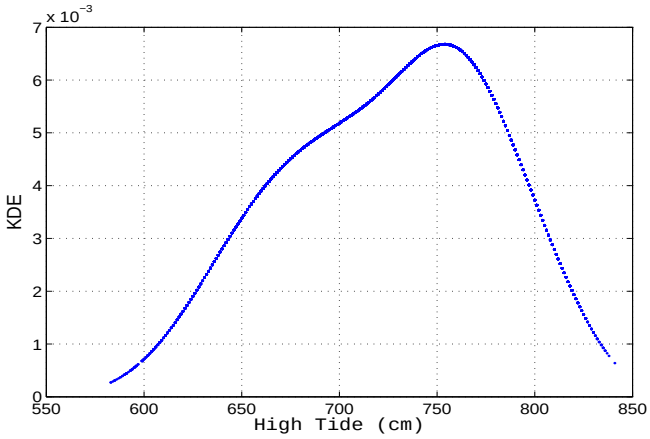

Figure 5.16: Kernel density of High tides.

from the empirical distribution. We accounted for the uncertainty in the dependence parameter between the hydraulic inputs using the following algorithm:

1. Pick at random ω in $[0,1]$ and the corresponding ω-cut of the dependence parameter contour plausibility on α $pl(\alpha)$: $[U^{\alpha}(\omega), V^{\alpha}(\omega)]$.

2. Propagate the focal element through Goda and overtopping discharge models. Estimate, via an optimization method, the focal element on the centennial overtopping $[U^{q_{100}}, V^{q_{100}}]$. This is performed by sampling (in the uniform distribution) m elements from $[U^{\alpha}(\omega), V^{\alpha}(\omega)]$, calculating for every element the centennial overtopping output q_{100}^{i} $(i = 1, ..., m)$, and then taking the maximum and minimum output values. The focal element on q_{100}, is approximated by:

$$U^{q_{100}} = \min_{i=1,...,m} q_{100}^{i}; \tag{5.19}$$

and

$$V^{q_{100}} = \max_{i=1,...,m} q_{100}^{i}. \tag{5.20}$$

These steps were repeated N times and provided N focal elements on the centennial overtopping under present-day conditions. The contour plausibility induced by the random interval on q_{100} is plotted in Figure 5.17. One can read from the figure that the most plausible value of the centennial overtopping discharge is 0.37 10^{-3} and that the statistical uncertainty on the correlation between the hydrographic variables is relatively important when estimating the design hazard.

3.2.4 Adapting to uncertain climate change

By combining the evidence on the magnitude of future SLR by 2100 with the statistical evidence on the centennial overtopping discharge, we evaluated the elevation of the crest so that the dike maintains its current level of protection from overtopping.

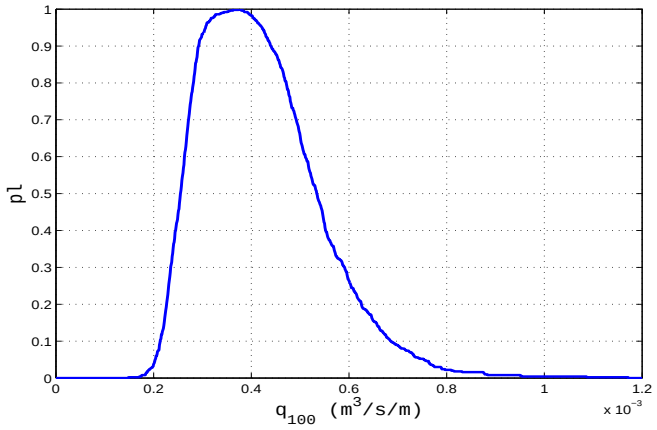

Figure 5.17: Contour plausibility induced by the belief function on the centennial overtopping (under current climate conditions).

The crest elevation was encoded by a random interval – the product of the random interval on SLR and the one on $(1 - 0.33 \times 0.52exp(4.2m)\gamma_f\gamma_\beta Ln(q_{100}))$ (note that the formula holds for q_{100} as $q_{100} < 5\dot{1}0^{-2}$). As the function is increasing in SLR and decreasing in q_{100}, the propagation of the random sets was performed using the vertices method.

The contour plausibility induced by the resulting belief function on the crest elevation ΔD is plotted in continuous line in Figure 5.18. Again, the imprecision in the projections of the elevation of sea water-levels significantly dominates the overall uncertainty in the estimate of the dike reinforcement. This conclusion stems from the visualization and comparison of the extent of the contour plausibilities on ΔD in cases where we consider (1) uncertainty in both SLR and q_{100}, (2) uncertainty in SLR (with $\alpha = \hat{\alpha}$) and (3) uncertainty in α (with $SLR = \hat{SLR} = 1m$). The two first contour plausibility functions are plotted in continuous and dashed lines, respectively. The curves nearly coincide, suggesting that most of the uncertainty in the output pertains to the SLR input. The uncertainty in the statistical correlation between the hydrographic variables was found to have negligible effect on the adaptation level as the third contour plausibility, plotted in dot-dashed line, is very narrow (around the value $\Delta\hat{D} = \Delta D(\hat{SLR}, \hat{\alpha}) = 1.85$ m).

The set of plausible values is relatively large (between 0 and 3.8 meters), with values ranging between 0.9 and 1.5 meters being the most plausible. The obtained results are conservative and reflect the difficulty of making adaptaion decisions consistent with the current limited state of knowledge of the climate evolution.

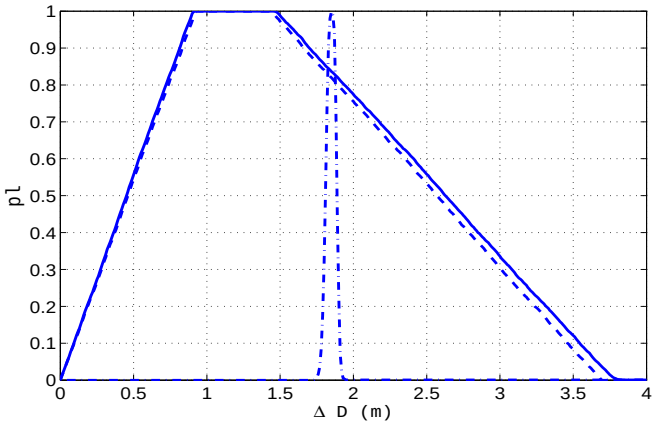

Figure 5.18: Contour plausibility induced by the random interval on the crest elevation required to maintain the hydraulic performance by 2100, accounting for uncertainty in q_{100} (dot-dashed), SLR projections (dashed) and both (continuous).

4 Conclusion

The objective of this study was to (1) estimate some coastal risk indicators and design metrics and (2) assess their evolution when climate changes. We used a DS-based approach to estimate these variables. Risk indicators under present day conditions were first inferred from the available hydraulic records. Statistical evidence has been modeled using the likelihood-based approach, which equates the contour function of a consonant belief function with the normalized likelihood. To assess the evolution of these variables when sea levels increase, we combined them with SLR projections. SLR projections correspond to the combination of IPCC, Rahmstorf, and Pfeffer estimates. Evidence on SLR has been represented by random closed intervals. Results shows that the uncertainty in the 21st century SLR is important and accounts for most of the uncertainty in the design and adaptation criteria.

The analysis we described in this work is methodologically-oriented. The objective was to propose a different mathematical approach for dealing with uncertainty in hydraulic engineering applications. Although this analysis only addressed two components of the coastal design uncertainty, it demonstrated the applicability of belief functions methods and tool in practical engineering applications. The uncertainty analysis conducted in this study can naturally be extended as the theory can handle other types of uncertainty, as those listed in Section 2.3.3.

Conclusion

In many scientific communities (engineering, risk), people are familiar and comfortable with the probabilistic approach when addressing uncertainties, and alternative uncertainty formalisms, such as imprecise probabilities or fuzzy sets, are not very welcomed. In addition to the complex theoretical background underlying these models, the main argument against these theories is the cumbersome calculations they lead to. Some of these arguments are justified while some others are pure clichés as they don't account for the substantial advances these theories are recording, mainly from a computational point of view. In addition, considering the probabilistic model as a Benchmark to evaluate the complexity of an uncertainty theory is not adequate as imprecise probability models in general process much more relevant information (the known and the unknown) than probabilities (only the known).

This thesis is concerned with the use of a particular uncertainty framework – the belief functions theory – in quantifying uncertainty. The objective is to propose a methodology for uncertainty processing (modelling, combination and propagation) based on belief functions and apply it in the assessment of future sea-level rise and the impact of the latter on some coastal risk indicators used in coastal design. Uncertainties in these applications being commonly addressed using probabilities, the second objective is to demonstrate that belief functions can be a promising alternative to probabilities both conceptually and computationally.

The method we proposed exploits the mathematical equivalence between belief functions and random intervals which we described in the opening chapter. When the uncertain quantity of interest θ is random (i.e., characterized by an aleatory uncertainty), a belief function is drawn from the statistical evidence using the likelihood-based inference approach. This method provides a simple way to draw inference conclusions as it leads to consonant belief functions that have simple analytical expression (the normalised likelihood). Otherwise, when the uncertainty is epistemic and the information is too poor to be represented by a precise probabilistic model (interval, quantiles, linguistic judgements, etc.), particular belief functions are assessed. For instance, intervals or confidence interval are better described by consonant belief functions, while quantiles are better represented by belief functions with a finite number of disjoint focal elements, etc. The term better refers here to a better informativeness given the evidence at hand. In the case where evidence on some quantity is provided by several sources (experts, observations and prior information, etc.), we suggested different fusion modes, and described the preconditions, basically on the dependence (between) and reliability of the sources, to their use. To combine belief functions assessed from expert's judgments, we explored some basic combination rules: Dempster's rule (without and with discounting) and the linear opinion pool. The latter method involves the tricky step of assigning weights to the different sources. Equal weighting scheme, as well as two differential schemes defined based on the available information, were explored. To propagate the uncertain quantities (model parameters, inputs) through some model, the extension principle (in the finite case) or Monte Carlo simulations (in the infinite case) allow to estimate (or approximate) the model response. This method allows to treat (represent, combine, and propagate) uncertainty originating from different sources.

The second and third chapters were concerned with the description and quantification of uncertainty on future sea-level rise projections. A review of the state of science on the physical processes controlling the elevation of sea level and their modeling demonstrated the difficulty of making projections because of the substantial uncertainty characterising some of the key processes, in particular the melting of ice sheets. We described three forecasting methods based on different pieces of evidence (historical observations, experts elicitation, and simulations).

Two of these forecasting methods were investigated. We were first concerned with the statistical approach. The method consisted in representing statistical evidence on the parameters of the semi-empirical model using the likelihood based-approach, and the annual temperature projections by consonant belief functions. The model response was then approximated by extending the belief functions on the model parameters and inputs using Monte Carlo simulations. In a second stage, we estimated future SLR projections by combining the most relevant and up-to-date pieces of evidence on the contribution of each of the SLR components. For the melting of mountain glaciers and the expansion of oceans, we used IPCC estimates, whereas for the melting of both ice sheets, we used the very recent expert elicitation by Bamber and Aspinall [Bamber 2013]. We expressed expert opinions, consisting on a set of quantiles, by means of belief functions with disjoint focal elements. We then tested and compared different combination rules to aggregate the individual assessments. A comparative analysis showed that the three methods to derive SLR projections (including the process-based approach) lead to very disparate projections and that the largest part of uncertainty in the estimates is due to the lack of scientific consensus in the climate community on the ice sheets contribution.

The second part of this thesis (chapters IV and IV) addressed the problem of coastal adaptation to climate change. We presented a methodologically-oriented case study that develops a climate change impact assessment and develops an uncertainty analysis based on belief functions. The proposed approach was applied to estimate two risk indicators ((a) extreme sea level and (b) extreme overtopping hazard) and provide elements of decision support for coastal adaptation. The analysis was performed using data from Le Havre site in France. For the uncertainty analysis, we considered two sources of uncertainty. The first is statistical and stems from the statistical analysis when estimating extreme sea conditions. The second is epistemic and is related to the magnitude of future SLR to be integrated when accounting for climate change. Our approach consisted in representing the statistical evidence on the statistical quantities (i.e., (a) and (b)) using the likelihood-based inference. This part involved the use of extreme value theory, as well as copulas to model the joint behaviour of extreme events. The impact of climate change was then analysed by combining the statistical evidence with the most relevant evidence on future SLR. We conducted a sensitivity analysis to assess the sensitivity of the results to the choice of the random interval on SLR projections. It suggests that the choice of the random interval has little impact on the results. Results reveal also that uncertainty in future SLR projections largely dominates statistical uncertainty, and that ignoring it leads to decisions that are inconsistent with the real state of

knowledge of the future evolution of the climate.

Through the several applications described in this work, belief functions theory, as a particular imprecise probability model, was shown to be able to cope naturally with several aspects of uncertainty. Indeed, it can be used to naturally represent different types of poor information (intervals, quantiles, etc.), as well as statistical evidence. We illustrated this fact by constructing several belief functions that describe different pieces of evidence, combining them using different rules and propagating them through monotonous and non-monotonous models. The implementation that we realized on Matlab did not raise particular computational issues.

Future directions

This work is methodologically-oriented. The principal focus was to develop a methodology to uncertainty processing and apply it in an important prediction problem. This work required, for the novice I am, an important bibliographical effort on the application, i.e., on climate modelling and coastal design (tide data processing, wave propagation, etc.). I believe this work would benefit from a closer interaction with climate experts and coastal engineers who would bring an additional insight on some points that have not been addressed with the desired rigor.

Some of the results obtained in this study were based on simplifying and not particularly defensible assumptions. For example, in Chapter II, we assumed independence between the contribution of the Greenland and the eastern and western caps of the Antarctica ice sheet to the overall sea-level rise. From a physical point of view, this assumption is objectionable, as ice sheet responses are more likely to be correlated positively or negatively. Closer interaction with climate experts would allow, inter alia, to better understand the nature of correlation between these components, and to rigorously account for it when combining ice sheets contributions.

In this work, I only addressed some sources of the overall uncertainty involved in the estimation of future SLR and coastal design and adaptation. The proposed methodology can be easily extended to (1) handle other sources of uncertainty, in particular model uncertainty (e.g., the overtopping model, the propagation model), and (2) conduct climate change vulnerability assessments for decision making.

This work raises some interesting theoretical perspectives, which deserve deep future investigations. They can be summarized by the following points:

- The elicitation and assessment of experts' judements: this is a promising research question. Standard elicitation is Bayesian as it assumes that expert's knowledge can be captured by subjective probabilities with behavioral interpretation. As mentioned previously, this is not always true, mainly because of the inevitable ambiguity in experts' knowledge. Belief functions can be more appropriate than probabilities for capturing more faithfully experts' state of knowledge. To our knowledge, no methodologies exist yet for eliciting directly belief functions from experts, and it will be interesting to think of a protocol for such an elicitation, including the survey questions types (comparative,

classificatory, etc.), the answers formats, etc.

- For the combination of expert's opinions, we restricted ourselves to three combination models. The choice of the linear opinion pool method may be questionable as this mode does not account for the conflict between the several sources and requires an extra information about the expert's reliability. Other fusion rules that overcome these shortcomings need to be explored, for instance, the maximal coherent subset rule [Destercke 2009].

- This work adopted the likelihood-based approach for performing statistical inference. This method has strong theoretical basis, as it is the translation of inference principles. In addition, it does not involve cumbersome calculations. However, it will be interesting to investigate some other inference methods and compare the inference conclusions these methods lead to.

Part VI

Appendices

1 Statistical inference

1.1 Frequentist perspective: an exemple to illustrate inconsistency

The following example, proposed by Pratt [Pratt 1965], illustrates the inconsistency of the frequentist inference perspective. It shows in particular how the inference conclusions depend on the sampling space.

Example 1 *An engineer draws a random sample of electron tubes and measures their voltage under certain conditions with a very accurate voltmeter, accurate enough so that the measurements error is negligible compared with the variability of the tubes. A statistician examines the measurements, which look normally distributed and vary from* 75 *to* 99 *volts with a mean of* 87 *and a standard deviation of* 4*. He makes the ordinary normal analysis, giving a confidence interval for the true mean. Later the statistician visits the engineer's laboratory and notices that the voltmeter reads only as far as* 100*, so the population appears to be 'censored'. This necessitates a new analysis, if the statistician is orthodox. However, the engineer says he has another meter reading to* 1000 *volts, which he would have used if any voltage had been over* 100*. This is a relief to the statistician, because it means the population was effectively uncensored after all. But, the next day the engineer informs the statistician that this second meter was not working at the time of the measuring. The statistician ascertains that the engineer would not have held up the measurements until the meter was fixed, and informs him that new measurements are required. The engineer is astounded and says "But the experiment turned out just the same as if the high range meter had been working. I obtained the precise voltages of my sample anyway, so I learned exactly what I would have learned if the high-range meter had been available. Next you'll be asking about my oscilloscope!"*

1.2 Formal description of Bayesian perspective of inference

In the Bayesian perspective, a posterior distribution on the unknown quantity to infer θ is derived by combining a prior belief on θ with the evidence brought by some observation x according to Bayes' rule:

$$p(\theta|x) = \frac{p(x|\theta)p(\theta)}{p(x)} \tag{6.1}$$

where $p(\theta)$ is the prior probability on θ, $p(x|\theta)$ is the probability of observing x given θ, and $p(x)$ is the marginal likelihood of the data: $p(x) = \int p(x|\theta)p(\theta)\mathrm{d}\theta$.

1.3 Axiomatic justification of the likelihood principle

The justification of the likelihood principle was given by Birnbaum [Birnbaum 1962], and is based on proving that it is equivalent to two prominent principles that should hold for inference to be relevant: the sufficiency (SP) and the conditionality (CP) principles. We state these principles based on Berger's book dedicated to the likelihood principle [Berger 1984] .

An experiment E defines a triple $(X, \theta, \{f_\theta\})$, where the random variable X taking values in $\mathbb{X}$ and having density $f_\theta(x)$ for some θ in Θ, is observed. From the experiment and the observation of X, we obtain evidence about θ. Evidence is function of E and the realization x, denoted $Ev(E, x)$.

Conditionality Principle (CP) *Suppose there are two experiments* $E_1 = (X_1, \theta, \{f_\theta^1\})$ *and* $E_2 = (X_2, \theta, \{f_\theta^2\})$*, where only the unknown parameter need to be common to both experiments. Consider the mixed experiment* E^**, whereby* $J = 1$ *or* 2 *is observed, each having probability* $1/2$ *(independent of* θ*,* X_1 *and* X_2*) and Experiment* E_J *is performed. Formally* $E^* = (X^*, \theta, \{f_\theta^*\})$ *where* $X^* = (J, X_J)$ *and* $f_\theta^*(x^*) = f_\theta^*((j, x_j)) = \frac{1}{2} f_\theta^j(x_j)$*. Then:*

$$Ev(E_j^*, x_j^*) = Ev(E_j, x_j).$$

The conditionality principle essentially states that only the experiment that was actually performed should be relevant for the interpretation of that experiment's results. Said differently, if an experiment is selected by a random mechanism independent of θ, then inference conclusions should depend solely on the performed experience and not on the possible but unrealized outcomes. The following example quoted by Berger in [Berger 1985] illustrates the conditionality principle.

Example 2 *Suppose a substance to be analyzed can be either sent to a laboratory in New York or a laboratory in California. The two laboratories seem to be equally competent, so a far coin is flipped to choose between them. The California laboratory is selected on the basis of the flip. A conclusion is based on the results of the analysis. Should the conclusion take into account that the coin could have fallen the other way (and the New York Laboratory could have been chosen)?*

The second principle that justifies the (LP) is the Sufficiency principle (SP) (or its weak version the Weak Sufficieny Principle). This principle introduced by Fisher [Fisher 1922] relies on the notion of *sufficient statistics*. A statistic T is a measurable function of the sample X, and it is said to be sufficient if knowing the actual observations of the sample does not provide any additional information about the quantity to infer θ beyond the information provided by knowing the exact value of this statistic (calculated for this same sample). According to Fisher, T is sufficient if and only if the likelihood function can be factorized as follows:

$$L(\theta; x) = g(t, \theta)h(x). \tag{6.2}$$

for all θ and x.

Weak Sufficiency Principle (WSP) *Consider an experiment* $E = (X, \theta, \{f_\theta\})$*, and suppose* $T(X)$ *is a sufficient statistic for* θ*. Then, if* x_1 *and* x_2 *are two data samples such that* $T(x_1) = T(x_2)$*, then* $Ev(E, x_1) = Ev(E, x_2)$*.*

This principle is obvious given the definition of sufficient statistics. Birnbaum [Birnbaum 1962] showed that accepting the (weak) sufficiency and conditionality principles leads to committing to the (LP), and vice-versa:

Theorem 1 *(Birnbaum (1962a)) The formal likelihood principle follows from the conditionality and the sufficiency principles. The converse is also true.*

The proof of the theorem in the discrete case as proposed by Birnbaum can be found in [Robert 2001, pages 18-19] and in [Berger 1984] for the continuous case. The formal statement of the (LP) is as follows:

Formal Likelihood Principle *Consider two experiments* $E_1 = (X_1, \theta, \{f_\theta^1\})$ *and* $E_2 = (X_2, \theta, \{f_\theta^2\})$*, where* θ *is the same quantity in each experiment. Suppose that for the particular realizations* x_1 *and* x_2 *from* E_1 *and* E_2*, respectively:*

$$L(\theta; x_1) = cL(\theta; x_2)$$

for some constant c*. Then*

$$Ev(E_1, x_1) = Ev(E_2, x_2).$$

It should be noted that frequentist inference clashes with the likelihood principle as it violates the conditionality principle (inference conclusions are drawn from hypothesized data), whereas Bayesian inference is compatible with it.

2 Correlation analysis in time series

Time series analysis concerns the analysis of data collected over time. Let $\{x_t\} = \{...x_t, x_{t+1}, ...\}$ be a time series indexed by a time subscript t.

Autocorrelation refers to the correlation of a time series with its past. Characterising the autocorrelation of a time series is often performed through the autocorrelation function – a set of autocorrelation coefficients between the time series itself and the time series lagged by successive time units. The autocorrelation coefficient between the time series and the time series shifted by k time steps, also called the autocorrelation coefficient at lag k, can be approximated by the statistic:

$$r_k = \frac{\sum_{t=1}^{N-1} (x_t - \overline{x})(x_{t+k} - \overline{x})}{\sum_{t=1}^{N-1} (x_t - \overline{x})^2} \tag{6.3}$$

with $\overline{x} = \sum_{t=1}^{N-1} x_t$. The autocorrelation function is often displayed graphically as a function of time lag k.

PACF is a conditional correlation. The partial autocorrelation at lag k is defined as the autocorrelation between X_t and X_{t-k} that is not accounted for by lags 1 through $k-1$.

The plots of the correlation and partial autocorrelations functions, referred to as correlogams. They are graphical tools used to identify an appropriate time series model. In particular, the correlogram can be used to detect (non)-randomness in data. This is performed by comparing computed correlation coefficients with a critical threshold of correlation that indicates whether the sample normality hypothesis should be rejected or not. For a sample of size N, the critical level of correlation for 95% significance is $\pm 1.96/\sqrt{N}$. This level corresponds to the confidence interval for the autocorrelation sequence of a white noise $\mathcal{N}(0,1)$.

If the data is found to be non-random, alternative models should be tested, as the autoregressive models:

$$AR(p) : X_t = c + \sum_{i=1}^{p} a_i X_{t-i} + \varepsilon_t, \tag{6.4}$$

or the ARMA models:

$$ARMA(p,q) : X_t = \sum_{i=1}^{p} a_i X_{t-i} + \sum_{i=1}^{q} b_i \varepsilon_{t-i} + \varepsilon_t, \tag{6.5}$$

where $a_1, ..., a_p, b_1, ..., b_q$ are the models parameters, (p,q) the order of the process and ε_t is a white noise. The identification of the properties of those models, such as their order, is based on both the PACF and ACF plots.

3 Multivariate analysis through copulas

3.1 Archimedean copulas family

Archimedean copulas are defined for the bivariate case by:

$$C(u,v) = \phi^{[-1]}(\phi(u) + \phi(v)) \quad \forall (u,v) \in [0,1]^2,$$

where ϕ is a continuous, strictly decreasing and convex function from $[0,1]$ to $[0,+\infty[$, such that $\phi(1) = 0$. Here, $\phi^{[-1]}$ is the pseudo-inverse of ϕ defined from $[0,+\infty[$ into $[0,1]$ by:

$$\phi^{[-1]}(t) = \begin{cases} \phi^{-1}(t) & 0 \leq t \leq \phi(0) \\ \\ 0 & \phi(0) \leq t \leq \infty. \end{cases}$$

If $\phi(0) = \infty$, the pseudo-inverse coincides with the inverse ϕ^{-1} and the copula is said to be strict. Function ϕ is called the *generator* of C. Note that it possible to extend Archimedean copulas to the multivariate case (refer to [McNeil 2005]).

Table 6.1 summarises the expressions of the generator functions of these basic Archimedean copulas.

	$\phi(t)$	$\alpha \in$
Clayton	$(t^{-\alpha} - 1)/\alpha$	$[-1, +\infty[\setminus \{0\}$
Gumbel	$(-Lnt)^{\alpha}$	$[1, +\infty[$
Frank	$-Ln\left(\frac{\exp(-\alpha t)-1}{\exp(-\alpha)-1}\right)$	$\mathbb{R} \setminus \{0\}$

Table 6.1: Generator and expressions of basic families of multivariate Archimedean copulas.

3.2 Genest and Rivest goodness-of-fit test

Different approaches exist to assess the GOF of copulas to data (a non-exhaustive survey can be found in [Matteis 2001]). Genest and Rivest [Genest 1993] proposed a graphical method based on the so-called *Kendall dependence function* for selecting the most adequate copula. We describe this approach in the bivariate case.

Let $((X_{11}, X_{12}), ..., (X_{n1}, X_{n2}))$ be an i.i.d sample from a two-dimensional random vector $\mathbf{X} = (X_1, X_2)$ with continuous marginal distribution functions $F_1(X_1)$ and $F_2(X_2)$ and joint distribution function F:

$$F(X_1, X_2) = C(F_1(X_1), F_2(X_2)).$$

The Kendall function is the (univariate) distribution function of C defined on the unit interval $[0,1]$ by:

$$K(t) = \mathbb{P}[C(U) \leq t] \quad ,$$

where $U_1 \sim N(0,1)$, $U_2 \sim N(0,1)$ and $U = (U_1, U_2) \sim C$. For a bivariate Archimedean copula C with generator ϕ and parameter α, the parametric Kendall function has a simple expression:

$$K_\alpha(t) = K(\alpha, t) = t - \frac{\phi(t)}{\phi'(t^+)} \quad \forall t \in]0,1].$$

A nonparametric estimator of Kendall function is the empirical distribution given by :

$$K_n(t) = \frac{1}{n+1} \sum_{i=1}^{n} I\left\{\hat{C}(\hat{U}_i) \leq t\right\},$$

where I is the indicator function, $\hat{C}$ is the empirical copula (introduced by Deheuvels [Deheuvels 1979]) defined for every $u = (u_1, u_2) \in [0,1]^2$ by:

$$\hat{C}(u) = \frac{1}{n+1} \sum_{i=1}^{n} I\left\{\hat{U}_{i1} \leq u_1, \hat{U}_{i2} \leq u_2\right\}$$

and $\hat{\mathbf{U}} = (\hat{U}_1, \hat{U}_2)$ is the vector of pseudo-observations:

$$\begin{cases} \hat{U}_{ij} = \frac{n}{n+1} \hat{F}_j(X_{ij}) & i \in \{1, ..., n\} \\ \\ \hat{F}_j(x) = \frac{1}{n} \sum_{i=1}^{n} I\{X_{ij} \leq x\} & j \in \{1, 2\}. \end{cases}$$

The estimator $\hat{\alpha}$ is adequate if the parametric distribution function $K_{\hat{\alpha}}(.)$ is close to the nonparametric function $K_n(.)$ and the the choice of the best fitting family is based on visualizing (or calculating) the closeness between both distributions. Graphically, GOF can be visualized from the QQ-plot of Kendall distribution or from the plot of function $\lambda(.)$ defined as $\lambda(t) = t - K(t)$.

4 Expert Elicitation: intermediate results

e_j \ e_i	**1**	**2**	**3**	**4**	**5**	**6**	**7**	**8**	**9**	**10**	**11**	**12**	**13**
1	0.59	0.9	0.75	0.34	0.54	0.9	0.34	0.34	0.7	0.36	0.34	0.34	0.34
2	-	0.59	0.9	0.9	0.9	0.34	0.72	0.9	0.7	0.9	0.52	0.9	0.9
3	-	-	0.59	0.36	0.54	0.9	0.52	0.34	0.9	0.54	0.7	0.52	0.36
4	-	-	-	0.59	0.36	0.9	0.54	0.36	0.9	0.34	0.72	0.52	0.38
5	-	-	-	-	0.59	0.9	0.56	0.36	0.9	0.54	0.72	0.52	0.36
6	-	-	-	-	-	0.59	0.7	0.9	0.72	0.9	0.52	0.9	0.9
7	-	-	-	-	-	-	0.59	0.54	0.54	0.34	0.54	0.34	0.54
8	-	-	-	-	-	-	-	0.59	0.9	0.54	0.74	0.54	0.56
9	-	-	-	-	-	-	-	-	0.59	0.7	0.54	0.54	0.9
10	-	-	-	-	-	-	-	-	-	0.59	0.54	0.54	0.54
11	-	-	-	-	-	-	-	-	-	-	0.59	0.34	0.74
12	-	-	-	-	-	-	-	-	-	-	-	0.59	0.52
13	-	-	-	-	-	-	-	-	-	-	-	-	0.59

Table 6.2: Conflict (in the sense of Dempster) among experts.

e_j \ e_i	**1**	**2**	**3**	**4**	**5**	**6**	**7**	**8**	**9**	**10**	**11**	**12**	**13**
1	0.24	0.3	0.29	0.15	0.23	0.31	0.14	0.15	0.24	0.15	0.14	0.14	0.15
2	-	0.16	0.28	0.31	0.3	0.1	0.24	0.32	0.2	0.3	0.17	0.29	0.32
3	-	-	0.22	0.15	0.21	0.3	0.2	0.14	0.3	0.21	0.27	0.2	0.15
4	-	-	-	0.26	0.16	0.32	0.24	0.17	0.33	0.15	0.31	0.22	0.18
5	-	-	-	-	0.25	0.31	0.24	0.16	0.32	0.23	0.3	0.21	0.16
6	-	-	-	-	-	0.17	0.24	0.33	0.21	0.31	0.18	0.3	0.33
7	-	-	-	-	-	-	0.25	0.24	0.19	0.14	0.23	0.14	0.25
8	-	-	-	-	-	-	-	0.27	0.33	0.24	0.33	0.23	0.27
9	-	-	-	-	-	-	-	-	0.17	0.24	0.19	0.18	0.33
10	-	-	-	-	-	-	-	-	-	0.24	0.27	0.22	0.24
11	-	-	-	-	-	-	-	-	-	-	0.25	0.14	0.33
12	-	-	-	-	-	-	-	-	-	-	-	0.22	0.22
13	-	-	-	-	-	-	-	-	-	-	-	-	0.28

Table 6.3: Conflict (in the sense of Dempster) among experts after discounting.

Bibliography

[Aickin 2000] M. Aickin. Connecting Dempster–Shafer belief functions with likelihood based inference. *Synthese*, vol. 123, pages 347–364, 2000. (Cited on page 34.)

[Allsop 2007] W. Allsop, A. Kortenhaus and M. Morris. *Failure Mechanisms for Flood Defence Structures. FLOODsite - Integrated Flood Risk Assessment and Management Methodologies.* 2007. (Cited on pages 91, 94 and 95.)

[Andronova 2001] N. G. Andronova and M. E. Schlesinger. Objective estimation of the probability density function for climate sensitivity. *Journal of Geophysical Research-Atmospheres*, vol. 106, pages 22605–22611, 2001. (Cited on page 45.)

[Apel 2004] H. Apel, A. H. Thikeken, B. Merz and G. Blosch. Flood risk assessment and associated uncertainty. *Natural Hazards and Earth System Sciences*, vol. 4, pages 295–308, 2004. (Cited on page 102.)

[Aspinall 2008] W. Aspinall. *Expert judgement elicitation using the classical model and EXCALIBUR, briefing notes.* 2008. (Cited on page 25.)

[Bamber 2013] J. L. Bamber and W. P. Aspinall. An expert judgment assessment of future sea level rise from the ice sheets. *Nature Climate Change*, vol. 3, pages 424–427, 2013. (Cited on pages 49, 52, 53, 54, 74, 76, 81, 83, 85 and 132.)

[Baudrit 2005] C. Baudrit. *Représentation et propagation des connaissances imprécises et incertaines : Application à l'évaluation des risques liés aux sites et aux sols pollués.* PhD thesis, Université Paul-Sébastier, Toulouse, 2005. (Cited on pages 61 and 75.)

[Ben-Abdallah 2013] N. Ben-Abdallah, N. Mouhous Voyneau and T. Denoeux. Combining statistical and expert evidence using belief functions: Application to centennial sea level estimation taking into account climate change. *International Journal of Approximate Reasoning*, 2013. (Cited on page 14.)

[Beraldi 2011] P. Beraldi and al. Monte Carlo and fuzzy interval propagation of hybrid uncertainties on a risk model for the design of a flood protection dike. *In Proceedings of the European Safety and Reliability Conference*, pages 2167–2175, 2011. (Cited on page 102.)

[Berger 1984] J.O. Berger and R. L. Wolpert. *The Likelihood Principle.* Institute of Mathematical Statistics, Hayward, CA, 1984. (Cited on pages 29, 32, 138 and 139.)

[Berger 1985] J.O. Berger. *Statistical Decision Theory and Bayesian Analysis.* Springer, second edition, 1985. (Cited on page 138.)

[Berleant 1998] D. Berleant and C. Goodman-Strauss. Bounding the results of arithmetic operations on random variables of unknown dependency using intervals. *Reliable Computing*, vol. 4, no. 2, pages 147–165, 1998. (Cited on page 28.)

[Bindoff 2007] N. Bindoff and al. *Contribution of Working Group I to the Fourth Assessment Report of the Intergovernmental Panel on Climate Change*. Cambridge University Press, Cambridge, 2007. (Cited on page 100.)

[Birnbaum 1962] A. Birnbaum. On the foundations of statistical inference (with discussion). *Journal of the American Statistical Association*, vol. 57, no. 298, pages 269–326, 1962. (Cited on pages 32, 138 and 139.)

[Bloch 1996] I. Bloch. Some aspects of Dempster–Shafer evidence theory for classification of multi-modality medical images taking partial volume effect into account. *Pattern Recognition Letters*, vol. 17, no. 8, pages 905–919, 1996. (Cited on page 13.)

[Boston 2000] J. R. Boston. A signal detection system based on Dempster–Shafer theory and comparison to fuzzy detection. *IEEE Transactions on Systems Man and Cybernetrics, Part C Applications and Reviews*, vol. 30, no. 1, pages 45–51, 2000. (Cited on page 13.)

[Chao 2008] B. F. Chao, Y. H. Wu and Y. S. Li. Impact of artificial reservoir water impoundment on global sea level. *Science*, vol. 320, pages 212–214, 2008. (Cited on page 64.)

[Charnes 1976] A. Charnes, E. L. Frome and P. L. Yu. The equivalence of generalized least squares and maximum likelihood estimates in the exponential family. *Journal of the American Statistical Association*, vol. 71, pages 169–171, 1976. (Cited on page 68.)

[Church 2006] J. A. Church and N. J. White. A 20th-century acceleration in global sea-level rise. *Geophysical Research Letters*, vol. 33, 2006. (Cited on pages 46 and 64.)

[Coles 1991] S. G. Coles and J. A. Tawn. Modelling extreme multivariate events. *Journal of Royal Statistical Society. B*, vol. 53, pages 377–392, 1991. (Cited on page 98.)

[Cooke 1988] R. M. Cooke. Uncertainty in risk assessment: A probabilist's manifesto. *Reliability Engineering and System Safety*, vol. 23, pages 277–283, 1988. (Cited on page 24.)

[Davison 1990] A. Davison and R. Smith. Models for exceedances over high thresholds. *Journal of Royal Statistics Society*, vol. 52, no. 3, pages 393–442, 1990. (Cited on page 97.)

[Dawson 2005] R. J. Dawson, J. W. Hall, P. D. Bates and R. J. Nichols. Quantified analysis of the probability of flooding in the Thames Estuary under imaginable worst case sea-level rise scenarios. *International Journal of Water Resources Development*, vol. 21, no. 4, pages 577–591, 2005. (Cited on page 102.)

[de Finetti 1974] B. de Finetti. *Theory of probability, vol. i.* John Wiley, New York, 1974. (Cited on page 11.)

[Deheuvels 1979] P. Deheuvels. La fonction de dépendence empirique et ses propriétés : un test non paramétrique d'indépendence. *Academic Royal Bel. Bull. Class Sc*, vol. 5, pages 274–292, 1979. (Cited on page 142.)

[Dempster 1966] A. P. Dempster. New methods for reasoning towards posterior distributions based on sample data. *Annals of Mathematical Statistics*, vol. 37, pages 355–374, 1966. (Cited on pages 13, 15 and 30.)

[Dempster 1967] A. P. Dempster. Upper and lower probabilities induced by a multivalued mapping. *Annals of Mathematical Statistics*, vol. 38, pages 325–339, 1967. (Cited on page 13.)

[Dempster 1968a] A. P. Dempster. A generalization of Bayesian inference (with discussion). *Journal of Statistical Society B*, vol. 30, pages 205–247, 1968. (Cited on pages 30 and 35.)

[Dempster 1968b] A. P. Dempster. Upper and lower probabilities generated by a random closed interval. *Annals of Mathematical Statistics*, vol. 39, no. 3, pages 957–966, 1968. (Cited on pages 17 and 30.)

[Dempster 2008] A. P. Dempster. The Dempster–Shafer calculus for statisticians. *International Journal of Approximate Reasoning*, vol. 48, no. 2, pages 365–377, 2008. (Cited on page 31.)

[Denoeux 2001] T. Denoeux and L. M. Zouhal. Handling possibilistic labels in pattern classification using evidential reasoning. *Fuzzy Sets and Systems*, vol. 122, no. 3, pages 409–424, 2001. (Cited on page 13.)

[Denoeux 2006] T. Denoeux. Constructing belief functions from sample data using multinomial confidence regions. *International Journal of Approximate Reasoning*, vol. 42, no. 3, pages 228–252, 2006. (Cited on page 31.)

[Denoeux 2008] T. Denoeux. Conjunctive and disjunctive combination of belief functions induced by nondistinct bodies of evidence. *Artificial Intelligence*, vol. 172, pages 234–264, 2008. (Cited on pages 20 and 23.)

[Denoeux 2009] T. Denoeux. Extending stochastic ordering to belief functions on the real line. *Information Sciences*, vol. 179, pages 1362–1376, 2009. (Cited on page 17.)

[Denoeux 2013a] T. Denoeux. Likelihood-based belief functions: justification and some extensions to low-quality data. *International Journal of Approximate Reasoning (In Press)*, 2013. (Cited on pages 30, 33, 34 and 35.)

[Denoeux 2013b] T. Denoeux. Maximum likelihood estimation from uncertain data in the belief function framework. *IEEE Transactions on Knowledge and Data Engineering*, vol. 25, no. 1, pages 119–130, 2013. (Cited on page 35.)

[Dessai 2004] S. Dessai and M. Hulme. Does climate adaptation decisions need probabilities? *Climate Policy*, vol. 4, pages 107–128, 2004. (Cited on page 44.)

[Dessai 2007] S. Dessai and J. van der Sluijs. *Uncertainty and climate change adaptation – a scoping study*. Copernicus Institute for Sustainable Development and Innovation, Department of Science Technology and Society, Universitat Utrecht, 2007. (Cited on page 41.)

[Destercke 2008a] S. Destercke. *Uncertainty representation and combination: new results with application to nuclear safety issues*. PhD thesis, Université Paul-Sébastier, Toulouse, 2008. (Cited on page 25.)

[Destercke 2008b] S. Destercke, D. Dubois and E. Chojnacki. Unifying practical uncertainty representations: Generalized p-boxes. *International Journal of Approximate Reasoning*, vol. 49, no. 3, pages 649–663, 2008. (Cited on page 19.)

[Destercke 2009] S. Destercke, D. Dubois and E. Chojnacki. Possibilistic information fusion using maximal coherent subsets. *IEEE Transactions on Fuzzy Systems*, vol. 17, no. 1, pages 79–92, 2009. (Cited on page 134.)

[Dong 1987] W. M. Dong and H. C. Shah. Vertex method for computing functions of fuzzy variables. *Fuzzy Sets and Systems*, vol. 24, no. 1, pages 65–78, 1987. (Cited on page 27.)

[Dubois 1986] D. Dubois and H. Prade. A set-theoretic view on belief functions: logical operations and approximations by fuzzy sets. *International Journal of General Systems*, vol. 12, no. 3, pages 193–226, 1986. (Cited on page 20.)

[Dubois 1987] D. Dubois and H. Prade. The mean value of a fuzzy number. *Fuzzy Sets and Systems*, vol. 24, pages 279–300, 1987. (Cited on page 18.)

[Dubois 1988] D. Dubois and H. Prade. *Possibility theory: An approach to computerized processing of uncertainty*. Plenum Press, New-York, 1988. (Cited on pages 13, 17, 18 and 36.)

[Dubois 1991] D. Dubois and H. Prade. Random sets and fuzzy interval analysis. *Fuzzy Sets and Systems*, vol. 42, pages 87–101, 1991. (Cited on page 26.)

[Dubois 1992] D. Dubois and H. Prade. On the combination of evidence in various mathematical frameworks. *Reliability Data Collection and Analysis*, vol. 3, pages 213–241, 1992. (Cited on page 20.)

[Dubois 2010] D. Dubois and T. Denoeux. Statistical inference with belief functions and possibility measures: a discussion of basic assumptions. *Combining Soft Computing and Statistical Methods in Data Analysis*, vol. 77, pages 217–225, 2010. (Cited on page 35.)

[Efron 1986] B. Efron. Why isn't everyone a Bayesian. *American Statistician*, vol. 40, pages 1–11, 1986. (Cited on page 29.)

[Efron 1998] B. Efron. R. A. Fisher in the 21st century. *Statistical Science*, vol. 13, no. 2, pages 95–122, 1998. (Cited on page 29.)

[Elouedi 2004] Z. Elouedi, K. Mellouli and Ph. Smets. Assessing sensor reliability for multi-sensor data fusion with the transferable belief model. *IEEE Transactions on Systems, Man and Cybernetics, Part B*, vol. 34, pages 782–787, 2004. (Cited on page 23.)

[Ferson 2003] S. Ferson, V. Kreinovich, L. Ginzburg, D. S. Myers and K. Sentz. *Constructing probability boxes and Dempster–Shafer structures. Technical Report SAND2002-4015*. Albuquerque, NM, 2003. (Cited on page 19.)

[Ferson 2004] S. Ferson, J. Hajagos, D. Berleant, J. Zhang, W. Tucker, L. Ginzburg and W. Oberkampf. *Dependence in probabilistic modeling, Dempster–Shafer theory, and probability bounds analysis. Technical Report SAND-2004-3072*. Albuquerque, NM, 2004. (Cited on page 28.)

[Fisher 1922] R. A. Fisher. On the mathematical foundations of theoretical statistics. *Philosophical Transactions of the Royal Society of London, Series A*, vol. 222, pages 309–368, 1922. (Cited on pages 32 and 138.)

[Fisher 1925] R. A. Fisher. Theory of statistical estimation. *In Proceedings of the Cambridge Philosophical Society*, volume 22, pages 700–725, 1925. (Cited on page 32.)

[Fisher 1933] R. A. Fisher. The concepts of inverse probability and fiducial probability referring to unknown parameters. *In Proceedings of The Royal Society of London, Series A*, volume 139, pages 343–348, 1933. (Cited on page 29.)

[Fisher 1935] R. A. Fisher. The fiducial argument in statistical inference. *Annals of Eugenics*, vol. 6, pages 391–398, 1935. (Cited on page 29.)

[Fisher 1973] R. A. Fisher. *Statistical Methods and Scientific Inference*. Hafner, New York, third edition, 1973. (Cited on page 29.)

[Forest 2002] C. E. Forest and al. Quantifying uncertainties in climate system properties with the use of recent climate observations. *Science*, vol. 295, pages 113–117, 2002. (Cited on page 45.)

[Fraser 1968] D. A. S Fraser. *The Structure of Inference*. Wiley, New-York, 1968. (Cited on page 30.)

[Gelman 2008] A. Gelman. Objections to Bayesian statistics. *Bayesian Analysis*, vol. 3, pages 445–450, 2008. (Cited on page 29.)

[Genest 1993] C. Genest and L. P. Rivest. Statistical inference procedures for bivariate Archimedean copulas. *Journal of the American Statistical Association*, vol. 88, pages 1034–1043, 1993. (Cited on pages 120 and 141.)

[Genest 2007] C. Genest and A. C. Favre. Everything you always wanted to know about copulas modeling but were afraid to ask. *Journal of Hydrology Enineering*, vol. 347, pages 561–566, 2007. (Cited on page 99.)

[Ghosh 1988] J. K. Ghosh. *Interval analysis*. Springer-Verlag, New-York, 1988. (Cited on page 32.)

[Goda 2000] Y. Goda. *Random Seas and Design of Maritime Structures*. World scientific Publishing, Singapore, 2 edition, 2000. (Cited on page 93.)

[Gregory 2002] J. M. Gregory and al. An observationally based estimate of the climate sensitivity. *Journal of Climate*, vol. 15, pages 3117–3121, 2002. (Cited on page 45.)

[Gumbel 1958] E. J. Gumbel. *The Statistics of Extremes*. Colombia University Press, New-York, 1958. (Cited on pages 96 and 118.)

[Guttorp 2012] P. Guttorp and al. Statistical prediction of global sea level from global temperature. 2012. (Cited on pages 66 and 67.)

[Ha-Duong 2003] M. Ha-Duong. Imprecise probability bridges scenario-forecast gap. *In Annual Meeting of the International Energy Workshop, Austria*, 2003. (Cited on page 44.)

[Ha-Duong 2008] M. Ha-Duong. Hierarchical fusion of expert opinions in the Transferable Belief Model, application to climate sensitivity. *International Journal of Approximate Reasoning*, vol. 49, no. 3, pages 555–574, 2008. (Cited on pages 46, 59 and 87.)

[Hall 2007a] J. Hall. Probabilistic climate scenarios may misrepresent uncertainty and lead to bad adaptation decisions. *Hydrological Processes*, vol. 21, pages 1127–1129, 2007. (Cited on page 44.)

[Hall 2007b] J. Hall, G. Fu and J. Lawry. Imprecise probabilities of climate change: aggregation of fuzzy scenarios and model uncertainties. *Climatic Change*, vol. 81, pages 265–281, 2007. (Cited on page 46.)

[Hawkes 2002] P. J. Hawkes, B. P. Gouldby, J. A. Tawn and M. W. Owen. The joint probability of waves and water levels in coastal engineering design. *Journal of Hydraulic Research*, vol. 40, pages 241–251, 2002. (Cited on pages 93 and 98.)

[Hawkes 2005a] P. Hawkes. *Use of Joint Probability Methods in Flood Management: A guide to Best Practice. R&D technical Report FD2308/TR2.* 2005. (Cited on page 98.)

[Hawkes 2005b] P. J. Hawkes. *Use of joint probability methods in flood management, R & D Technical Report FD2308/tR2.* 2005. (Cited on page 118.)

[Holgate 2007] S. Holgate, S. Jevrejeva, P. Woodorth and S. Brewer. Comment on "A semi-empirical approach to projecting future sea-level rise ". *Science*, vol. 1866, 2007. (Cited on pages 52, 66 and 74.)

[Hunter 2010] J. Hunter. Estimating sea-level extremes under conditions of uncertain sea-level rise. *Climatic Change*, vol. 99, pages 331–350, 2010. (Cited on page 100.)

[Inagaki 1991] T. Inagaki. Independence between safety-control policy and multiple-sensor schemes via Dempster–Shafer theory. *IEEE Transactions on Reliability*, vol. 40, no. 2, pages 182–188, 1991. (Cited on page 13.)

[IPCC 2007] IPCC. *Climate Change 2007. Contribution of Working Group I to the Fourth Assessment Report of the Intergovernmental Panel on Climate Change.* Cambridge University Press, Cambridge, UK, 2007. (Cited on pages 41, 42, 43, 45, 47, 48, 50 and 85.)

[IPCC 2013] IPCC. *Climate Change 2013. The Pysical Science Basis, http://www.ipcc.ch/report/ar5/wg1/.* 2013. (Cited on page 51.)

[Joe 1996] H. Joe and J. J. Xu. *The Estimation Method of Inference Functions for Margins for Multivariate Models. Technical Report no. 166.* University of British Columbia, Department of Statistics, 1996. (Cited on pages 99 and 119.)

[Jousselme 2001] A. L. Jousselme, D. Grenier and E. Bossé. A new distance between two bodies of evidence. *Information Fusion*, vol. 2, no. 2, pages 91–101, 2001. (Cited on page 23.)

[Jousselme 2012] A. L. Jousselme and P. Maupin. Distances in evidence theory: comprehensive survey and generalizations. *International Journal of Approximate Reasoning*, vol. 53, no. 2, pages 118–145, 2012. (Cited on page 23.)

[Kahneman 1982] D. Kahneman, P. Slovic and A.Tversky. *Judgment under uncertainty: heuristics and biases.* Cambridge University Press, 1982. (Cited on page 9.)

[Kay 2007] R. Uwe Kay. Fundamentals of the Dempster–Shafer theory and its applications to system safety and reliability modeling. *Reliability, Quality and Safety Engineering*, vol. 14, no. 6, pages 173–185, 2007. (Cited on page 13.)

[Kim 2007] G. Kim and P. Silvapulle. Comparison of semi-parametric and parametric methods for estimating copulas. *Computational Statistics and Data Analysis*, vol. 51, pages 2836–2850, 2007. (Cited on page 120.)

[Klein 2010] J. Klein and O. Colot. Automatic discounting rate computation using a dissent criterion. *In Proceedings of the Workshop on the Theory of Belief Functions*, pages 1–6, 2010. (Cited on page 24.)

[Knutti 2002] R. Knutti and al. Constraints on radiative forcing and future climate change from observations and climate model ensembles. *Nature*, vol. 416, pages 719–723, 2002. (Cited on page 45.)

[Knutti 2008] R. Knutti and al. A review of uncertainties in global temperature projections over the twenty-first century. *Journal of Climate*, vol. 21, pages 2651–2663, 2008. (Cited on page 45.)

[Komatina 2005] D. Komatina and N. Branisavljevic. Uncertainty analysis as a complement to flood risk assessment - Theoretical background. 2005. (Cited on page 102.)

[Kriegler 2005] E. Kriegler. *Imprecise Probability Analysis for Integrated Assessment of Climate Change*. PhD thesis, Postdam Institute for Climate Impact Research (PIK), 2005. (Cited on pages 46, 52 and 59.)

[Krupnick 2006] A. Krupnick, R. Morgenstern, M. Batz, P. Nelsen, D. Burtraw, J. Shih and M. McWilliams. *Not a Sure Thing: Making Regulatory Choices Under Uncertainty- Technical Report*. 2006. (Cited on page 10.)

[Laplace 1814] P. S. Laplace. *A philosophical essay on probabilities*. Dover Publications Inc., New York, 1814. (Cited on page 11.)

[Leaf 2012] D. E. Leaf and C. Liu. Inference about constrained parameters using the elastic belief method. *International Journal of Approximate Reasoning*, vol. 53, no. 5, pages 709–727, 2012. (Cited on page 31.)

[Leggett 2003] J. W. Leggett, W. Pepper, A. Sankovski, J. Smith, R. Tol and T. Wigley. Climate change risk analysis framework - a probabilistic tool for analyzing climate change uncertainties. *Geophysical Research Abstracts*, 2003. (Cited on page 44.)

[Martin 2008] A. Martin, A. L. Jousselme and C. Osswald. Conflict measure for the discounting operation on belief functions. *In Proceedings of the International Conference on Information Fusion*, Cologne, Germany, 2008. (Cited on pages 23 and 24.)

[Martin 2010] R. Martin, J. Zhang and C. Liu. Dempster–Shafer theory and statistical inference with weak beliefs. *Statistical Science*, vol. 25, pages 72–87, 2010. (Cited on pages 30 and 31.)

[Martins 2000] E. S. Martins and J. R. Stedinger. Generalized maximum-likelihood generalized extreme-value quantile estimators for hydrological data. *Water Resources Research*, vol. 36, no. 3, pages 737–744, 2000. (Cited on page 109.)

[Matteis 2001] R. De Matteis. *Fitting copulas to Data*. PhD thesis, Institute of Mathematics of the University of Zurich, 2001. (Cited on pages 120 and 141.)

[McInnes 2009] K. L. McInnes, J. G. O'Grady and I. Macadam. *The effect of climate change in extreme sea levels in port Phillip Bay. Report to Victorian Department of Sustainability and Environment*. 2009. (Cited on page 100.)

[McNeil 2005] A. McNeil, R. Frey and P. Embrechts. *Quantitative Risk Management: Concepts, Techniques and Tools*. Princeton University Press, Princeton, USA, 2005. (Cited on pages 99 and 141.)

[Mercier 2005] D. Mercier, B. Quost and T. Denoeux. Contextual discounting of belief functions. *Symbolic and Quantitative Approaches to Reasoning with Uncertainty (Lecture Notes in Computer Science)*, vol. 3571, pages 552–562, 2005. (Cited on page 23.)

[Mercier 2008] D. Mercier, B. Quost and T. Denoeux. Refined modeling of sensor reliability in the belief function framework using contextual discounting. *Information Fusion*, vol. 9, no. 2, pages 246–258, 2008. (Cited on page 23.)

[Michele 2005] C. De Michele, G. Salvadori, M. Canossi, A. Petaccia and R. Rosso. Bivariate statistical approach to check adequacy of dam spill-way. *Journal of Hydrological Engineering*, vol. 10, no. 1, pages 50–57, 2005. (Cited on page 99.)

[Millner 2012] A. Millner and al. Do probabilistic expert elicitations capture scientists' uncertainty about climate change? *Climatic Change*, vol. 116, no. 2, pages 427–436, 2012. (Cited on pages 12, 46 and 75.)

[Moore 1966] R. E. Moore. *Interval analysis*. Prentice-Hall, Englewood Cliffs, 1966. (Cited on page 13.)

[Moore 2005] J. C. Moore, A. Grinsted and D. Jevrejeva. New tools for analyzing time series relationships and trends. *EOS, Transactions American Geophysical Union*, vol. 86, no. 24, pages 226–232, 2005. (Cited on page 65.)

[Morellato 2010] D. Morellato and M. Benoit. Vagues et changement climatique - Simulation des états de mer dans l'Océan Atlantique de 1960 à 2100 pour trois scénarios de changement climatique. *Journées Scientifiques et Techniques, Brest 2010*, vol. 25, 2010. (Cited on page 100.)

[Morgan 1990] M. G. Morgan and M. Henrion. *Uncertainty: A guide to dealing with uncertainty in quantitative risk and policy analysis*. Cambridge University Press, Cambridge, UK, 1990. (Cited on pages 10 and 11.)

[Morgan 1995] M. G. Morgan and D. W. Keith. Subjective judgments by climate experts. *Environmental Science and Technology*, vol. 29, pages 468A–476A, 1995. (Cited on page 52.)

[Morgan 2006] M. Morgan, P. Adams and D. keith. Elicitation of expert judgments of aerosol forcing. *Climate Change*, vol. 75, no. 1, pages 195–214, 2006. (Cited on page 52.)

[Murphy 2000] C. K. Murphy. Combining belief functions when evidence conflicts. *Decision Support Systems*, vol. 29, no. 1, pages 1–9, 2000. (Cited on pages 20, 24 and 45.)

[Neill 2004] B. C. O' Neill. Conditional probabilistic population projections: An application to climate change. *International Statistical Review*, vol. 72, no. 2, pages 157–284, 2004. (Cited on page 44.)

[Nelsen 2006] R. Nelsen. *An introduction to copulas*. Springer, New York, second edition, 2006. (Cited on page 99.)

[Nguyen 2006] H. T. Nguyen. *An introduction to random sets*. Chapman and Hall - CRC Press, Boca Raton, Florida, 2006. (Cited on pages 15 and 17.)

[O'Hagan 2006] A. O'Hagan and al. *Uncertain Judgements: Eliciting Experts' Probabilities*. John Wiley & Sons, 2006. (Cited on page 52.)

[Oumeraci 2004] H. Oumeraci, A. Kortenhaus, N. W. H. Allsop, M. B. Degroot, R. Crouch, J. K. Vrijling and H. G. Koortman. Probabilistic design tools for vertical breakwaters. *International Statistical Review*, vol. 72, pages 1505–1506, 2004. (Cited on page 102.)

[Pfeffer 2008] W. T. Pfeffer, J. T. Harper and S. O'Neel. Kinematic constraints on glacier contributions to 21-st century sea-level rise. *Science*, vol. 321, pages 1340–1343, 2008. (Cited on pages 49, 51 and 59.)

[POLO 2012] SAO POLO. *Stratégies d'adaptation des Ouvrages de Protection Marine ou des Modes d'Occupation du Littoral vis-à-vis de la montée du niveau des mers et des Océans - Rapport Technique*. 2012. (Cited on pages 91, 92, 93, 101, 107 and 118.)

[Pratt 1965] J. W. Pratt, H. Raiffa and R. Schlaifer. *Introduction to Statistical Decision Theory*. The MIT Press, USA, 1965. (Cited on pages 29 and 137.)

[Pugh 2003] D. T. Pugh and J. M. Vassie. Extreme sea levels from tide and surge probability. *In Proceedings of the International Conference on Coastal Management*, pages 911–930, 2003. (Cited on pages 97 and 98.)

[Pullen 2004] T. Pullen and al. *Die Kuste: Archive for Research and Technology on the North Sea and Baltic Coast*. Hamburg, Germany, 2004. (Cited on page 93.)

[Pullen 2007] T. Pullen. *EurOtop - Wave Overtopping of Sea Defences and Related Structures: Assessment Manual*. Wallingford, UK, 2007. (Cited on pages 94, 95 and 102.)

[Purvis 2008] M. Purvis, B. D. Bates and C. M. Hayes. Probabilistic methodology to estimate future coastal flood risk due to sea level rise. *Coastal Engineering*, vol. 55, pages 1062–1073, 2008. (Cited on page 102.)

[Radič 2010] V. Radič and R. Hock. Regional and global volumes of glaciers derived from statistical upscaling of glacier inventory data. *Journal of geophysical Research-Earth Surface*, vol. 115, page F01010, 2010. (Cited on page 47.)

[Rahmstorf 2007a] S. Rahmstorf. A semi empirical approach to projecting future sea level rise. *Science*, vol. 315, pages 368–370, 2007. (Cited on pages 49, 50 and 65.)

[Rahmstorf 2007b] S. Rahmstorf. Technical notes *http://www.realclimate.org/index.php/archives/2007/03/the-ipcc-sea-level-numbers/*. 2007. (Cited on page 49.)

[Rahmstorf 2012] S. Rahmstorf, M. Perrette, and M. Vermeer. Testing the robustness of semi-empirical sea level projections. *Climate Dynamics*, vol. 39, pages 861–875, 2012. (Cited on pages 49 and 66.)

[Rahmstorf 2013] S. Rahmstorf. Sea-level rise: Where we stand at the start of 2013 - *http://www.realclimate.org/index.php/archives/2013/01/sea-level-rise-where-we-stand-at-the-start-of-2013/*. 2013. (Cited on pages 50 and 52.)

[Ramasso 2013] E. Ramasso and T. Deneoux. Making use of partial knowledge about hidden states in HMMs: an approach based on belief functions. *IEEE Transactions on Fuzzy Systems (submitted)*, 2013. (Cited on page 35.)

[Ramon 1991] P. Ramon, T. Wiley and A. P. Salvi. Adaptive selection of sensors based on individual performance in multisensor environment. *In SPIE Proceedings, Data Structures and Target Classification*, volume 1470, pages 30–36, 1991. (Cited on page 23.)

[Regan 2004] H. M. Regan, S. Ferson and D. Berleant. Equivalence of methods for uncertainty propagation of real-valued random variables. *International Journal of Approximate Reasoning*, vol. 36, pages 1–30, 2004. (Cited on page 28.)

[Reilly 2001] J. Reilly and al. Uncertainty and climate change assessments. *Science*, vol. 293, pages 430–433, 2001. (Cited on page 52.)

[Robert 2001] C. Robert. *Bayesian choice*. Springer Verlag, second edition, 2001. (Cited on pages 29 and 139.)

[Salvadori 2004a] G. Salvadori. Bivariate return periods via 2-copulas. *Statistical Methodology*, vol. 1, 2004. (Cited on page 99.)

[Salvadori 2004b] G. Salvadori and C. De Michele. Frequency analysis via copulas: theoretical aspects and applications to hydrological events. *Water Resources Research*, vol. 40, 2004. (Cited on page 99.)

[Sandri 1995] S. A. Sandri, D. Dubois and H. W. Kalfsbeek. Elicitation, assessment and pooling of expert judgments using possibility theory. *IEEE Transactions on Fuzzy Systems*, vol. 3, no. 3, pages 313–335, 1995. (Cited on pages 24, 25 and 75.)

[Savage 1954] L. J. Savage. *The foundation of statistics*. John Wiley & Sons, New York, 1954. (Cited on pages 11 and 12.)

[Savage 1963] L. J. Savage. Discussion. *Bulletin of the International Statistical Institute*, vol. 40, pages 925–927, 1963. (Cited on page 29.)

[Schmith 2007] T. Schmith, S. Johansen and P. Thejll. Comment on "A Semi-Empirical Approach to Projecting Future Sea-Level Rise ". *Science*, vol. 317, page 368, 2007. (Cited on pages 52 and 66.)

[Schubert 2011] J. Schubert. Conflict management in Dempster–Shafer theory using the degree of falsity. *International Journal of Approximate Reasoning*, vol. 52, no. 3, pages 449–460, 2011. (Cited on page 24.)

[Schuttrumpf 2008] H. Schuttrumpf, A. Kortenhaus, P. Froohle and K. Peters. Analysis of uncertainties in coastal structure design by expert judgment. *In Proceedings of the Chinese-German Joint Symposium on Hydraulic and Ocean Engineering*, 2008. (Cited on page 102.)

[Sentz 2002] K. Sentz and S. Ferson. *Combination of evidence in Dempster–Shafer theory. Technical Report SAND2002-0835*. USA, 2002. (Cited on pages 20 and 22.)

[Shafer 1976] G. Shafer. *A Mathematical Theory of Evidence*. Princeton University Press, Princeton, N. J, 1976. (Cited on pages 13, 15, 16, 21 and 22.)

[Shafer 1979] G. Shafer. Allocations of probability. *Annals of probability*, vol. 7, no. 5, pages 827–839, 1979. (Cited on page 17.)

[Shafer 1981] G. Shafer. Constructive probability. *Synthese*, vol. 48, no. 1, pages 1–60, 1981. (Cited on pages 15 and 21.)

[Shafer 1982] G. Shafer. Belief functions and parametric models (with discussion). *Journal of Royal Statistical Society, Series B*, vol. 44, pages 322–352, 1982. (Cited on pages 33, 34 and 35.)

[Shenoy 1992] P. P. Shenoy. Using Dempster–Shafer's belief functions theory in expert systems. *In Proceedings of SPIE The International Society for Optical Engineering*, pages 2–14, 1992. (Cited on page 13.)

[Shiau 2003] J. T. Shiau. Return period of bivariate distributed extreme hydrological events. *Stochastic Environmental Research and Risk Assessment*, vol. 17, pages 42–57, 2003. (Cited on pages 99 and 100.)

[Shubert 1996] J. Shubert. Specifying nonspecific evidence. *International Journal of Intelligent Systems*, vol. 11, pages 525–563, 1996. (Cited on page 24.)

[Sklar 1959] A. Sklar. Fonction de répartition à n dimensions et leurs marges. *Publications de l'Institut de Statistique de l' Université de Paris*, vol. 8, pages 229–231, 1959. (Cited on page 99.)

[Smets 1993] Ph. Smets. Belief functions: the disjunctive rule of combination and the generalized Bayesian theorem. *International Journal of Approximate Reasoning*, vol. 9, pages 1–35, 1993. (Cited on pages 20 and 35.)

[Smets 2005] Ph. Smets. Belief functions on real numbers. *International Journal of Approximate Reasoning*, vol. 40, no. 3, pages 181–223, 2005. (Cited on page 17.)

[Smets 2007] Ph. Smets. Analyzing the combination of conflicting belief functions. *Information Fusion*, vol. 8, pages 387–412, 2007. (Cited on page 22.)

[Tawn 1989] J. A. Tawn, J. M. Vessie and E. J. Gumbel. Extreme sea levels: the joint probability method revisited and revised. *In Institution of Civil Engineering Proceedings*, volume 87, pages 429–442, 1989. (Cited on page 97.)

[Thunnissen 2003] D. P. Thunnissen. Uncertainty classification for the design and development of complex systems. *In Proceedings of the 3 rd Annual Predictive Methods Conference, Veros Software*, 2003. (Cited on page 10.)

[Titus 1995] J. G. Titus and V. K. Narayanan. *The Probability of Sea Level Rise.* Environmental Protection Agency, Washington, 1995. (Cited on page 59.)

[Turner 2009a] J. Turner and al. *Antarctic climate change and the environment.* Scientific committee on Antarctic Research, Cambridge, UK, 2009. (Cited on page 51.)

[Turner 2009b] J. Turner and al. *The effect of climate change on extreme sea levels along Victoria's coast.* National Research Flagships Climate adaptation, Cambridge, UK, 2009. (Cited on page 92.)

[Vermeer 2009] M. Vermeer and S. Rahmstorf. Global sea level linked to global temperature. *Proc Natl Acad Sci USA*, vol. 106, pages 21527–21532, 2009. (Cited on pages 49, 50, 51, 52, 63, 64, 66 and 69.)

[Wagenmakers] E. J. Wagenmakers and al. *Bayesian cognitive modeling: A practical course*. (Cited on page 29.)

[Wahl 2012] T. Wahl, C. Muderbach and J. Jensen. Assessing the hydrodynamic boundary conditions for risk analyses in coastal areas: a multivariate statistical approach based on copula functions. *Natural Hazards and Earth System Sciences*, vol. 12, pages 495–510, 2012. (Cited on page 99.)

[Walley 1987] P. Walley. Belief function representations of statistical evidence. *The Annals of Statistics*, vol. 15, no. 4, pages 1439–1465, 1987. (Cited on page 35.)

[Walley 1991] P. Walley. *Statistical Reasoning with Imprecise Probabilities*. Chapman and Hall, London, 1991. (Cited on pages 12, 13 and 28.)

[Wasserman 1988a] L. A. Wasserman. *Belief functions and likelihood. Technical Report 420*. Carnegie-Mellon University, Department of Statistics, 1988. (Cited on page 33.)

[Wasserman 1988b] L. A. Wasserman. *Some applications of belief functions to statistical inference*. PhD thesis, University of Toronto, Department of Preventive Medicine and Biostatistics, 1988. (Cited on page 33.)

[Wasserman 1990] L. A. Wasserman. Belief functions and statistical evidence. *The Canadian Journal of Statistics*, vol. 18, no. 3, pages 183–196, 1990. (Cited on page 33.)

[Webster 2002] M. D. Webster and al. Uncertainty in emissions projections for climate models. *Atmospheric Environment*, vol. 36, pages 3659–3670, 2002. (Cited on page 44.)

[Wigley 2001] T. M. L. Wigley and S. C. B. Raper. Interpretation of high projections for global-mean warming. *Science*, vol. 293, pages 451–454, 2001. (Cited on page 45.)

[Williamson 1990] R. C. Williamson and T. Downs. Probabilistic Arithmetic I: numerical methods for calculating convolutions and dependency bounds. *International Journal of Approximate Reasoning*, vol. 4, pages 89–158, 1990. (Cited on page 28.)

[Yager 1978] R.R. Yager. On the Dempster–Shafer framework and new combination rules. *Information Science*, vol. 41, pages 93–137, 1978. (Cited on pages 20 and 22.)

[Yager 1986] R.R. Yager. Arithmetic and other operations on Dempster–Shafer structures. *International Journal Man-Machine Studies*, vol. 25, pages 357–366, 1986. (Cited on page 26.)

[Yang 2013] Y. Yang, D. Han and C. Han. Discounted combination of unreliable evidence using degree of disagreement. *International Journal of Approximate Reasoning*, vol. 54, no. 8, pages 1197–1216, 2013. (Cited on pages 23 and 24.)

[Zabell 1992] S. L. Zabell. R. A. Fisher and the fiducial argument. *Statistical Science*, vol. 7, pages 369–387, 1992. (Cited on page 29.)

[Zadeh 1965] L. A. Zadeh. Fuzzy sets. *Information and Control*, vol. 8, pages 338–353, 1965. (Cited on page 13.)

[Zadeh 1978] L. A. Zadeh. Fuzzy sets as a basis for a theory of possibility. *Fuzzy Sets and Systems*, vol. 1, pages 3–28, 1978. (Cited on pages 13, 17, 18 and 36.)

[Zadeh 1979] L. A. Zadeh. *On the validity of Dempster's rule of combination of evidence. Memo M79/24*. University of Califonia, Berkeley, USA, 1979. (Cited on page 21.)

[Zadeh 1986] L. A. Zadeh. A simple view of the Dempster–Shafer theory of evidence and its implication for the rule of combination. *AI Magazine*, vol. 7, no. 2, pages 85–90, 1986. (Cited on page 21.)

[Zeng 2007] C. Zeng and P. Wu. A reliability discounting strategy based on plausibility function of evidence. *In Proceedings of the 10th International Conference on Information Fusion*, pages 1–6, 2007. (Cited on page 22.)

[Zhang 1994] L. Zhang. *Advances in the Dempster–Shafer Theory of Evidence - representation, independence and combination of evidence in the Dempster–shafer theory*. John Wiley & Sons, Inc., New York, USA, 1994. (Cited on pages 20 and 22.)

[Zickfeld 2010] K. Zickfeld and al. Expert judgments about transient climate response to alternative future trajectories of radiative forcing. *PNAS*, pages 12451–12456, 2010. (Cited on page 52.)